IntechOpen

Evolving BCI Therapy

Engaging Brain State Dynamics

Edited by Denis Larrivee

EVOLVING BCI THERAPY - ENGAGING BRAIN STATE DYNAMICS

Edited by **Denis Larrivee**

Evolving BCI Therapy - Engaging Brain State Dynamics
http://dx.doi.org/10.5772/intechopen.71592
Edited by Denis Larrivee

Contributors

Irving Weinberg, Lamar Mair, Sahar Jafari, Jose Miguel Algarin Guisado, Jose Maria Benlloch Baviera, James Baker-McKee, Bradley English, Sagar Chowdhury, Pulkit Malik, Jamelle Watson-Daniels, Olivia Hale, Pavel Stepanov, Alek Nacev, Ryan Hilaman, Said Ijanaten, Christian Koudelka, Ricardo Araneda, Jens Herberholz, Luz J Martinez-Miranda, Benjamin Shapiro, Pablo S S Villar, Ilya Krivorotov, Sakhrat Khizroev, Stanley Fricke, Jzau-Sheng Lin, Ray Fhih, Maryam Alimardani, Shuichi Nishio, Hiroshi Ishiguro, Yoshibumi Bunno, Rajesh Singla, Bijay Guragain, Ali Haider, Reza Fazel-Rezai, Haitham Hasan, Denis Larrivee

Notice

First published in London, United Kingdom, 2018 by IntechOpen
eBook (PDF) Published by IntechOpen, 2019
IntechOpen is the global imprint of INTECHOPEN LIMITED, registered in England and Wales, registration number: 11086078, The Shard, 25th floor, 32 London Bridge Street
London, SE19SG – United Kingdom
Printed in Croatia

British Library Cataloguing-in-Publication Data
A catalogue record for this book is available from the British Library

Additional hard and PDF copies can be obtained from orders@intechopen.com

Evolving BCI Therapy - Engaging Brain State Dynamics
Edited by Denis Larrivee

p. cm.

Print ISBN 978-1-78984-069-8

Online ISBN 978-1-78984-070-4

eBook (PDF) ISBN 978-1-83881-588-2

Meet the editor

Professor Denis Larrivee is a Visiting Scholar at Loyola University Chicago and the Mind and Brain Institute, University of Navarra, Pamplona Spain, having held prior associate professor appointments at Weill Cornell University Medical College, New York City and Purdue University, Indiana, USA. A former fellow at Yale University Medical School, he received the Association for Research in Vision and Ophthalmology's first place award for studies on photoreceptor degenerative and developmental mechanisms. He currently maintains an active research interest in mechanisms of global brain integration and is an editorial board member of the journals Neurology and Neurological Sciences (USA) and EC Neurology (UK). An International Neuroethics Society Expert, he is the author of more than 60 papers and book chapters.

Contents

Preface XI

Section 1 New Conceptions in BCI Therapy: Syntax and Semantics in Rehabilitation 1

Chapter 1 **Introductory Chapter: Multilevel Representational Content in BCI Therapy - Extending Syntactic and Semantic Architectures 3**
Denis Larrivee

Section 2 Classification and Precision in Assessing Dynamical States 13

Chapter 2 **A Motor-Imagery BCI System Based on Deep Learning Networks and Its Applications 15**
Jzau-Sheng Lin and Ray Shihb

Chapter 3 **Rotation Invariant on Harris Interest Points for Exposing Image Region Duplication Forgery 29**
Haitham Hasan Badi, Bassam Sabbri and Fitian Ajeel

Section 3 The Motor Image: Reconstructing Semantic Output 51

Chapter 4 **The Application of Motor Imagery to Neurorehabilitation 53**
Yoshibumi Bunno

Chapter 5 **Brain-Computer Interface and Motor Imagery Training: The Role of Visual Feedback and Embodiment 73**
Maryam Alimardani, Shuichi Nishio and Hiroshi Ishiguro

Section 4 Advancing Syntactical Options in BCI Therapy 89

Chapter 6 **SSVEP-Based BCIs 91**
Rajesh Singla

Chapter 7 **Hybrid Brain-Computer Interface Systems: Approaches, Features, and Trends 113**
Bijay Guragain, Ali Haider and Reza Fazel-Rezai

Chapter 8 **Image-guided Placement of Magnetic Neuroparticles as a Potential High-Resolution Brain-Machine Interface 141**
Irving N. Weinberg, Lamar O. Mair, Sahar Jafari, Jose Algarin, Jose Maria Benlloch Baviera, James Baker-McKee, Bradley English, Sagar Chowdhury, Pulkit Malik, Jamelle Watson-Daniels, Olivia Hale, Pavel Y. Stepanov, Aleksandar Nacev, Ryan Hilaman, Said Ijanaten, Christian Koudelka, Ricardo Araneda, Jens Herberholz, Luz J. Martinez-Miranda, Benjamin Shapiro, Pablo S. Villar, Ilya Krivorotov, Sakhrat Khizroev and Stanley Fricke

Preface

This book proves the need for BCI to adjust its therapeutic role to accommodate the distinct syntactic and semantic levels of dynamical coding architectures that characterize the more complex circumstances of motor cognition. In doing so, the book draws from up-to-date and forward looking imaging technologies, including advances in classification methods using artificial intelligence and feature element recognition, as well as a cross-fertilization from methodologically related technologies, novel frequency configurations, in situ and interfacial implanting technology, output driven therapy based on dynamical language architectures, perceptual imaging therapy based on form reconstruction, and neurorehabilitation that links form imaging to cognitive and sensorial feedback.

The book begins with a thematic chapter discussing the pertinence of the brain's operational dynamics for BCI and how this entails shifting the needs of syntax, semantics, and resulting in construction related to the performance demands of the body. Their impact on modifying the current BCI therapeutic model is then discussed. Subsequent chapters show how these novel aspects will require new analytical approaches that can respond to the motive and modular meaning of dynamical elements, now being developed in the classification technologies, and even more distant information and intelligence disciplines. In this vein, Chapter 2 discusses the use of deep learning intelligence schemes that can be applied to decompose wavelets, information bearing, deconstructed forms that promise improved data extraction over fourier analysis. Chapter 3 then takes the eclectic tack of improving classification parcellation by borrowing from technologies that detect false from real signal content in forgery detection.

A critical feature for BCI administered therapy is that, at deeper dynamical levels, the brain is not merely attempting to communicate completed imagery with defined semantic content, but is instead investing meaning to the perceptual form. This can be seen in BCI rehabilitation approaches that seek to elicit motor imagery in the attempt to repair central events, as presented in Chapter 4. Chapter 5 furthers this use of BCI beyond motor image generation to the processes involved in assembling the motor image. This entails the use of realistic sensorial feedback that generates an embodied sense, akin to what happens in normal cognition, that is, through a recreation of the dynamical elements used to generate the form image on an online-updated basis.

While the primary intent of any therapy is the restoration of the endogenous physiology, BCI therapy has frequently resorted to a replace and restore strategy, meaning the substitution of normal performance with implant devices, a concession to the inherent difficulty in fully healing these nerve processes. In such instances, BCI will need to advance technology so as to interface with dynamical elements in order to not only convey formulated action intentions but also to assist in their construction.

Three final chapters consider this dimension in their discussion of the advantages and performance constraints of mediating brain-based output. Chapter 6 discusses a cue related potential, the SSVEP, as an interpretive element that conveys intended actions. Such potentials are proposed to engage synchronous oscillatory activity; hence, they are promising for exploring mechanisms of oscillatory transfer that lead to new behavioral states. Chapter 7 explores the evolution of single mode BCI to multimode hybrid configurations that combine the advantages of multi-classification and multi-command modes.

Chapter 8 considers an entirely new form of interfacial elements, magnetic nanoparticles, that are capable of frequency modulation. Because these are subject to navigational control, they can be mobilized to any region of the brain; hence, they are potentially capable of dynamically interacting with resonating neural ensembles throughout the brain.

It is my hope that this text will generate a thoughtful discussion about how these challenges lead BCI to undertake new therapeutic roles and administer new strategic responses to the motor impaired patient.

I am grateful to Loyola University Chicago for their kindness in supporting this project and for ready access to their informational facilities.

Prof. Denis Larrivee
Loyola University Chicago
Chicago, USA

Section 1

New Conceptions in BCI Therapy: Syntax and Semantics in Rehabilitation

Chapter 1

Introductory Chapter: Multilevel Representational Content in BCI Therapy - Extending Syntactic and Semantic Architectures

Denis Larrivee

Additional information is available at the end of the chapter

http://dx.doi.org/10.5772/intechopen.80232

1. Introduction

The often expressed, but usually trite cliché about history duplicating fiction, nonetheless, reflects a deeper reality, about the human penchant for mystery behind modern technological marvels like brain-computer interfacing (BCI). Indeed, by combining the elusiveness of mental representations with unseen links to motor movements, BCI seemingly appealed to fictional accounts of unlimited mobility and teleportation. This mystique behind the mechanism has lessened somewhat since Jacque Vidal first coined the term in the 1970s [1]. Nevertheless, there remains ongoing excitement over therapeutic prospects that continue to drive interest in advancing BCI applications. Recent domains for example have included the rehabilitation of stroke victims, improved learning with artificial sensory feedback, and real-time control over fine motor movements, as well as the traditional mobilization of external devices usually associated with BCI.

As a strategic response to cognitive and CNS impairments, BCI is a theoretical outgrowth of several generations of endogenous devices that have as a prime strategy the direct replacement of lost neural function. Devices like pacemakers, cochlear implants, and vagal stimulators for example have all been successfully deployed in the relatively simpler anatomical substrate of sensorial and motor nerves where nerve transmission is largely unidirectional and composed of sequences of transmitting signals [2, 3]. In these applications the premise of administering therapy by replacing lost function has been limited to the restoration of signal-generating capacity [4]. Cochlear implants, for instance, transduce pitch vibrations that occur outside the ear to coded electrical signals within the cochlea in order to elicit action potentials in the frequency to place receptors that form the auditory nerve. Implants sited more internally are similarly designed but require the presence of a bidirectional interface for nerve signals, that is, one that can both receive electrical impulses from the intact nerve tissue and yield an

equivalently spaced temporal output beyond the point of lesion. For these devices the replacement of action potentials is akin to the restoration of language syntax, here linearly related to temporal spiking sequences.

In building on these earlier devices, BCI has appropriated not only a similar premise but also a similar design and has, therefore, been largely sequence based and output driven. One consequence of this approach, for example, has been the search for an electrical feature that can be used in a fashion analogous to that of spiking in implant devices for peripheral nerves, such as the local field potential [5]. The premise of a temporally defined syntax is increasingly challenged, however, as knowledge of the anatomical recurrency of the brain is made manifest and the need to distinguish transmitted signals from a dominant background of noise becomes evident [6–8]. How the brain resolves the challenges posed by its complex operation is now thought to occur through the structuring of temporally independent and cyclically repetitive activity, that is, nonlinear dynamical elements that, while using spiking activity as a fundamental mechanistic feature, nonetheless relate only indirectly to it for communication. This is to say that the brain employs a very different type of coding syntax from that of the peripheral nerves. Such fundamentally distinct conditions for communicating information in turn require a different premise on which to base BCI therapy.

Qualitatively different premises for technology, in fact, are hardly new in science, often exerting profound influences on the subsequent course a field may take. The difference in the way information content is represented, when transitioning from peripheral to central nervous tissue resembles, for example, the transition made in computational programming architectures before and after the introduction of autonomous robotic design [9]. Attempts to endow field-situated robotic agents with autonomous mobility initially employed basic program planning formats where decision-making points were encoded in a series of steps telling the robot how to respond. In the field however, it became apparent that programmed contingencies were incapable of responding to the vast array of circumstances that could act as input variables. The need to accommodate this nearly unlimited variability resulted in a new approach to program planning that adopted a more interactive format where plans comprised only one among several input resources that autonomous robots could call upon [10]. In their formatting, these plans adopted a parallel architecture to accommodate multiple and simultaneous inputs. World information was thus assimilated and assembled as blocks of knowledge rather than temporally consecutive incidents.

An analogous shift is now needed for conceiving of BCI as a therapeutic medium, that is, as one that no longer entails only the restoring of signal transmission capacity but also the repairing of processes that structure basic functions. The direction in which this shift will need to evolve, therefore, is not merely in duplicating how the brain transmits information but also in a larger grasp of organismal design that is mediated globally. This becomes apparent when analogized to a linguistic hierarchy, which is used to structure multilevel representational content.

2. Syntactical generation for cognitive representations

In the distinct circumstances of brain cognition, this is apparent, first, at a syntactical level. Given a prevailing background of noise, signal preservation is prioritized, by use of recurrent

connectivities that possess reciprocal inhibitory and excitatory contributions [11–13]. The emphasis of this anatomical architecture is to create circumstances of signal stability, to enable information-bearing signals to persist, thereby minimizing any corruption of information content. Hence, the physical architecture of the brain is anatomically configured to create patterns of cyclical flow, where the pattern of the cycle contains the information representation. Current estimates indicate that nearly 95% of brain neurons exhibit some form of feedback, with some zones noted for especially dense innervation [14, 15]. The physiological consequence of this arrangement is the generation of energetically favored zones where signal propagation is retained. Such persistent activity is a necessity to enable the brain to monitor ongoing bodily activity. However, persistent activity also makes brain operation susceptible to the pervasive influence of a noisy background. This susceptibility is overcome by structuring flow within energetically favorable zones, which minimizes the influence of noise and maximizes signal retention.

The dynamical motifs that are generated adapt spiking activity to exhibit a periodicity that frees syntactical expression from its temporal dependence. This periodicity fundamentally restructures the representation of information content. Hence, basic elements of syntax in the brain are not pulsed sequences, but blocked patterns.

Critically, these stabilized patterns are unique outcomes determined by the resolution of numerous physical forces; that is, they emerge from a high-dimensional state space within the global activity of the brain. They can therefore potentially assume an indefinite number of mathematical configurations that are defined by these physical circumstances. In a simple model, like a fixed point attractor, the rate of change of the attractor back to its original configuration is linearly related to the brain state, which is typically represented by a signal feature related to that state. More complex models entail the continuous and repetitive traversal of brain states by the attractor, which are described mathematically by a second derivative function, while still other models are complex and multiparameterized [16, 17]. The result of this variation is a significant expansion of syntactical range that is likely to substantially differ from that in peripheral nerves.

For BCI therapy the use of a different syntactical expression can be expected to have several consequences. The transposition of one syntax for another means, first, that an interfacial medium relying only on the original syntax introduces gaps in syntactical interpretation, with the immediate consequence of interpretive redundancy [18, 19]. That is, the mapping from one coding structure to the second is not one to one, but instead elicits multiple readouts. For a therapy premised on signal restoration, this overextends the intended output range and diminishes if not obviates therapeutic effectiveness. Hence, bidirectional interfacing premised on duplicating spiking sequences alone is likely to be inadequate for information transfer.

By acquiring temporal independence additionally, the manner in which syntactical elements are assembled is also altered. As cyclical patterns it is only through their modular assembly into larger architectures that they can yield representational variation, a feature that is seen, for instance, in cases of stable heteroclinic channels [20, 21]. Such variation is potentially amenable to exploitation for constructing extended symbolical architectures [22]. Rodrigues et al., for example, have shown that simple combinations of dynamical elements can be exploited to significantly expand the range of syntactical elements [23]. Using an attractor and repellor, they were able to demonstrate that networks generating these elements not only variably combine in specific ratios but also generalize from external inputs; that is, they learned to

represent external input information. This is significant for relating the structure of the network in its connectivity features to a dynamical generation of symbolical structures that establish equivalency with external representation, that is, as codes that map content.

3. Feature-specific representation and semantic construction in BCI therapy

Yet, the generation of symbolical content is not the only consequence of acquiring temporal independence. The manner in which syntactical elements are assembled is also altered. As cyclical patterns it is only through their modular assemble into larger architectures that they can yield representational variation. Significantly, this change offers the immediacy of parallel-based representation. Hence, the role of syntax as representational sign, that is, as in a symbolical, Peircean coding, is itself transformed, linked instead to semantic elements that duplicate through self-organization feature-specific content of the external world [24]. For BCI, information extraction premised on symbolical articulation alone and not accounting for such modular assembly reduces structural content, diminishing the capacity for representation.

The complexity and magnitude of dynamical variation encountered in the state space of the brain, moreover, is a capacity amenable to environmental exigencies, in much the manner that field-situated robotic artifacts become amenable to local input by transferring responsivity from programmatic architectures to distributed processing. Here, sensorial input can elicit motor responsivity directly, structuring forms that directly respond to molding stimuli [25].

Some of the essence of this process of feature-specific duplication can be seen in the motor image, a covert action that is a representation of a non-executed action. The concept of the motor image itself evolved from several experimental legacies. Classical observations made by Lashley [26, 27] in a subject with a deafferented limb showed that humans, and animals, were able to generate actions without sensorial input, in contrast to the broadly assumed hypothesis prevalent in the nineteenth century. Later, experiments in monkeys showed that with deafferentation of spinal dorsal motor roots the animals nonetheless could execute pointing movements in all the phases of motion [28]. This indicated that the movement was predetermined centrally. How this was done and how executed became apparent in studies of ongoing motion. Held [29] observed that limb movements in such circumstances usually do not correspond to their expected trajectories, but entail a misreaching followed by progressive compensatory movements. To explain his finding he proposed Von Holst and Mittelstaedt [30] hypothesis that the command for the executed movement was stored as an efference copy, sent to the sensory cortex, where it was then compared with the actual movement undertaken so as to correct the misaligned motions. The experimental observation of misalignment and correction seen experimentally served as evidence of the memorized storage. A corollary of this hypothesis was that self-made motions could be contextualized to the individual who initiated the actions, a conclusion drawn by Frith in his comparator model [31, 32]. This is to say that the comprehension of the actions as those of one's own was a necessary feature of movement; while the actions could be initiated without afferences, they nonetheless required them for motor cognitions in order to be understood as self-executed functions.

In continuous motions the sensory cues are coupled to motor execution in a mutually reciprocal and sustained process [33]. This is necessary, since as the body undergoes motion, its spatiotemporal position is continually changing and so also the sensory cues that reference it. While these cues entail contributions from all the senses, those having the greatest influence are of somatotopic origin due to their capacity to delimit the three-dimensional topological perimeter of the body [34]; this is also to say that it is necessary to know where the body is situated in space and time in order to know where next to move it. Linda Smith has described this as a point of criticality, analogous to a phase transition in a material substance, where the body is framed as a stable reference that is transitioning to a fluid and behaviorally flexible state [35].

The validity of this observation, and also as a demonstration of the need to frame the whole body, is well documented in the Piaget A not B error where a young infant continues to perseverate toward an object goal despite having been informed of its prior displacement. This error is explained by the delay in development of maturational processes of the brain needed to formulate and execute goal-directed actions [36]. From these, and other experimental studies, it is intuitive to see why the observed events and processes hypothesized by Von Holst and Mittelstaedt and by Frith require a "predictive processing" to engage motion [37]. Predictions are needed if one is to engage in actions, that is, actions that are intended to be carried out by the self, and are not merely passive responses to external events. Since all external contingencies cannot be known beforehand, like the field-situated autonomous artifact, neither can all consequences of the intended actions. The expectation of the action, its prediction, affords a first approximation that is open to correction that can structure the sequence that follows and that is energetically efficient.

This interplay between predictive actions, goals, and a holistic bodily sense point, further, to the presence, indeed need of mechanisms that involve a simulation of intended actions. Covert actions are thus a motor planning stage needed for subsequent motor execution. In this, the motor image is the key element. The construction of the image, its contextualization to the whole, and its traversal of stability flexibility bifurcations are all basic elements that entail feature duplications of the projected events. That is, they constitute semantic representation of objective events directly and not coded symbols of what is intended.

Hence, at deeper levels, linguistic primitives function as determinants for assimilating semantic content. That is, the assembly of these elements creates the semantic content of what is communicated through the action. For BCI therapy, this expands the role of therapy from interpretive assessment to the construction of semantic form, like that occurring when coupling sensorial input to the elicitation of motor imagery [25]. Here, semantic content is added by combining the specific motions that are undertaken to their semantic representation in the whole form of the individual, a process likely to the precision of motor processing primitives of the cerebellum [38, 39].

4. BCI therapy and biological design

Taken together, what is made apparent in analogizing from a linguistic perspective is the strategical implementation of multilevel representational content to structure goal-oriented

motor actions. By extension, there is thus also the implicit subordination of this strategy to ontological demands, that is, actions undertaken for the good of the organism. Hence, they entail more than the execution of actions, a traditional objective performed in BCI, and so also include the formulation of organismal goals. For BCI therapy, accordingly, this formulation of representational content will be a critical objective for therapeutic strategy, encompassing diagnosis and therapy, and dictated at syntactic and semantic levels.

For the motor image, notably, it is apparent that representational content is articulated at multiple levels, built upon a dynamical syntax that acquires semantic content by binding representational, feature-specific, i.e., simulated, forms together. Distinguishing the level of functional disturbance therefore is an objective needed in order to administer therapy adequately. Yet, in decoding approaches that have evolved to date, the central technical concern is that of classification, that is, the mapping of a brain state in its activity patterns to an external object or event. Older techniques like mass univariate analysis sequentially evaluate brain regions for a specific activity at a specific location. Measuring covariance between multiple single units is thereby taken as a diagnostic feature of how select images are encoded, like the activation of long regions of the occipital cortex on presentation of a single object. Discerning the underlying structure of the representational content, therefore, remains unknown and an obstacle to focal BCI therapy [40].

In more recently developed multivariate classification approaches, previously determined activity patterns are linked to specific object features that can assess or predict the content of a specific activity. While this approach can be employed without the presentation of an object, many potential representations are left unclassifiable. These limitations have led to current model-based classification approaches that use models to predict patterns not elicited by training data. Such promising efforts seek to extract greater information content from patterned activity than obtained from linear mapping strategies alone. These latter strategies are likely to be strengthened by expanding the capacity to extract information content by combining deep neural learning with wavelet analysis, like that seen in Chapter 2. Hence, they can be expected to extrapolate from syntactical structure to simulated actions; that is, they will be better capable of extracting how meaning is formulated in the assembly of simulated executable sequences. Enlisting technological methods that can optimize distinctions between signal and noise, like that of Chapter 3, can be expected to further this capacity and particularly evident where discerning the syntactical expression of dynamical architectures is key, in order to communicate the motor image, as in Chapters 6, 7, and 8 of this text.

Crucially, issues of deciphering multilevel representational content and formulating semantic architectures for action-oriented goal seeking enter into primitive motor assembly levels, where, for example, the capacity for assimilating meaningful content is impaired. These will require new therapeutic paradigms where BCI may be one among several adjunct approaches used together to restore the functional modalities needed for simulated motor articulation. In practice, these paradigms will need to recreate the multilevel, brain-based operation that occurs in motor planning, like that used in sensory motor coupling. Models of such therapy, for example, are presented in Chapters 4 and 5 of the current volume.

5. Conclusion

Novel insights into the multilevel construction of representational content promise a new phase of BCI therapy, embracing not only the restoration of executable actions but also the formulation of the motor image and motor planning sequences. Built upon the fundamentally distinct syntactic and semantic architecture of dynamic cognition, new forms of therapy will undertake to simulate the brain's approach to information transfer and to attain goal-directed planning. These will likely entail enhanced information extraction in classification and predictive technology, dynamically structured command and communication methodologies, and integrative, mixed-mode BCI approaches that can restructure motor semantics.

Author details

Denis Larrivee[1,2]*

*Address all correspondence to: sallar1@aol.com

1 Loyola University Chicago, USA

2 Mind and Brain Institute, University of Navarra, Spain

References

[1] Vidal J. Toward direct brain-computer communication. Annual Review of Biophysics and Bioengineering. 1973;**2**:157-180

[2] Cong P. Neural interfaces for implantable medical devices: Circuit design considerations for sensing, stimulation, and safety. IEEE Solid States Circuits Magazine. Fall, 2016;**48**:1-6

[3] Larrivee D. Implantable medical devices and brain attractors: Network modulation and design practice. IEEE Transactions on Systems Man and Cybernetics-Part A Systems and Humans. pp. 2018-2023. DOI: 10.1109/SMC.2017.8122915

[4] 2nd International Conference on Neurological Rehabilitation. 2017. Available from: https://www.allcongress.com/medical-congress/2nd-international-conference-on-neurorehabilitation

[5] Jackson A, Hall TM. Decoding local field potential for neural interfaces. IEEE Transactions of Neural Systems and Rehabilitation Engineering. 2010;**2010**:1-10

[6] Schoner G. Development as change of system dynamics: Stability, instability, and emergence. In: Spencer J, Thomas MSC, McClelland JL, editors. Toward a Unified Theory of Development. Oxford: Oxford University Press; 2009

[7] Friston K. Free energy and global dynamics. In: Rabinovich M, Friston KJ, Varona P, editors. Principles of Brain Dynamics. London: MIT Press; 2013

[8] Rabinovich MI, Abarbanel HD. The role of chaos in neural systems. Neuroscience. 1998; **87**:5-14

[9] McDermott J, Hendler D. Planning: What it is, what it could be, an introduction to the special issue on planning and scheduling. Artificial Intelligence. 1995;**76**(1):1-16

[10] Arkin RC. Integrating behavioral, perceptual, and world knowledge in reactive navigation. In: Maes P, editor. Designing Autonomous Agents. Cambridge: MIT Press; 1993

[11] Wilson HR, Cowan JD. Excitatory and inhibitory interactions in localized populations of model neurons. Biophysics Journal. 1972;**12**:1-24

[12] Canavier CC. Phase-resetting as a tool of information transmission. Current Opinion in Neurobiology. 2015;**31**:206-213

[13] Fornito A, Zalesky A, Bullmore E. Fundamentals of Brain Network Analysis. London: Elsevier Press; 2016

[14] Muldoon SF, Bassett DS. Network and multilayer network approaches to understanding human brain dynamics. Philosophy of Science. 2016;**83**(5):710-720

[15] Tononi G, Sporns O, Edelman GM. A measure for brain complexity: Relating functional segregation and integration in the nervous system. Proceedings of the National Academy of Sciences USA. 1994;**91**:5033-5037

[16] McClelland JL, Vallabha G. Connectionist models development: Mechanical, dynamical models with emergent dynamical properties. In: Spencer J, Thomas MSC, McClelland JL, editors. Toward a Unified Theory of Development. Oxford: Oxford University Press; 2009

[17] Eliasmith C. Attractor Network. 2007. Available from: http://www.scholarpedia.org/article/Attractor_network

[18] Bedny M, Pascual-Leone A, Dodell-Feder D, Fedorenko E, Saxe R. Language processing in the occipital cortex of congenitally blind adults. Proceedings of the National Academy of Sciences. 2011;**108**(11):4429-4434

[19] Boroditsky L. How language shapes thought. Scientific American. Feb 2011:62-65

[20] Deco G, Jirsa V, Friston K. The dynamical and structural basis of brain activity. In: Rabinovich M, Friston, KJ, Varona P, editors. Principles of Brain Dynamics. London: MIT Press; 2013. pp. 9-26

[21] Rabinovich M, Huerta R, Laurent G. Neuroscience-Transient dynamics for neural processing. Science. 2008;**321**:48-50

[22] Tabor W. Dynamical insight into structure in connectionist models. In: Spencer J, Thomas MSC, McClelland JL, editors. Toward a Unified Theory of Development. Oxford: Oxford University Press; 2009

[23] Rodrigues P. Simple recurrent networks learn context free and context sensitive languages by counting. Neural Computation. 2001;**13**(9):2093-2118

[24] Friston K, Sengupta B, Auletta G. Cognitive dynamics: From attractors to active inference. Proceedings IEEE. 2014;**102**(4):427-445

[25] Varela F, Thompson E, Rosch E. The Embodied Mind: Cognitive Science and Human Experience. Cambridge: MIT Press; 1991

[26] Lashley KS. The problem of serial order in behavior. In: Jeffress LA, editor. Cerebral Mechanisms and Behavior. New York: Wiley Press; 1951. pp. 112-136

[27] Bizzi E, Kalil RE, Tagliasco V. Eye-head coordination in monkeys. Evidence for centrally patterned organization. Science. 1971;**173**:452-454

[28] Jeannerod M. Levels of representation of goal-directed actions. In: Fruend HJ, Jeannerod M, Hallett M, Leiguarda R, editors. Higher-order Motor Disorders. Oxford: Oxford University Press; 2005

[29] Held R. Exposure-history as a factor in maintaining stability of perception and coordination. Journal of Nerve and Mental Disorders. 1961;**132**:26-32

[30] Von Holst E, Mittelstaedt H. Das reafferenzprinzip. Wechselwirkungen zwischen Zentralnervensystem und Peripherie. Die Naturwissenschaften. 1950;**37**:464-476

[31] Frith C. Explaining delusions of control: The comparator model 20 years on. Consciousness and Cognition. 2012;**21**(1):52-54

[32] Bayne T, Pacherie E. Narrators and comparators: The architecture of agentive self-awareness. Synthese. 2007;**159**:475-491

[33] Shapiro L. Embodied Cognition. New York: Routledge Publishing; 2011

[34] Damasio A. Self Comes to Mind: Constructing the Conscious Brain. New York: Pantheon Books; 2012

[35] Smith L. Stability and flexibility in development. In: Spencer J, Thomas MSC, McClelland JL, editors. Toward a Unified Theory of Development. Oxford: Oxford University Press; 2009

[36] Corbetta D. Brain, body, and mind: Lessons from infant motor development. In: Spencer J, Thomas MSC, McClelland JL, editors. Toward a Unified Theory of Development. Oxford: Oxford University Press; 2009. pp. 51-56

[37] Allen M, Friston K. From cognitivism to autopoiesis: Toward a computational framework for the embodied mind. Synthese. 2016;**195**(6):2459-2482. DOI: 10.1007/s11229-016-1288-5

[38] Jeannerod M. The sense of agency and its disturbances in schizophrenia: a reappraisal. Experimental Brain Research. 2009;**192**:527-532

[39] D'Angelo E, Casali S. Seeking a unified framework for cerebellar function and dysfunction: From circuit operations to cognition. Front Neural Circuits. 2013;**6**(116):1-23. DOI: 10.3389/fncir.2012.00116

[40] Hayes JD. Decoding mental states from patterns of brain activity. In: Rabinovich M, Friston KJ, Varona P, editors. Principles of Brain Dynamics. London: MIT Press; 2013. pp. 9-26

Section 2

Classification and Precision in Assessing Dynamical States

Chapter 2

A Motor-Imagery BCI System Based on Deep Learning Networks and Its Applications

Jzau-Sheng Lin and Ray Shihb

Additional information is available at the end of the chapter

http://dx.doi.org/10.5772/intechopen.75009

Abstract

Motor imagery brain-computer interface (BCI) by using of deep-learning models is proposed in this paper. In which, we used the electroencephalogram (EEG) signals of motor imagery (MI-EEG) to identify different imagery activities. The brain dynamics of motor imagery are usually measured by EEG as non-stationary time series of low signal-to-noise ratio. However, a variety of methods have been previously developed to classify MI-EEG signals getting not satisfactory results owing to lack of characteristics in time-frequency features. In this paper, discrete wavelet transform (DWT) was applied to transform MIEEG signals and extract their effective coefficients as the time-frequency features. Then two deep learning (DL) models named Long-short term memory (LSTM) and gated recurrent neural networks (GRNN) are used to classify MI-EEG data. LSTM is designed to fight against vanishing gradients. GRNN makes each recurrent unit to capture dependencies of different time scales adaptively. Similar scheme of the LSTM unit, GRNN has gating units that modulate the flow of information inside the unit, but without having a separate memory cells. Experimental results show that GRNN and LSTM yield higher classification accuracies compared to the existing approaches that is helpful for the further research and application of relative RNN in processing of MI-EEG.

Keywords: motor imagery, brain-computer interface (BCI), recurrent neural network (RNN), long-short-term memory (LSTM), gated recurrent neural network (GRNN)

1. Introduction

Brain-computer interface (BCI) system provides one of the most important aspects, which is an alternative way of communication through brain signals. It is just to translate electroencephalogram

(EEG) signals from a reflection of brain activity into user action through system's hardware and software. A BCI system provides a communication channel not based on nerves and muscles that allow users to communicate by electrodes contacting on scalp. It has attracted increasing attention of a variety of research fields including neuroscience, machine learning, pattern recognition, rehabilitation medicine, and so on.

Motor imagery (MI) is an important research topic in the field of BCI that mentally simulates a given action, e.g., imaging the motions of the limbs [1]. It refers to visualization of a limbic activity, or any other movement, without the actual execution of the motion imagined. It leads to various changes in the connectivity between the neurons present in the cortex. This results in either an event-related desynchronization (ERD) or event-related synchronization (ERS) of mu rhythms. These effects are due to the changes in the chemical synapses of the neurons, the change in strength between the interconnections or the change of intrinsic membrane properties of local neurons. Since extracted from scalp EEG, MI-EEG has the characteristics of nonlinear, nonstationary, and time-varying.

In the research field of MI-EEG-based BCI, several researchers have proposed different strategies. Tomida et al. [2] presented an active data selection method for MI-EEG classification in 2015. Rejecting or selecting data from multiple trials of EEG recordings is crucial in the selection method. To aim at brain machine interfaces (BMIs), they proposed a sparsity-aware method to select data from a set of multiple EEG recordings during MI tasks. An extraction approach with transform-based feature for MI tasks classification was proposed by Baali et al. [3]. A signal-dependent orthogonal transform was used, referred to as linear prediction singular value decomposition (LP-SVD), for feature extraction. They used a logistic tree-based model classifier to classify the extracted features into one of four motor imagery movements. In 2016, Wu et al. [4] used the fuzzy integral with particle swarm optimization (PSO), which can regulate subject-specific parameters for the assignment of optimal confidence levels for classifiers. Lin and Lo [5] constructed a MI-based BCI system to control an electric wheelchair. They used discrete wavelet transform (DWT) to transform EEG signals into frequency domain and applied SVM to classify them into different commands. Chatterjee and Bandyopadhyay [6] used SVM and multilayered perceptron (MLP) for MI-EEG classification in 2016. They showed that both SVM and MLP were suitable for such MI classifications with the accuracy of 85 and 85.71%, respectively. The symmetric positive-definite (SPD) covariance matrices of EEG signals carry important discriminative information proposed by Xie et al. [7] for MI BCI system in 2016. Chatterjeel et al. [8] examined the quality of feature sets obtained from wavelet-based energy entropy with variation of scale and wavelet type for MI classification in 2016. They have verified their study with three classifiers—Naive Bayes, MLP and SVM. Jois et al. [9] compared several classification techniques for motor imagery-based BCI in 2015. They indicated that common features, e.g., band power values, present that the single EEG trials can be extracted by suitable methods for classification using SVM, neural networks, or ensemble classifiers. The classifiers yield different efficiencies and are compared to find the optimal technique for same number of features. They believed the neural net techniques were proved to be the most efficient. One obstacle of the traditional neural networks for their broader application is the initial weights need to be chosen carefully. Generally, small values could make the multilayer

network untrainable owing to weight diffusion, while large initial values of the weights could result in poor local minima [10]. In order to resolve this problem and construct high descriptive-ability neural networks, a new model of strategies and algorithms, called deep learning (DL), has been successfully developed and becomes prevailing in several fields [11].

There are many ways in machine learning for data classification. The most popular and proven method in recent decades is "Artificial Neural Network (ANN)." We know how artificial neural networks adjust weights so that the error between output and input becomes smaller. But even so, this is far from the "artificial intelligence" that we want. If the computer can analyze the data to find the features, then it is closer to the artificial intelligence we want, that is to say, the created computer can think. DL allows computers to analyze their own data to find "features," rather than decided by human beings with features, just as computers can have deep thinking to learn. DL uses not only a multilayer neural network but also an autoencoder for unsupervised learning.

Recurrent neural networks (RNN), one of the models in DL, have proved promising results in many field [12–15] recently, especially when input and/or output are of variable length. In the application of EEG signals classification, Petrosian et al. [16] first applied RNN and wavelet transform to classify EEG signals. RNN is not satisfied in scalp EEG owing to the scalp EEG containing interference resulted from external noises. Besides, the input of the RNN does not have a special signal preprocessing, the RNN network has some problems such as gradient explosion and gradient vanish. Fully using characteristics in time-frequency features of signals, RNN with LSTM [17], have recently emerged as an effective deep learning model in a wide variety of applications that involve sequential data. The LSTM-based RNN can not only solve the problems in RNN but also store the long time information. In 2016, Li et al. [18] proposed an LSTM-based RNN integrated with DWT to classify the EEG signals. The LSTM is designed to fight against vanishing gradients through a gating mechanism. Gated recurrent neural network (GRNN), proposed by Cho et al. [19] in 2014, makes each recurrent unit to capture variable-length sequences adaptively. Similar scheme of the LSTM unit, GRNN has gating units that modulate the flow of information inside the unit, but without having a separate memory cell. In GRNN, the parameters at each level are shared through the whole network.

In this chapter, LSTM and GRNN combined with the DWT to classify the EEG signals were proposed. The average power spectrum of MI-EEG signals was calculated and the effective time segment was also determined. Then, DWT is applied to each channel of MI-EEG to extract the effective time-frequency characteristics. Finally, LSTM and GRNN were used as classifiers to recognize the MI-EEG signals. The experimental results showed that GRNN and LSTM methods can make full use of the time-frequency information of MI-EEG, as well as time sequence information, and can get better recognition performance.

The rest of this chapter is organized as follows: Section 2 describes the system architecture; wavelet transform is described in Section 3; Section 4 presents the LSTM-based recurrent network; the GRNN is discussed in Section 5; Section 6 shows the experimental results; the application to control an electric wheelchair is shown in Section 7; and finally, the discussions are given in Section 8.

2. System architecture

The proposed BCI system is integrated as EEG signals extracting subsystem through the Emotiv EPOC chip, g.SAHARAbox system, and g.SAHARA electrodes. The g.SAHARAbox system and g.SAHARA electrodes are shown in **Figure 1**. The system's electrodes are dry manner and nonintrusive conductive system that allows 16 EEG channels to be embedded into the input of EPOC chip at the same time. The electrode locations C3, C4, and Cz based on the international 10–20 system, shown in **Figure 2**, were used to extract EEG signals, while locations A1 and A2 were used as reference points. For the MI-EEG signals, two motion-imagination brain signals were recognized, respectively. One is "imagining right-hand action" and the other is "imagining left-hand action." In order to establish a sampling model, we captured 9-s EEG signals for every imagining action from every channel. And, the extracted brainwave signal is transformed through DWT to obtain the spectrums in frequency domain. Then, the frequency feature was calculated and classified into different categories by using LSTM and GRNN.

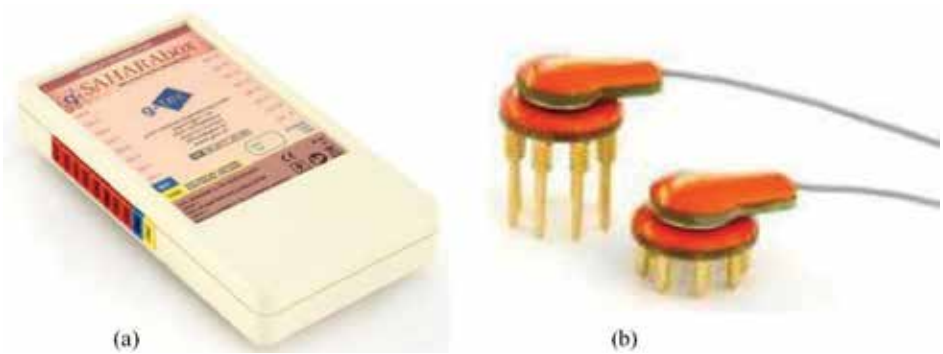

Figure 1. The subsystems in the proposed BCI: (a) g.SAHARAbox system and (b) g.SAHARA electrodes.

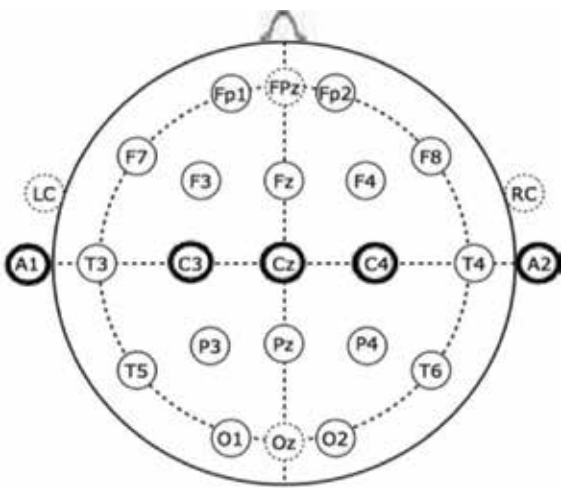

Figure 2. Locations C3, C4, and Cz are used in the 10–20 system.

In order to speed up the processing of DWT and update the classification performance in the deep learning algorithms, the NVIDIA Jetson TK1 is used in the proposed system. In the platform, NVIDIA Tegra K1 SoC is embedded with a super computing core NVIDIA Kepler. So that it is a high-speed computing system for rapid development and deployment in computer vision, robotics, medical applications, and more. Additionally, an FPGA module named Xilinx Virtex4 XC4VFX12 is also applied to control external system such as electric wheelchair.

3. Discrete wavelet transform

The concept of wavelet was proposed by Jean Morlet in 1981. In this chapter, The Daubechies wavelet, proposed by Dr Daubechies in 1988 [20], was used to extract the features from EEG signals. It is often used in signal compression, digital signal analysis and noise filtering, and so on. In Daubechies wavelet, several series db wavelets can get better performance in signal analysis. In this chapter, db4 wavelets were used to extract main features from EEG signals. Multiresolution analysis in the WT algorithm was proposed by Mallat [21] in 1989. When a signal resolution has a high-degree variation in a proper area, it is difficult to get detailed features while the multiresolution strategy can decompose the lower layer signal to get more information. Therefore, the decomposed low-frequency signal can be decomposed continuously to display more features. However, the decomposed iterations of the signal are so many to make the number of samples so few that results in less obvious characteristics of the signal.

Therefore, the number of signal decomposition layer is limited. In the wavelet decomposition, the original signal is input to a low-pass filter g[k] and a high-pass filter h[k], respectively. The low-pass filter retains the consistency of the original signal, and the high-pass filter reserves the variability of the original data. Discrete wavelet transform can be combined with wavelet function and scale function. In the low-frequency part, it has a high frequency resolution and low temporal resolution, while there was a lower frequency resolution and a higher time resolution in the high-frequency part. The discrete wavelet transform decomposition and recombination is shown in **Figure 3** and the multiresolution analysis in the WT is shown in **Figure 4**.

The left half is wavelet decomposition, after the high-pass and low-pass decomposition and then downsampling to get two groups of detailed signal and the approximate signal. The right half in **Figure 3**, the decomposition of the series for the rise of sampling, and then through the high-frequency synthesis filter and low-frequency synthesis filter can be reconstructed.

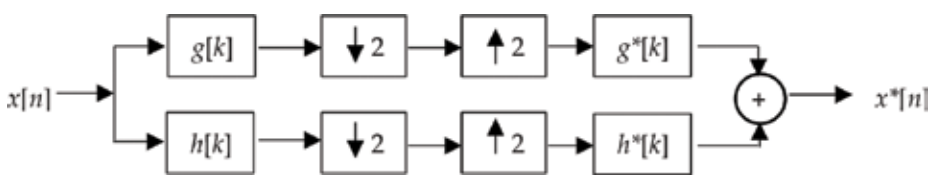

Figure 3. Discrete wavelet decomposition and reconstruction.

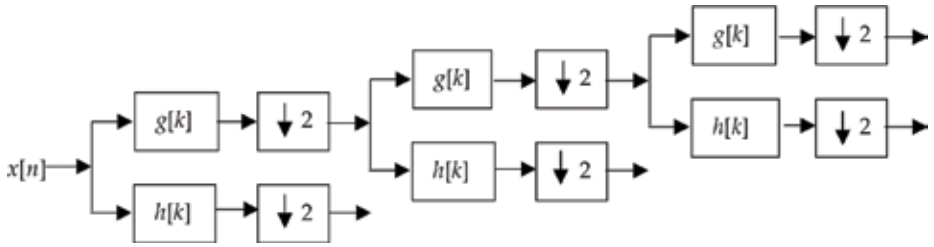

Figure 4. Discrete wavelet multiresolution decomposition.

4. LSTM-based recurrent network

RNNs are popular networks that have shown great promise in many sequential tasks. RNNs are called recurrent because they perform the same task for every element of a sequence, with the output being depended on the previous states. Recently, several researchers have developed more sophisticated types of RNNs to deal with some of the shortcomings of the vanilla RNN model. Training an RNN is similar to training a traditional neural network (TNN). Because RNNs trained by TNN's style have difficulties in learning long-term dependencies due to the vanishing and exploding gradient problem. LSTMs do not have a fundamentally different architecture from RNNs, but they use a different function to calculate the states in hidden layer. The memory in LSTMs is called cells and can be thought as black boxes that take as input the previous state and current input. Internally, these cells decide what to be kept in (and what to be erased from) memory. They then combine the previous state, the current memory, and the input. It turns out that these types of units are very efficient at capturing long-term dependencies. In this chapter, a peephole-connection LSTM, proposed by Gers and Schmidhuber [22], is applied and shown in **Figure 5**. In **Figure 5**, the state of forget gate $f(t)$, shown as in Eq. (1), is decided by a sigmoid function from the previous cell state C_{t-1}, the previous hidden layer state h_{t-i}, and input data x_t.

$$f_t = \sigma\left(w_{c,f}C_{t-1} + w_{x,f}x_t + w_{h,f}h_{t-i}\right) + b_f \tag{1}$$

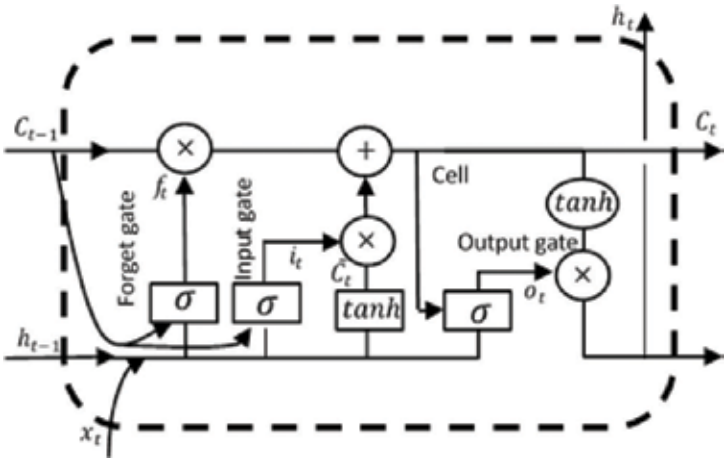

Figure 5. The block diagram of LSTM.

http://dx.doi.org/10.5772/intechopen.75009

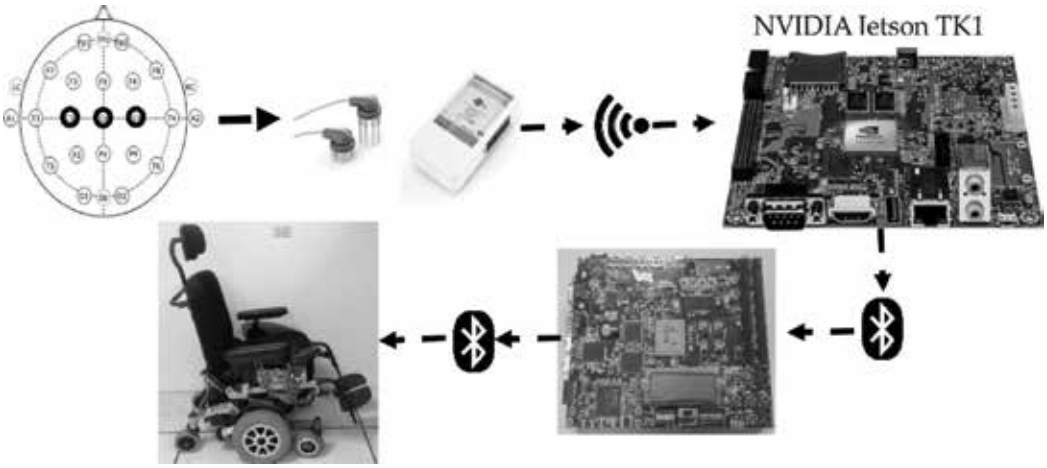

Figure 6. The proposed BCI control system.

From **Figure 6**, we can find the cell state shown as Eq. (2), calculated with the previous cell state C_{t-1}, forget-gate state f_t, and $i_t * \tilde{C}_t$.

$$C_t = f_t * C_{t-1} + i_t \tilde{C}_t \tag{2}$$

where

$$i_t = \sigma\left(W_{c,i} * C_{t-1} + w_{x,i} * x_t + w_{h,i} * h_{t-1} + b_i\right) \tag{3}$$

and

$$\tilde{C}_t = \tanh\left(w_{x,c} * x_t + w_{h,c} * h_{t-1} + b_c\right) \tag{4}$$

Finally, the output-gate state O_t and hidden-layer state h_t are computed by Eq. (5) and Eq. (6), respectively.

$$o_t = \sigma\left(w_{c,o} * C_t + w_{x,o} * x_t + w_{h,o} * h_{t-1} + b_o\right) \tag{5}$$

$$h_t = o_t \tanh(C_t) \tag{6}$$

5. Gated recurrent neural network (GRNN)

The GRNN was proposed by Cho et al. [19] in order to make each recurrent unit to extract dependencies of different timescales adaptively. The GRNN, shown in **Figure 7**, has gating units that modulate the flow of information inside the unit like the LSTM unit but without having a separate memory cell. The parameters in the GRNN are updated as follows:

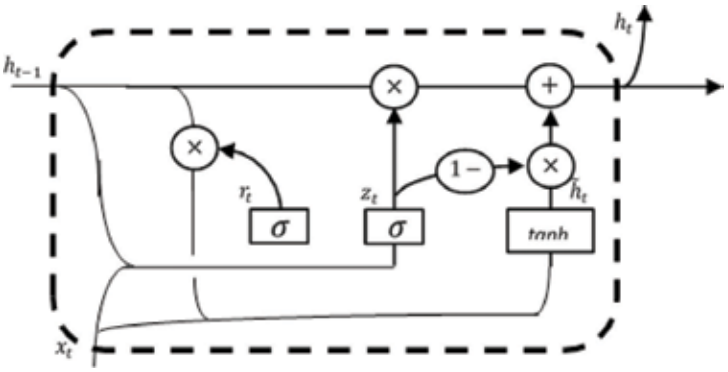

Figure 7. The block diagram of GRNN.

$$z_t = \sigma\left(w_{x,z} * x_t + w_{h,z} * h_{t-1} + b_z\right) \tag{7}$$

$$r_t = \sigma\left(w_{x,r} * x_t + w_{h,r} * h_{t-1} + b_r\right) \tag{8}$$

$$\tilde{h}_t = \tanh\left(w_{x,h} * x_t + w_{h,r} * \left(r_t * h_{t-1}\right) + b_h\right) \tag{9}$$

$$h_t = z_t * h_{t-1} + \left(1 - z_t\right) * \tilde{h}_t \tag{10}$$

where x_t is the input vector, h_t is the output vector in hidden layer, z_t is the vector of update gate, and r_t is the vector of reset gate, respectively.

6. Experimental results

In this chapter, C3, Cz, and C4 are used to capture brainwave signals. Each subject wore an Ultracortex helmet connected with g.tec dry electrode and Emotiv EPOC chip to record MI-EEG signals including to imagine right-hand and left-hand movements. Each imaginary action was consumed 9 s for a data set. The EEG signals were extracted 28 times and transformed by wavelet transform to obtain their features. Therefore, we can obtain 140 sets for 5 subjects and these data sets were divided into 112 groups for training and 28 groups for testing. The experimental data acquisition process is down to obtain a data set every 9 s with an interval of 2 min. The waiting time is set on the first 2 s, then a stimulus signal was sound indicating that the testing process is started and a cross sign "+" is displayed for 1 s. Then, the left or right arrow is displayed to hint a subject imaging the moving of left or right hand. The sampling rate is 128 Hz for the acquisition process.

In this chapter, LSTM and GRNN are used as the EEG classifiers. MI-EEG features were extracted for C3, Cz, and C4 and classified into two groups. Therefore, the neurons of input and output layers of LSTM and GRNN were set three and two, respectively. In order to obtain

http://dx.doi.org/10.5772/intechopen.75009

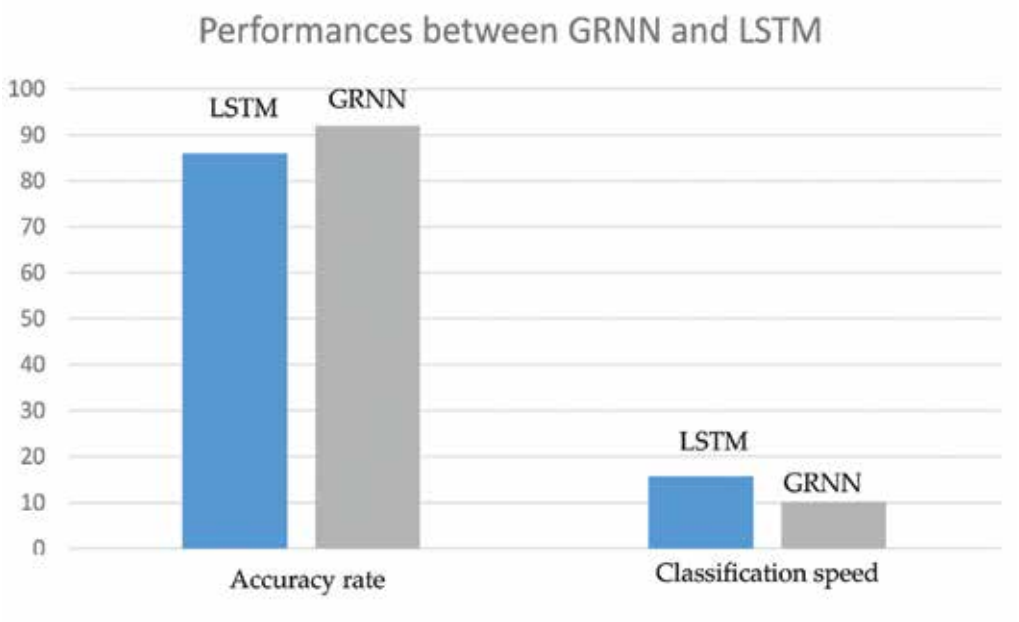

Figure 8. The performance competition between GRNN and LSTM.

Authors	Features	Classifiers	Accuracy rates
Christin Schafer [24]	Wavelet	Bayes	89.29%
GAO Xiaorong [24]	ERD	LDA	86.43%
Akash Narayana [24]	AR	LDA	84.29%
The proposed LSTM	DWT	LSTM	92.83%
The proposed GRNN	DWT	GRNN	94.50%

Table 1. The accuracy rates of different strategies for BCI Competition 2003.

better performance for classification, the hidden layer is set into 7 neurons, and therefore, we can obtain the length of MI-EEG characteristic sequence being 15, while the channel number of MI-EEG-based BCI is 3. In order to evaluate the classification results and obtain a reliable and stable model, this model performs 500 cross validation to calculate the classification accuracy. In 2009, Smith [23] indicated that the nervous system is significantly important to integration of information and to the range of behaviors in which the system can stably engage and among which the system can flexibly switch. However, the nervous system, the body, and the environment each possess their own complex intrinsic dynamics, and these are always in continuous interaction with each other. Human intelligence reveals both remarkable stability and nimble flexibility. Stability emerges from the incorporation of the past into the present. Flexibility, requires an abandonment of (or selection among) past ways, a shifting of responses to meet new circumstances. For the consideration of stability and flexibility, the proposed methods are compared to other strategies based on "BCI Competition 2003" [24]. The experimental results

are shown in **Table 1**. From **Table 1**, we can find that the proposed method can get better performance than others. Additionally, the GRNN is better than the LSTM with 2.67% and 5 ms in the performances of accuracy and classification speed that is shown in **Figure 8**.

7. Applications to control an electric wheelchair

In this section, the proposed BCI system was applied to control an electric wheelchair. During the online experiment, each subject wore the EEG acquisition system with integrated g.SAHARAsys and EPOC chip in the proposed BCI system. Additionally, the EEG signal for eye blinking was added in order to easily control an electric wheelchair to go ahead or emergency stop. For MI-EEG signals, imagining left hand and right hand are translated into turning wheelchair left and right as well as the eye blinking signal is converted into going ahead/emergency stopping. For the purpose of speeding up the extraction and processing EEG signals, the sapling interval was adjusted to 1 s. But these modifications result in losing a few features. Therefore, the db4 wavelet is adjusted to two levels as well as additional one layer is added into hidden layer of LSTM and GRNN networks.

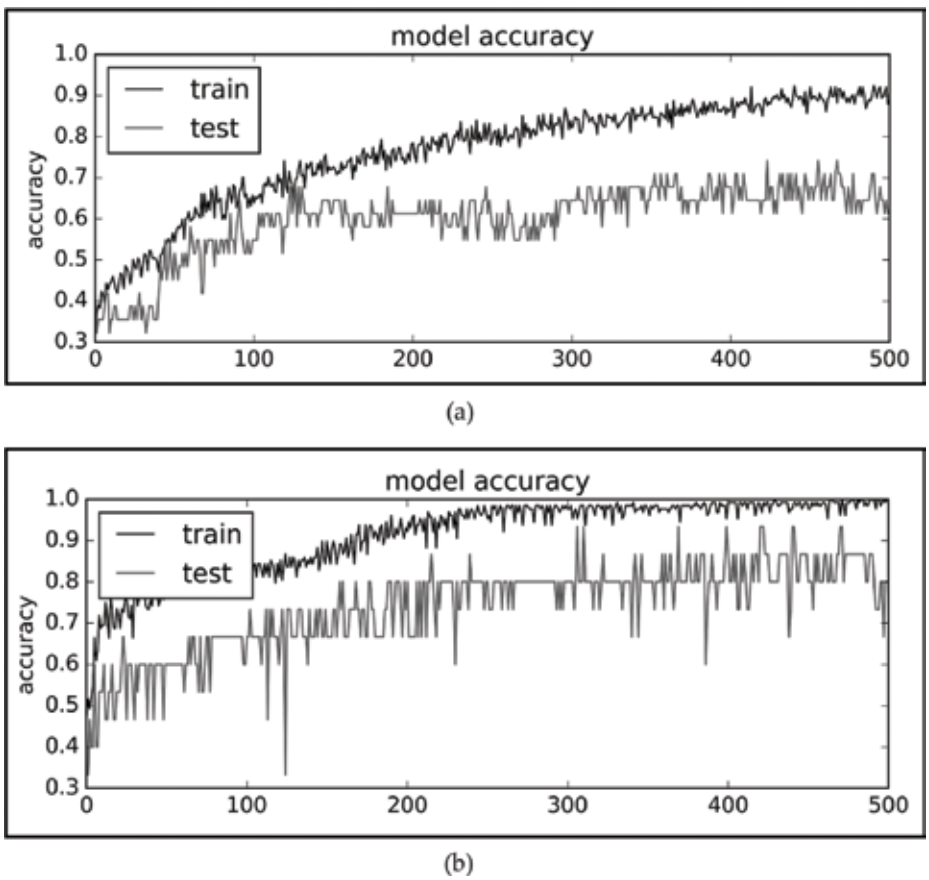

Figure 9. The accuracy rates in LSTM and GRNN with db4 wavelets and seven hidden layers. (a) LSTM. (b) GRNN.

Increasing the level number of DWT can directly reduce length of the EEG signals. If the db4 DWT is still used, the extracted signals will lose some features. Thus, reducing the DWT levels can retain more features in the original EEG signals. Increasing the number of hidden layers is due to the increased complexity of the input EEG signals. The more hidden layers are conducive to processing the data with higher complexity. However, too many hidden layers will cause the network to be difficult to converge during the learning process. In this section, additional one layer is added into hidden layer for obtaining better convergence properties. The classification accuracy rates for db4 wavelets by LSTM and GRNN networks with seven layers in hidden layer are shown in **Figure 9**, while the classification accuracy rates for db2 wavelets by LSTM and GRNN networks with eight layers in hidden layer are shown in **Figure 10**. From **Figures 9** and **10**, we can find that the accuracy rates of test data are obviously increased and nearby the accuracy rates of training data for both LSTM and GRNN networks.

Then, two BCI systems have respectively embedded LSTM and GRNN with db2 wavelets and eight hidden layers are applied to control an electric wheelchair. They can smoothly control an electric wheelchair and the GRNN model can always get better performance than the LSTM.

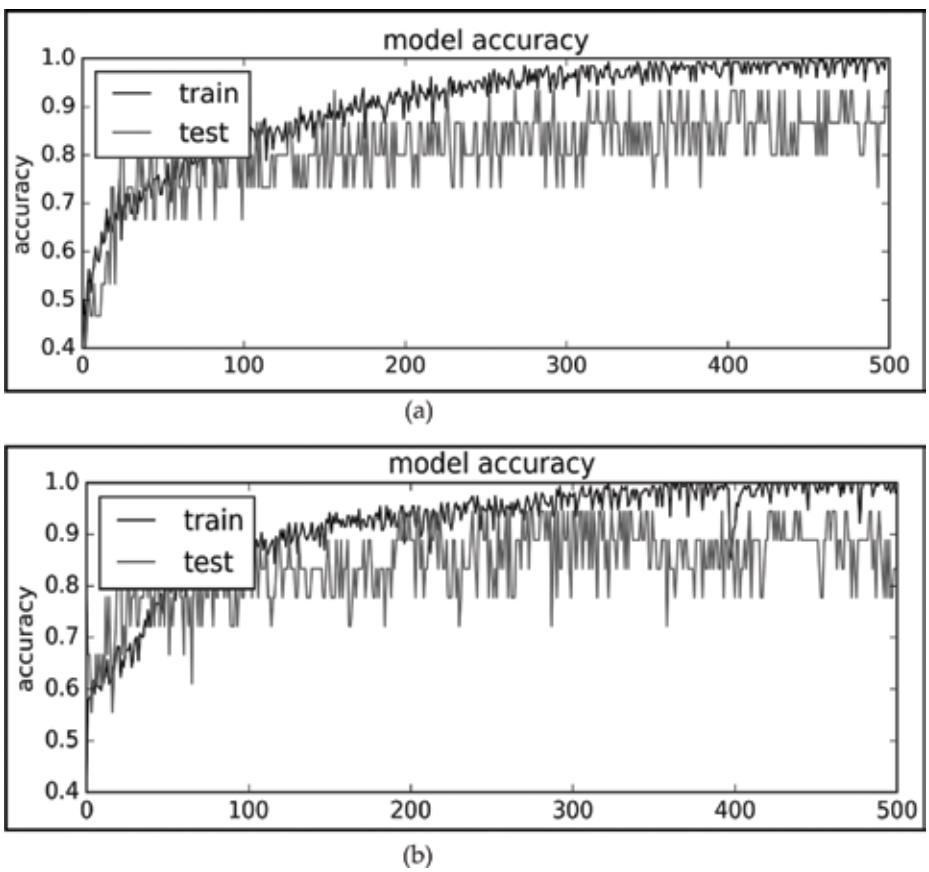

Figure 10. The accuracy rates in LSTM and GRNN with db2 wavelets and eight hidden layers. (a) LSTM. (b) GRNN.

8. Conclusions and future prospects

In this chapter, two deep-learning models named LSTM and GRNN were applied to be embedded into a BCI system for MI-EEG signal classification to identify two imagery movements such as imagining right-hand and left-hand actions. In the proposed BCI system, the Emotiv EPOC IC with tg.SAHARAbox system and g.SAHARA electrodes are used to capture MI-EEG signals on C3, Cz, and C4. In this chapter, we use the Daubechies wavelet to get feature values on db4 and db2 coefficients. The GRNN can make each recurrent unit to capture variable-length sequences adaptively. Modified from LSTM, the GRNN has gating units that modulate the flow of information inside the unit, but without having a separate memory cell. In the GRNN, the parameters at each level are shared through the whole network. From the experimental results, the GRNN can get better performance than other strategies. Additionally, the GRNN can always obtain better performance than the LSTM in the application to control an electric wheelchair.

Acknowledgements

In this chapter, the research was sponsored by the Ministry of Science and Technology of Taiwan under the Grant 106-2221-E-167-031.

Author details

Jzau-Sheng Lin * and Ray Shihb

*Address all correspondence to: jslin@ncut.edu.tw

Department of Computer Science and Information Engineering, National Chin-Yi University of Technology, Taiwan

References

[1] Decety J, Ingvar DH. Brain structures participating in mental simulation of motor behavior: A neuropsychological interpretation. Acta Psychologica. 1990;**73**:13-34

[2] Tomida N, Tanaka T, Ono S, Yamagishi M. Active data selection for motor imagery EEG classification. IEEE Transactions on Biomedical Engineering. 2015;**62**:458-467

[3] Baali H, Khorshidtalab A, Mesbah M, Salami MJE. Transform-based feature extraction approach for motor imagery tasks classification. Rehabilitation Devices and Systems. 2015;**3**:1-8. DOI 10.1109/JTEHM.2015.2485261

[4] Wu S-L, Liu Y-T, Hsieh T-Y, Lin Y-Y, Chen C-Y, Chuang C-H, Lin C-T. Fuzzy integral with particle swarm optimization for a motor-imagery-based brain computer interface. IEEE Transactions on Fuzzy Systems. 2016;**2016**. DOI: 10.1109/TFUZZ.2016.2598362

[5] Lin J-S, Lo C-H. Mental commands recognition on motor imagery-based brain computer Interface. International Journal of Computing, Consumer and Control. 2016;**25**:18-25

[6] Chatterjee R, Bandyopadhyay T. EEG based motor imagery classification using SVM and MLP. In: Proceeding of International Conference on Computational Intelligence and Networks; 2016. pp. 84-89

[7] Xie X, Yu ZL, Lu H, Gu Z, Li Y. Motor imagery classification based on bilinear sub-manifold learning of symmetric positive-definite matrices. IEEE Transactions on Neural Systems and Rehabilitation Engineering. 2016;**25**:504-516. DOI: 10.1109/TNSRE.2016.2587939

[8] Chatterjeel R, Bandyopadhyal T, Sanyal DK. Effects of wavelets on quality of features in motor imagery EEG signal classification. In: Proceedings of IEEE WiSPNET 2016 Conference; 2016. pp. 1346-1350

[9] Jois K, Garg R, Singh V, Darji A. Comparative analysis of classification techniques for motor imagery based BCI. IEEE Workshop on Computational Intelligence: Theories, Applications and Future Directions (WCI); 2015. DOI: 10.1109/WCI.2015.7495507

[10] Hinton GE, Salakhutdinov RR. Reducing the dimensionality of data with neural networks. Science. 2006;**313**(5786):504-507

[11] Bengio Y, Courville A, Vincent P. Representation learning: A review and new perspectives. IEEE Transactions on Pattern Analysis and Machine Intelligence. 2013;**35**:1798-1828

[12] Graves A. Supervised Sequence Labelling with Recurrent Neural Networks. Studies in Computational Intelligence. Cham Switzerland: Springer; 2012

[13] Graves A, Mohamed A-R, Hinton G. Speech recognition with deep recurrent neural networks. In: Proceedings of IEEE International Conference on Acoustics, Speech and Signal Processing; May, 2013

[14] Li N, Chen J, Cao H, Zhang B, Natarajan P. Applications of recurrent neural network language model in offline handwriting recognition and word spotting. In: Proceeding of 14th International Conference on Frontiers in Handwriting Recognition; 2014. pp. 134-139

[15] Moghadam SM, Seyyedsalehi SA. Nonlinear analysis of video images using deep recurrent auto-associative neural networks for facial understanding. In: Proceedings of 3rd International Conference on Pattern Recognition and Image Analysis; 2017. pp. 20-25

[16] Petrosian A, Prokhorov D, Homan R, Dasheiff R, Wunsch DII. Recurrent neural network based prediction of epileptic seizures in intra-and extracranial EEG. Neurocomputing. 2000;**30**(1):201-218

[17] Hochreiter S, Schmidhuber J. Long short-term memory. Neural Computation. 1997;**9**: 1735-1780

[18] Li M, Zhang M, Luo X, Yang J. Combined long short-term memory based network employing wavelet coefficients for MI-EEG recognition. In: Proceedings of IEEE International Conference on Mechatronics and Automation; Aug., Harbin, China; 2016. pp. 1971-1976

[19] Cho K, van Merrienboer B, Bahdanau D, Bengio Y. On the properties of neural machine translation: Encoder-decoder approaches. arXiv Preprint. 2014;**arXiv**:1409.1259

[20] Daubechies I. Orthonormal bases of compactly supported wavelets. Communications on Pure and Applied Mathematics. 1988;**41**:909-996

[21] Mallat S. A theory for multiresolution signal decomposition: The wavelet representation. IEEE Transactions on Pattern Analysis and Machine Intelligence. 1989;**11**:674-693

[22] Gers FA, Schmidhuber J. Recurrent nets that time and count. In: Proceedings of the IEEE-INNS-ENNS International Joint Conference on Neural Networks; 2000. pp. 189-194

[23] Smith L. Dynamic Systems, Sensorimotor Processes, and the Origins of Stability and Flexibility. In: Spencer J, Thomas MSC, McClelland JL, editors. Toward a Unified Theory of Development. Oxford: Oxford University Press; 2009

[24] Blankertz B, Müller KR, Curio G. The BCI Competition 2003: Progress and perspectives in detection and discrimination of EEG single trials. IEEE Transactions on Biomedical Engineering. 2004;**51**:1044-1051

Chapter 3

Rotation Invariant on Harris Interest Points for Exposing Image Region Duplication Forgery

Haitham Hasan Badi, Bassam Sabbri and Fitian Ajeel

Additional information is available at the end of the chapter

http://dx.doi.org/10.5772/intechopen.76332

Abstract

Nowadays, image forgery has become common because only an editing package software and a digital camera are required to counterfeit an image. Various fraud detection systems have been developed in accordance with the requirements of numerous applications and to address different types of image forgery. However, image fraud detection is a complicated process given that is necessary to identify the image processing tools used to counterfeit an image. Here, we describe recent developments in image fraud detection. Conventional techniques for detecting duplication forgeries have difficulty in detecting postprocessing falsification, such as grading and joint photographic expert group compression. This study proposes an algorithm that detects image falsification on the basis of Hessian features.

Keywords: copy-move detecting, doubled region, Harris pursuit point

1. Introduction

Brain-computer interface (BCI) technology provides a means of communication that allows individuals with severely impaired movement to communicate with assistive devices using the electroencephalogram (EEG) or other brain signals. The practicality of a BCI has been made by advances in multi-disciplinary areas of research related to neuroscience, brain-imaging techniques and human-computer interfaces. The end goal of a BCI is to enable monitoring of the underlying brain processes and subsequent utilization of this information for communicating and controlling devices solely through the brain without depending on the normal output pathways of peripheral nerves and muscles. Photographs capture reality. However, this belief no longer holds true in the current digital era given that the

manufacture of counterfeit images has increased [1]. The development of powerful photo editing software, such as Photoshop, has simplified the production of fake digital images [2]. A case of image counterfeiting is shown in **Figure 1**. Image forgery has severe consequences. For example, by modifying faces in an image, image counterfeiting can be applied to ruin a person's reputation. Academic documents may also include manipulated images that misrepresent experimental data. In addition, image forgery can be applied to remove a reference object from a standard image. As a result, the validity of the image can no longer be accepted [3]. These multilevel protection issues have different implications in different fields, such as detective work.

In simple terms, a brain-computer interface (BCI) is a direct interface between the human brain and an artificial system. Its purpose is to control the actuation of a device, say a robotic system or a wheelchair, with brain activity but without the use of peripheral nerves or muscles [4]. BCI in a literal sense means interfacing an individual's electrophysiological signals with a computer [5]. Thus, in a true sense, the BCI only uses signals from the brain and must consider eye and muscle movements as artifacts1 or noise. Information from various knowledge domains is necessary to create a complete BCI system. Thus, an artificial neural network (ANN) is an information-processing paradigm that is inspired by the way in which biological nervous systems, such as the brain, process information. This network is composed of a large number of highly interconnected processing elements referred to as neurons that work in unison to solve specific problems. Enhancing the noisy electroencephalogram (EEG) signal utilizes a layer of neurons in the spatial dimension within the neural network framework. The incoming noisy input signal sample is treated as a probability density function (pdf) by the layer of neurons and it recurrently evolves under the influence of the SWE and appropriate learning rules. This approach has made possible the development of an efficient computational algorithm referred to as the recurrent quantum neural network algorithm (RQNN) which to some extent has solved the complex problem under consideration. In general, two methods can be applied to detect image fraud: active and passive certification [6]. These two methods are illustrated in **Figure 2**. Active certification is categorized into two classes. The first class is based on the identification of a digital watermark. A watermark is hidden in the image at the end of capture, the detection program checks if the image certificate has been edited [7, 8]. The watermark is inserted when the image is taken using a specially equipped photographic camera or after acquisition by an expert [1]. The successive editing

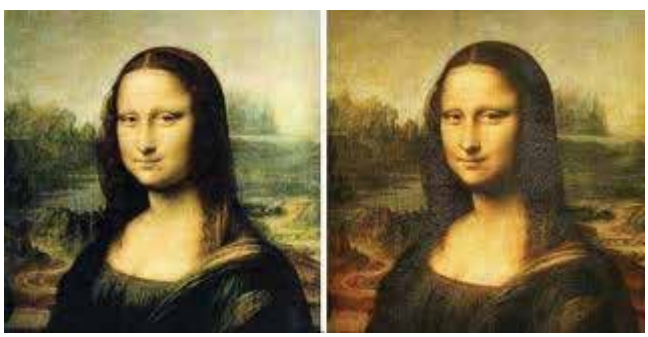

Figure 1. Image forgery has severe consequences.

http://dx.doi.org/10.5772/intechopen.76332

Figure 2. Detect image fraud: active and passive certification.

of the original image may degrade image quality. Passive certification methods are based on digital signatures. These methods identify the distinguishing characteristics of an image as a signature after image acquisition. At the end of certification, signatures are renewed in accordance with a similar method, and the genuineness of the image can be identified by comparison. Digital signatures and watermarks have similar disadvantages. Negative image certification, also referred to as forensic digital image certification, is highly practical. Digital image certification does not require extra information and is independent of the image theme [9]. Negative methods have two parts: (1) identification of the original edit and (2) detection of tampering [10]. Certification for the first class is based on digital fingerprint certification, effects allowed by image acquisition, and storage. The methods used in this class use the digital fingerprint of the camera to differentiate among similar or dissimilar camera models. The detection methods of passive falsification can either be false or independent. Fraud detection methods are employed in particular cases of counterfeiting, similar to making copies or linking images. To discover universal forgery, researchers use autonomous techniques and exploit three different types of artifacts: the effects of resampling, pressure, and contradictions [10]. The types of counterfeiting techniques can be categorized into two classes: copy-detecting technique (image forging) and image-binding technique (two-fold image-based counterfeiting).

2. Copy-move forgery detecting

The ease and effectiveness of counterfeiting facilitates its application in changing image content [11]. The important features, like the pallet and the active range, of replicated areas are compatible with the rest of the image given that these areas are obtained from the same image [12]. Nevertheless, in practice, counterfeiting may imply more than simple replication. Numerous image-editing processes may be applied in serious counterfeiting, as shown in **Figure 3**. The processes can be divided into two groups: intermediator processes and post-processes. Intermediator processes are applied to synchronicity and homogeneity between a replicated region and its neighbor [13]. Intermediator processes include rotation, scaling,

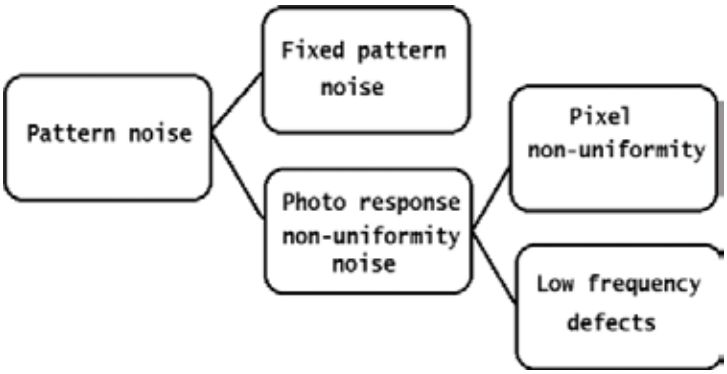

Figure 3. Image processing operations associated with image forgery.

reflection, lighting adjustment, or color adjustment. In serious cases, intermediator processes can be combined. Postprocesses, such as noise addition, joint photographic expert group (JPEG) compression, or blurring, can be applied to delete all retraces that can be detected in the copy process, such as sharp edges [2]. A broad range of easily available algorithms has been proposed to detect replicated images and functions, as shown in **Figure 4**.

To detect image forgery, an image is first selected (e.g., converted to gray scale). The image is divided into an auction block of nested pixels. The size of the image *m_n*, size of block *B*, and the number of overlapping blocks is given by:

$$\text{No of blocks} = (m - k + 1) \times (n - k + 1) \tag{1}$$

The vector is an extractable characteristic in each block. The vector-matching function is highly similar to pairing functions. Known pairing methods include the arrangement of miracle dictionaries on the element vectors and the identification of the nearest neighbor in the tree *Kd*. The similarity between two attributes can be determined on the basis of similarities between different parameters, such as Euclidean length. In the verification step, extreme values are suppressed and holes are filled up through a basic filtration step, such as morphing.

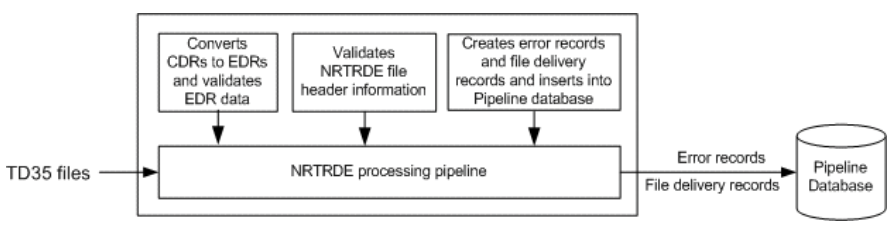

Figure 4. Pipeline of a fraud detection algorithm.

http://dx.doi.org/10.5772/intechopen.76332

3. Copy-move detecting algorithm

Numerous articles on the negative detection of displacement in images have been and continue to be published. Existing methods for displacement detection are primarily distinguished on the basis of the case and sizing of the function applied to match the image block. This article classifies existing methods in accordance with the extracted properties applied to test block similarities. In the following sections, different cases or classes of detection algorithms are presented.

3.1. Algorithm based on invariant keypoints

In contrast to other algorithms, this algorithm does not divide the image into auction blocks to extract features but instead extracts features from the intact image. Feature extraction is performed with SIFT and speeded-up robust feature (SURF). This technique is applied to derive the characteristic local feature of an image and produce a keypoint in accordance with preset requirements. The vector sum/descry values are fixed for rotational, translational, and scale measurements and are partially fixed for strong illumination changes in local geometric distortion [14, 15]. The first attempt to exploit this algorithm was reported by [16]. In the algorithms, only the correspondence of the keypoint can be achieved by its maximum bin, including the identity of the nearest neighbor [17]. SIFT has been adopted to identify replicated regions in a counterfeit image. The SIFT signifier is applied to detect copied areas by coping with keypoints rather than clusters. This algorithm has excellent detection accuracy but otherwise poor performance.

3.1.1. SIFT algorithm

He proposed the SIFT algorithm, which could be used to detect and evaluate the geometrical shifts applied to forged displacement copy-and-paste images. The detection procedure involves three steps: In the first step, SIFT functions are extracted and main points are associated. The second step is committed to keypoint compilation and fraud detection. The third step estimates the engineering shifts, if any, that occurred. SIFT can be executed under the conditions of eminent real rate (TPR) and abject fake positive degree ratio (FRE), JPEG compression, and additional noise. In addition, SIFT can accurately estimate different arguments for affine transmutation. **Figure 5** shows different arguments for affine transmutation.

The first attempts to take advantage of SIFT have been reported in [16]. In SIFT, the correspondence of the key indicator is achieved by first identifying the neighbor closest to the best bin [17]. SIFT has been adopted to identify a single copy in the counterfeit image. SIFT descriptors are usually applied to identify keypoints of copied areas instead of blocks, whereas other algorithms cope with object indicators. Although SIFT exhibits excellent detection performance, its false–positive rate remains unknown. In [18], the main SIFT points were extracted from the image and were then associated to obtain the corresponding keypoints. A vote scheme based on vector direction was applied to distinguish between origin and direction. Then, an

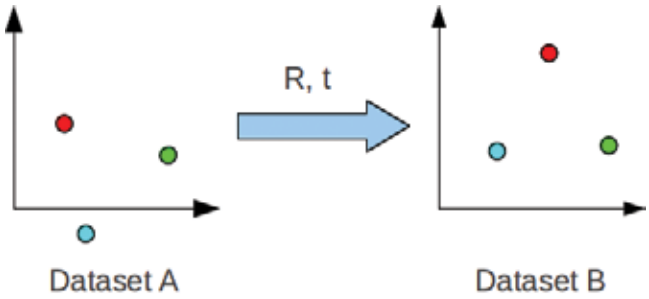

Figure 5. Different arguments for affine transmutation.

efficient two-fold sub-window search algorithm (EES) was used to locate duplicated areas within the border box. Finally, a pixelwise partition was identified. The experiment solutions demonstrated that the proposed algorithm remains robust even with background noise and engineering manipulation [19]. He suggested a SIFT algorithm that could detect and then estimate the geometrical transformation applied to forge displacement copy-and-paste images. The detection process involves three steps. In the first step, the SIFT function is extracted and corresponding keypoints are identified. The second step involves the consolidation and detection of fraud. The third step identifies changes that occurred. SIFT has high positive identification rate and low false positive rate even under JPEG image compression and added noise conditions. In addition, it accurately estimates several affine transformation parameters. Refs. [20, 21] suggested a SIFT-established detecting algorithm that can be used to estimate the geometrical transformation applied to the copy. The algorithm begins by converting the suspected image into grayscale. SIFT is then applied to collect image characteristics for the detection of keypoint sources. In SIFT, the keypoint sources are initially adapted in accordance with the characteristics of the vector sum used in the better bin-first algorithms. The potential geomagnetic distortion of the refined areas is estimated on the basis of the assumed paired keypoints by applying RANSACK. SIFT is more robust than intermediary processes even when JPEG compression or noise are added to the processed image. Furthermore, affine transformation is exactly estimated, particularly in larger duplicated areas. A different scenario is to integrate SIFT into copy detection systems [22]. Instead of applying SIFT to detect keypoints, the Harris quicker from SIFT is applied. After all keypoints are revealed, SIFT is applied to generate the descriptive characteristics of extracted features. Then, the *Kd* trees algorithms are applied to match the keypoints to identify duplicated areas. The algorithms can effectively detect copied areas, such as unrotated scanlines or Gaussian noise conditions, that have undergone transformation [5, 22]. Harris detection, which is quicker than SIFT, has been used to detect keypoints. After keypoint detection, SIFT is applied to identify a unique characteristic from extracted keypoints. The *Kd* tree algorithm is then applied to match keypoints to determine duplicate areas. This algorithm can efficiently detect areas, such as scanlines, that have undergone transformation.

3.1.2. SURF algorithm

SURF has been adopted to detect image editing processes, such as rotation and gradation. SURF is superior to SIFT in detecting image strengths and performs as well as SIFT. The

http://dx.doi.org/10.5772/intechopen.76332

complicated automatic reinstallation of duplicate areas hinders the practical applications of these algorithms. We propose a novel algorithm for the detection and description of scale and constant rotation in images. The algorithm is based on SURF and thus has powerful acceleration functions. SURF approximates or even exceeds the proposed thresholds for redundancy, excellence, and sustainability and rapidly performs calculation and comparison. This operation is performed by relying on image confluence. The exit detection and prescriptive prescriptions are based on their strengths (if a Hessian scale is used to detect and describe the established distribution), and kernel methods are simplified to allow the combination of new detection, description, and correspondence. Correspondence between two images of the same view and the objective is partly achieved by using many computers. In this study, photography, three-dimensional reconstruction, image recording, and objective recoding were conducted. The search for a separate image match—the purpose of our research—can be separated into three principal steps. First, points of interest are specified in the characteristic locations of the image, such as angles, points, and plus T-intersections. The most important property of a detection method is its repeatability, that is, its reliability in finding similar indicators of interest under different conditions. Then, each point of interest is represented by a transmitter characteristic. This description must be distinct and must have similar time strengths under noise conditions, mistake detection, and geometrical and photometrical distortions. Finally, vector descriptors are adapted in different images. Correspondence is based on vector distance. Descriptor size directly affects computational time. Thus, fewer dimensions are desired. We aimed to develop an algorithm for the detection and the identification of fraud. We compared the performance of our proposed algorithm with that of a state-of-the-art detection algorithm. Our algorithm exhibits computational time and robust performance. Downsizing after description and complexity must be balanced while providing sufficient distinction. Various detection and description algorithms have been proposed in the literature (e.g., [1–3, 6, 7, 23]). Furthermore, detailed datasets for comparison and standard assessment have been established [8–10]. We build upon the knowledge gained from previous work to better understand the aspects that contribute to algorithm performance. When used in experiments on standard image sets, as well in the application of actual objective recognition, the algorithm exhibited rapid detection and description, as well as distinctive and reproducible performance. While working with local features, stability is the first issue that requires resolution and depends on the expectation of geometrical and photometrical distortions. This turn of events is identified by the possibility changing in conditioning. We concentrate on the detectors and constant descriptions of the balance and rotation of the image. These detectors offer better compromises among the complexity of the functionality and the durability of the distortions that usually occur. The discrepancy and gradient of anomalies and the effects of perspective are secondary to the effect covered by the overall durability of the description [2]. The additional complexity of affine invariance negatively affects sustainability, unless significant changes are anticipated. In some cases, even analog rotation can be abandoned with solutions in a fixed static version of our description. We refer to this ability as "erect SURF" (U-SURF). In fact, in some applications, such as cell robotic navigation or visual guidance, the camera often only revolves around the vertex. Taking advantage of avoidance of the exaggerated stability of rotation in similar events not only increases speed but also increases discriminatory force. As for the photometric, we assumed a simple linear accelerator example with a scaled factor and displacement. Note that our detection and description do not apply color.

4. Related work

The most commonly used detection method is the Harris-cornered method [24], which was proposed in 1988. It is based on the intrinsic values of the secondary-momentary matrix. However, Harris angles are not fixed. The Lindberg detection method introduces the principle of automatic scaled selection [1], which allows the detection of a full point of interest in an image together with its scope. He experimented with the Hessian matrix operation identifier and Laplacian (corresponding to the Hessian matrix operation effect) to detect bulb structure. The detectors, which were developed by Harris-Laplace and Hessian-Laplace, are robust and stable with high reproducibility [25]. The Harris (Adaptive Scale) or the Hessian Matrix Locator and Laplacian have been applied to determine scale. Focusing on speed, [26] estimates Laplace Gaussians (LoG) on the basis of the candidate Gauss (DoG). Several fixed-interest rate detectors that increase the entropy in the area and the edged-based zone detection have been proposed [11]. Nevertheless, these detectors are inflexible. Several detection methods have been proposed for fixed properties that can adapt to long-term changes but are not discussed in this article. A review of the literature [9, 12] shows that (1) Harris-based detection methods are stable and replicable. The use of a specific Hessian matrix addition instead of its effect (the Laplacians) is useful because fires occur less on elongated and nonlocal structures. In addition, (2) an approximation, such as DoG, has low-cost computational speed and low loss of precision. A wider set of attribute descriptions has been suggested, such as the Gaussian-derived function [13], a fixed moment [27], complex feature [4, 28], guiding filters [29], and phase-localized functions [30], to represent the distribution of small features in a region of interest. The latter [2] has been shown to surpass the others [8] because they capture a basic quantity of information on the special intensity of level models when large to small deformations or localization mistakes occur. In [2], SIFT has been applied as a general level gradient diagram around the indicator of interest and is stored in boxes in a 128-dimension vector (eight routing boxes for each 4 × 4 box). Various improvements have been proposed on this basic scheme [3]. PCA has been applied to slope images. These operations (PCA, SIFT) provide a 36-dimension characteristic that is rapidly harmonized but is less distinct from SIFT in terms of secondary comparison [9]. The slow calculation function reduces the impact of quick coping. In similar papers [9], the authors suggested a variation on SIFT, named GLOH, which proved to be more distinct with the same dimensional count. However, GLOH is computationally expensive. SIFT is the most attractive for practical application and is currently the most widely applied algorithm. It is distinct and relatively quick, which is crucial for online applications. Recently, [31] used a field-programmable area grid to improve its order of magnitude relation. However, the height dimensions of the descriptions in SIFT are defective when compared with those of corresponding methods. For online applications on an ordinary computer, each of the three steps (detection, description, and correspondence) must be fast. Alternatively, best-bin-first [2] accelerates computation but provides inaccurate solutions. A novel detection method based on SURF has been proposed by [1, 25]. However, basic approximation was applied because DoG [2] is a basic Laplacian-based detector. Given that it depends on the embedded image to reduce computing time, we designated this algorithm as the "Quick Hessian" detector. Description, on the other hand, describes the distribution of the Haar-wavelength reactions in the area of interest. We operate the built-in speed images repeatedly. In addition, only 64

http://dx.doi.org/10.5772/intechopen.76332

dimensions are used, thus decreasing the calculation time of the corresponding characteristic and simultaneously increasing durability. We again propose a new index step based on the Laplacian marker. This step accelerates correspondence and increases the robustness of the description. To illustrate the self-sufficiency of the algorithm, we briefly discussed the conception of an integrated image, as defined in [32]. It allows the quick execution of filter to wrap a box type. The insertion of an integrated image IΣ (z) into $x = (z, y)$ represents the amount of all the pixels of the income I of a rectangularity area formed by the z and the origin.

$$I_{\Sigma}(\mathbf{x}) = \sum_{i=0}^{i \leq x} \sum_{j=0}^{j \leq y} I(i, j) \tag{2}$$

The calculated IΣ only requires four additions to calculate the total intensity on any vertical and rectangular surface, regardless of its shape.

5. Quick-Hessian detection

We based our detection method on Hessian matrix addition because of its superior calculation time and accuracy. Therefore, instead of using an applied range to select position and scale (as in the Hessian-Laplace [25]), we used a Hessian identifier for both. Given the indicators $z = (z, y)$ in **Figure 1**, the matrix Hessian H (z, σ) in x is defined on the scale as follows.

$$\mathcal{H}(\mathbf{x}, \sigma) = \begin{bmatrix} L_{xx}(\mathbf{x}, \sigma) & L_{xy}(\mathbf{x}, \sigma) \\ L_{xy}(\mathbf{x}, \sigma) & L_{yy}(\mathbf{x}, \sigma) \end{bmatrix}, \tag{3}$$

where, similar to L,zy(z, σ) and L,yy(z, σ), L,zz(z, σ) is the rotation of the Gaussian second-order differential ∂2 ∂,z2 g(σ) with the image I in indicator z. Gaussian analysis has been optimized for large-scale analysis, as shown in [33]. However, in practice, Gaussian analysis should be reduced (**Figure 1** of the allowed half) because filtering Gaussians with aliases will result in image subsamples. In addition, a property that cannot show new structures when resolutions are decreased has been proven in one-dimensional images and cannot be applied in two-dimensional images [34]. Thus, the importance of the Gaussian filter may have been exaggerated in this respect, and here we test a simple alternation. Given that the Gaussian filter is not idealistic in any event because of the success of the LoG with the approximations of the newspaper, we push the rounding with the filters of the box (**Figure 6** on the right). These approximate Gaussian second-class derivatives can be rapidly evaluated with an integrated image irrespective of size. It can be evaluated very quickly using embedded images regardless of size. The algorithm's performance is similar to that used for esterized crops and Gaussians.

When applied to rectangular areas, SURF remains simple and arithmetically efficient. However, we need additional relative weight in equilibrium. This weight is specifically expressed with

$$\frac{|L_{xy}(1.2)|_F |D_{xx}(9)|_F}{|L_{xx}(1.2)|_F |D_{xy}(9)|_F} = 0.912... \simeq 0.9, \tag{4}$$

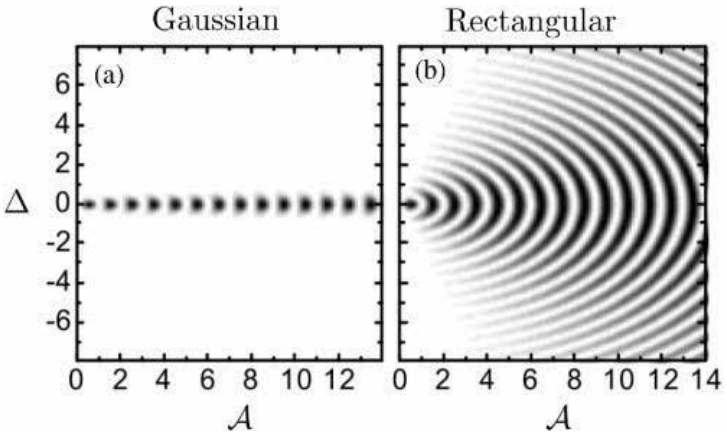

Figure 6. Left to right: (intact and trimmed) Gaussian secondary arrangement partly derived in the *y*-direction and *zy*-direction, and our approximation of the applied box filter. Gray areas are null.

where |z|F is the Frobenius norm.

$$\text{let}(\mathcal{H}_{\text{approx}}) = D_{xx}D_{yy} - (0.9D_{xy})^2. \tag{5}$$

In addition, the responses to the filters are normalized to mask size to ensure that the continuous Frobenius is standard for any filter size. In an image, space generally takes the form of a triangle. The image is repeated with a Gaussian filter and subsamples to reach the apex of the triangle. Given the application of box filter and plot image, we do not duplicate the filtering to output a previous filter layer. Nevertheless, filters of any size can be used at the same speeds when applied to the original image (even parallel to the latitude, if not used here). Therefore, size spacing is analyzed by increasing filter size rather than decreasing image size. The output of the 9 × 9 filters above is considered as the primary gauge level. Thus, scaling s = 1.20 (corresponding to the derivate Gaussian with σ = 1.20). The following levels are obtained by filtering the image with a progressively larger mask, taking into account the distinct nature of the integrated image and the specific structure of our filter. Specifically, this phenomenon leads to sizes 9 × 9, 15 × 15, 21 × 21, and 27 × 27. On a large scale, the increment in filter size must also vary accordingly. Thus, for each new Octavian, the volume of the filter doubles from 6 to 12 to 24. At the same time, sampling periods can be doubled to enable the extraction of points of interest. Given that our filter arrangement ratios remain constant after expansion, the bypass scale is approximately matched. For example, 27 × 27 filters correspond to σ = 3 × 1, 2 = 3, 6 = s. Moreover, given that the Frobenius base remains constant in our filtering, they soon normalize [35]. To locate points of interest in the image and the scaling, maximizing suppression is not applied on the 3 × 3 × 3 neighbor. The maximum limit for the Hessian matrix is then encountered in the range and proposed spacing of the image [36]. The spatial interpolation scale is particularly important in our case, and the difference in size among the first levels of each Octavian is relatively large.

http://dx.doi.org/10.5772/intechopen.76332

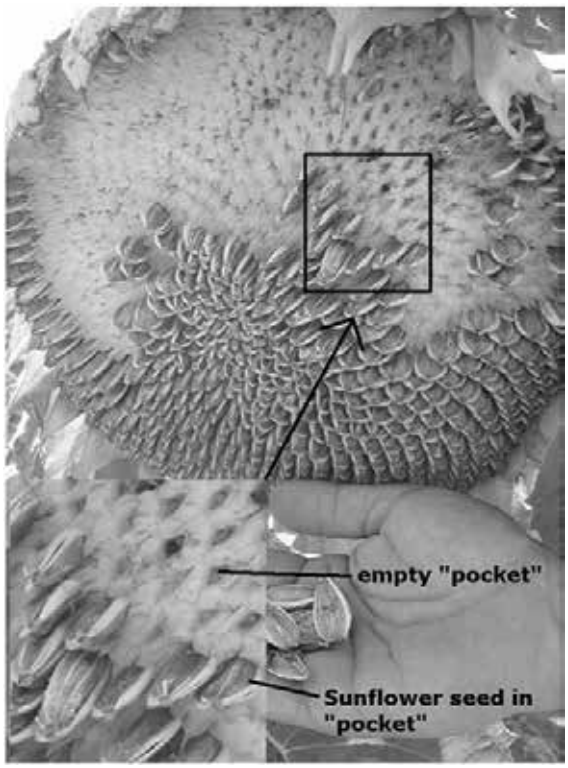

Figure 7. Left: points of interest detected in an image of a sunflower field.

This view clearly shows the Hessian-detecting characteristics. Medium: Warp types applied in SURF. Right: Image of graffiti showing the size of the window descriptors on different scales.

The first levels of each Octavian are relatively large. **Figure 7** (left) shows the points of interest detected when quick-Hessian detection is applied.

6. SURF description

The superior performance of SIFT compared with that of other [9] benchmarks is remarkable. Their mixing with local informatics and the distribution of gradient-related characteristics provide fine characteristic resistance that mitigates the effect of settlement faults in terms of size or surface area. The application of relative resistance and gradient directions decreases the effect of illumination changes. The proposed SURF descriptor is based on similar properties, further complicating the process. The first step is to identify a direction that can be reproduced from data from a circular area surrounding the indicator of interest. Next, we

construct a square area aligned with a specific orientation and extract the description from it. In addition, we also offer a vertical version number of our descriptor (U-SURF), which is not fixed for in image rotation and rapidly calculates and improves camera location.

6.1. Orientation assignments

To fix the rotation, we define a reproducibility orientation for points of interest. To this end, we first compute the Haars wavefunction that corresponds to the X and Y direction. It is located in a boundary with a radius vector 7 s surrounding the indicator of interest, with the image being detected as the point of interest. The sampling step depends on the scale and its selection is s. Wavelet responses are also computed in the current range s. Thus, the size of the wavelet on a large scale is also large. We therefore use the integrated image as a quick filter. Only seven operations are required for SURF to calculate the corresponding Z or Y direction at any scale. The lateral distance of the wavelength is 4 s. Once the responses are calculated and weighed with Gaussians (σ = 2.51 s) centered around the indicators of interest, the responses are represented as vectors in range with the horizontal angle corresponding to force alongside the output and the vertical angle corresponded to the force along the coordinate. The trend is estimated by calculating the amount of all responses in navigation windows with an angle of π 3.1. The horizontal and vertical angle responses are summarized in the windows. The synthesized questionnaires then produce new vectors. The long vectors of its kind are directed towards the indicator of interest. The range of the slide windows is the argument, which was chosen empirically. Smaller sizes focus on one dominant, maximizing yield size in vectorial lengths that are not expressive. Both lead to an unstable trend in the area of interest. Note that U-SURF skips over this step.

6.2. Description component

To extract a description, a window centered around the indicator of interest must be constructed. The area must be oriented in the direction specified in the previous section. This transformation is unnecessary for a vertical copy. The size of this window is 20 s. The area is regularly divided into small 4 × 4 subregions to preserve crucial data in each subregion. We calculate some simple characteristics in a 5 × 5 regularized subregion. For simplification, we designated the DEX response waveform Haars in the horizontal direction and colored the prepared Haars corresponding to the vertical angle direction (2S filters size). Here, the terms "horizontal" and "vertical" are defined with respect to the orientation of the specified point of interest. To increase robustness to geometrical distortions and localization faults, the DEX and dy responses are first weighted with a Gaussian (σ = 3.4 s) centered around the indicator of interest. Then, the wavelength and dz. and dy wavelet responses are summarized above each subregion and are the first place of inputs in the vectorial function. To provide data on changes in polarity density, we also extract total absolute value for the replay of |dz| and |dy|. Thus, each sub region has a four-dimensional descriptor for the underlying intentional structure that leads to a vectorial description of all 4 × 4 sub regions of distance 64. Wavelength response is constant to polarize the illuminated "offset." Contrast (factor range) is obtained by converting the description into a vector unit. The characteristics of three different image

intensities in a subregion. Imaging groups of these general density models can be applied to produce a distinct description. To access the SURF descriptor, we experimented by subtracting and adding waves, applying d2z and d2y, adding first-order waves, applying PCA, and identifying the intermediate and average values. From a comprehensive evaluation, the outer part performs best among all parts (**Figure 8**).

$$\mathbf{v} = (\sum d_x, \sum d_y, \sum |d_x|, \sum |d_y|) \tag{6}$$

Left: the state of a homogeneous zone. All values are relatively small. Center: in the presence of frequency in the direction of z, the value $\sum |d_x|$ increases but remains low. If the density increases progressively in the direction of x, the two values $\sum d_x$ and $\sum |d_x|$ increase.

We change the sampling count for indicators and subfields. A sampling subregion of 4 × 4 provides good results. Given the fine divisions, it appears to be less powerful, significantly increasing the timing of correspondence. In other methods, the shortage circuit with 3 × 3 subregions (SURV-35) provides poor results but allows for rapid computation e and is relatively acceptable compared with other descriptors in the literature. **Figure 9** shows just some of the compared results (SURV-126 will be explained soon).

The two different match strategy tests performed on the "Graffiti" image with width changes of 30 points from the current description. Points of interest are calculated through the "Quick Hessian" detection method. Note that rates are unfixed per affine. Therefore, the results are not identical to those of [9]. Surf-126 corresponds to the expanded description. Left: similarity between threshold element and match strategy. Right: strategy for closer contact.

We test another section of the SURF descriptor by adding two similar characteristics (SURV-126). It repeatedly uses the same quantities as before but has additional divisors. The values of dz and |dz| are calculated individually for dy < 0 and dy ≥ 0. Likewise, the values of dy and |dy| are separate and agree with the signal of dz, thereby duplicating the count of the feature. Description is more distinct and does not require long computation time. However, matching time is slow because of the high dimensions of the features. The argument choice is equated for the "Graffiti" sequence [9] because it contains out-of-play rotation in the rotation map, as well illumination changes. The general description of 4 × 4 sub regions (SURF-126) improves

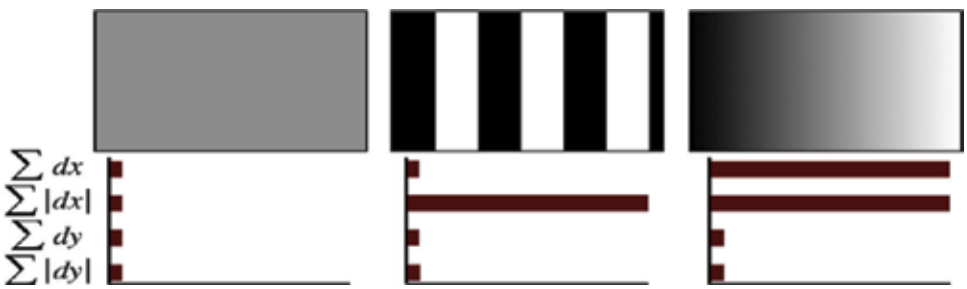

Figure 8. Descriptive entries for a subregion representing the universal base density model.

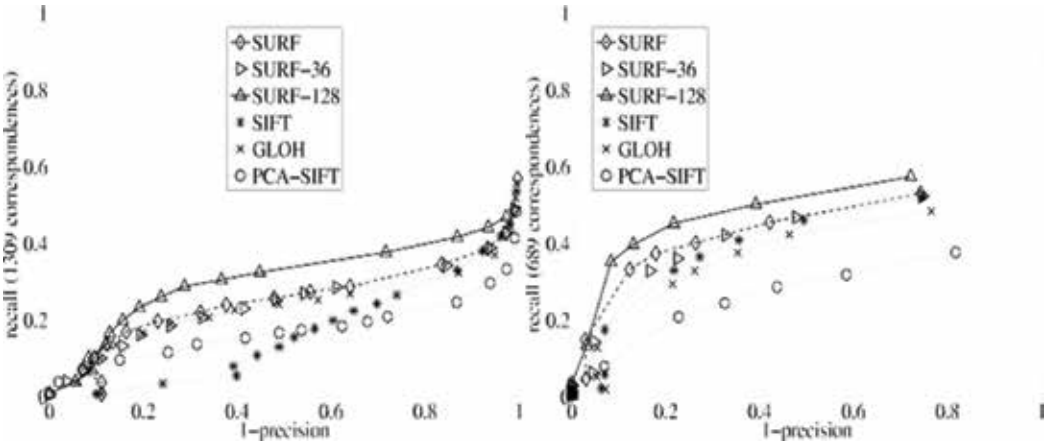

Figure 9. Line graphs for different methods.

performance. In addition, SURF has excellent performance that surpasses that of the latest state-of-the-art algorithm. To provide an index of the pairing phase, Laplacian signs (i.e., the Hessian matrix effect) are included for the basic point of interest. Typically, the points of interest are in plug-type structures. The label marks luminous points on the darker background of the reversed situation. This functionality is available at an additional price, which has already been calculated throughout the detecting process. During matching, we compare the feature only if they have the similar contrast types. Thus, this minimum data speeds up matching and improves performance.

7. Experimental results

We provide solutions for a standard evaluation set without detection and description. Then, we discuss the solutions obtained during when applying the algorithm to apply the real object. All detectors and descriptions are based on comparison with the original application of the authorizer. In standard evaluation, we test our detectors and describe the applied sequence of images and software tests. The test set included images of actual, narrow, and structured scenes. Given the limited page count of this manuscript, we cannot provide the results of all sequences. To compare the performances of the detectors, we selected images with changes in perspective (Graffiti and Wall), magnification and rotation (Boats), and illumination (Leuven). Test notes for all sequences are presented in addition to the base sequence. We applied the degree of repetition, as described in [10], to detect the number of points of interest in two images relative to the indicator of interest (which is only the visible part of both images). The performance of the detection algorithm was compared with that of the Gaussian (DOG) [2], Harris, and Hessian Laplace [12] algorithms. All algorithms provided similar number of points of interest. This finding applies to all images, including the database used in the object recognition experiment (see **Table 1** for an example). In addition,

Detecting	Threshold	Nb of indicators	Compu. time (ms)
Quick Hessian	601	1417	119
Hessian-Laplace	900	1980	651
Harris-Laplace	2400	1665	1799
DoG	Default	1521	401

Table 1. Threshold element, numbers of points detected, and computational time (the first image of the graffiti sequence, 900 × 640).

the computational speed of our Quick Hessian detector was more than three times faster than that of DOG and five times quicker than that of Hessian Laplace. At certain timepoints, the repetitions of our detector approximated (Graffiti, Leuven, Boat) or exceeded (Walls) that of the competition. The Graffiti and Walls sequences contained out-of-play gyration, and solutions in affine contortions when the detection compared only gyration and were scaled invariantly. Therefore, distortions must be addressed through the overall durability of features. The descriptors were evaluated by the applied call diagrams (1 precisely) in [3, 9]. In each evaluation, we applied the first and fourth images of the sequence, except for the Graffiti image and the Walls scenario. The corresponding perspective change was 30 and 50 points., we compared our SURF signifier (GLOH0, SIFT, and PCA-SIFT) with our "Quick Hessian" detector. SURF outperformed the other signifiers in almost all tests. In **Figure 4**, we equated the solutions applied to two different corresponding techniques—one established on the same threshold element and one founded on the closest neighbor proportion (see [9] for a discussion of this technique). This phenomenon affected the order of descriptors but SURF performance is better in both events because of limited spacing. However, the only solutions on likeness similar to the similarity threshold are shown in **Figure 7** because this technique is most appropriate for representing the runner distribution in its advantage spacing [9] and used more routinely. SURF descriptor is systematically and extensively superior to other descriptors and exhibited 11% improvement. Its computational time is rapid (**Table 2**). The microprocessor (Surf-126) seems to be slightly superior to the general SURF system. However, its matching process was slow. Thus, it may be unsuitable for applications that require speed. Object recognition was performed under a similar set of standards and threshold element (**Table 1**). The moment was evaluated on a standard Unix computer (Pentium IV, 2.5GHZ). The objects are recognized because we experienced new

	U-SURF	SURF	SURF-126	SIFT
Time (ms)	254	355	390	1035

The threshold element is adjusted to detect the same number of indicators of interest for all methods. The relatively shorter calculation time also represents the other image.

Table 2. Calculation time for common detectors—descriptive applications, testing on the first image of the Graffiti sequence.

Figure 10. Example images of the reference group (left) and the test group (right). Note the difference in perspective and colors.

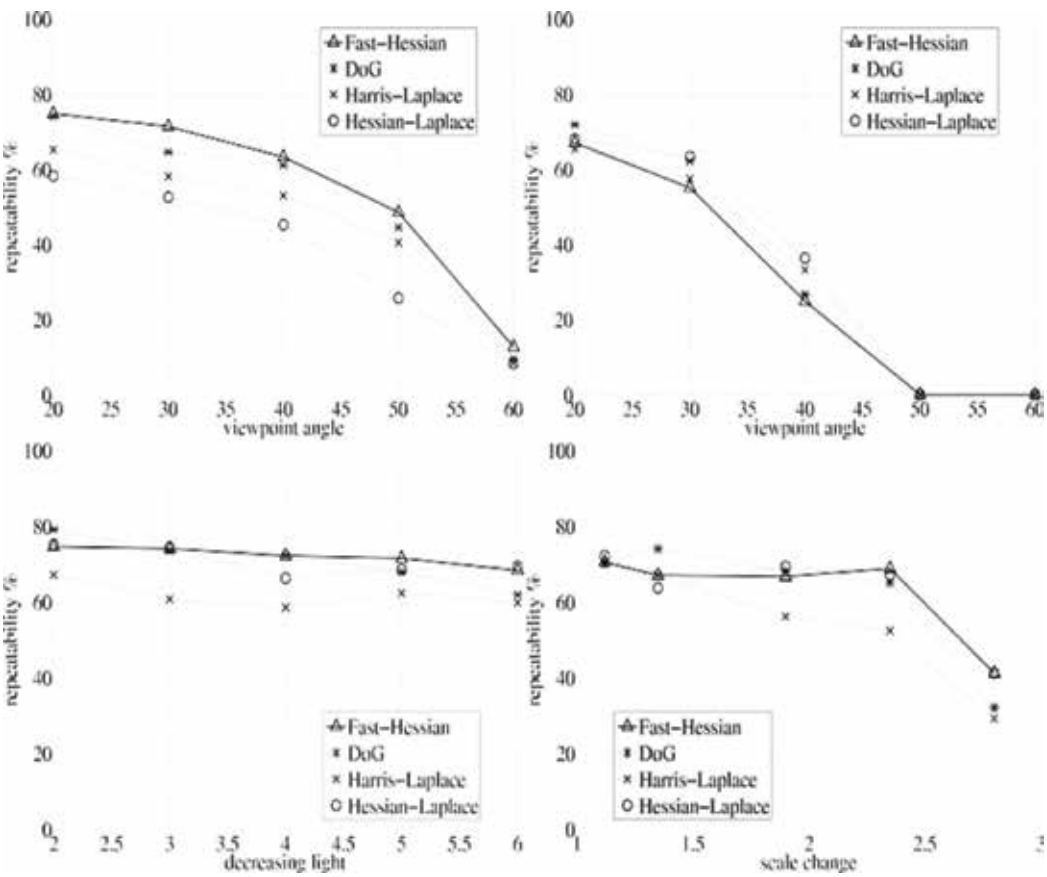

Figure 11. Left to right and from top to bottom: Frequency of Walls-Graffiti (perspective change), Leuven (illumination change), and Boats (magnification and rotation).

functionalities on the practical application, aiming to identify the art object in the museum. The data consisted of 216 images of 22 objects. The test group images comprised 116 images.

Under different conditions, including extreme illumination changes, object reflections in glass cabinetry, changes in perspective, magnification, and differences in camera quality, images are small (319 × 240) and difficult to recognize because they lose detail. To identify the objects in the database management, we proceed as follows: The images of the test group are compared with all the images of the reference group by associating their respective indicators of interest. The object represented on the reference image is selected with the greatest amount of correspondence with respect to the test image as a recognized object. Correspondence is performed as follows: A perspective of interest in the test image is compared with a perspective of interest in the referenced image by computing the value of Euclidean space between the vector and its descriptors. A corresponding pair is detected if the vision distance is closer by 0.6 times than that from the closest neighbor to the second. It is the closest strategy that corresponds to the ratio of the neighbors [2, 8, 27]. Extra engineering restrictions reduced the impact of false-positive matching, and this can be performed over any situation. For comparative reasoning, this does not make sense because it may be hiding the lack of the basic tables. On average, the rating reflection of the solutions of our performed appraisal is established. The leaders are SURF-126 with a recognizability rate of 85.7%, followed by U-SURF (84.8%), and SURF (83.7%). The other descriptors were 78.4% for GLOH, 78.2% for SIFT, and 72.3% for PCA-SIFT (**Figures 10** and **11**).

8. Discussion and conclusions

A brain-computer interface (BCI) is a direct interface between the human brain and an artificial system. Its purpose is to control the actuation of a device.

Many researchers have proposed modern algorithms to solve the problem of image authentication. This study explored and compared the application of different algorithms that detect common types of image forgery. The characteristics of the algorithms are shown in **Table 2**. The algorithms we examined in this study are undoubtedly important for the detection of image counterfeiting. Previous researchers have attempted to improve the reliability of image fraud detection algorithms. They have achieved this objective by (1) reducing algorithm complexity and computational time. This objective was achieved by using small vector dimensions, as shown in Refs. [18, 37–41] increasing the robustness of the algorithms. This aim was achieved by adopting a powerful feature that is consistent for a wide range of image processes, as shown in Refs. [42–48]. The algorithm based on fixed key indicators and fixed instances exhibits remarkable performance, as shown in **Table 2**. However, several barriers and challenges remain. We summarize the defects of available algorithms in **Tables 1** and **2**: (1) the algorithms cannot handle all possible types of image processing that can be applied to forge images; (2) some algorithms rely heavily on several threshold elements or initial value, and the identification of these threshold elements and values require experimentation and improvements; and (3)

most current methods take time [49, 50]. The development of complex and reliable algorithms that quickly and rapidly detect image forgery has been proposed. However, future work must overcome the following challenges: (1) the lack of standardized datasets for false counterfeiting limits the comparability and reproduction of existing algorithms, as well the design of improved algorithms and (2) the lack of common quantitative methods for measuring and evaluating algorithm performance prevents the comparison of different algorithms under different conditions. We believe that this reason accounts for the absence of studies that compare

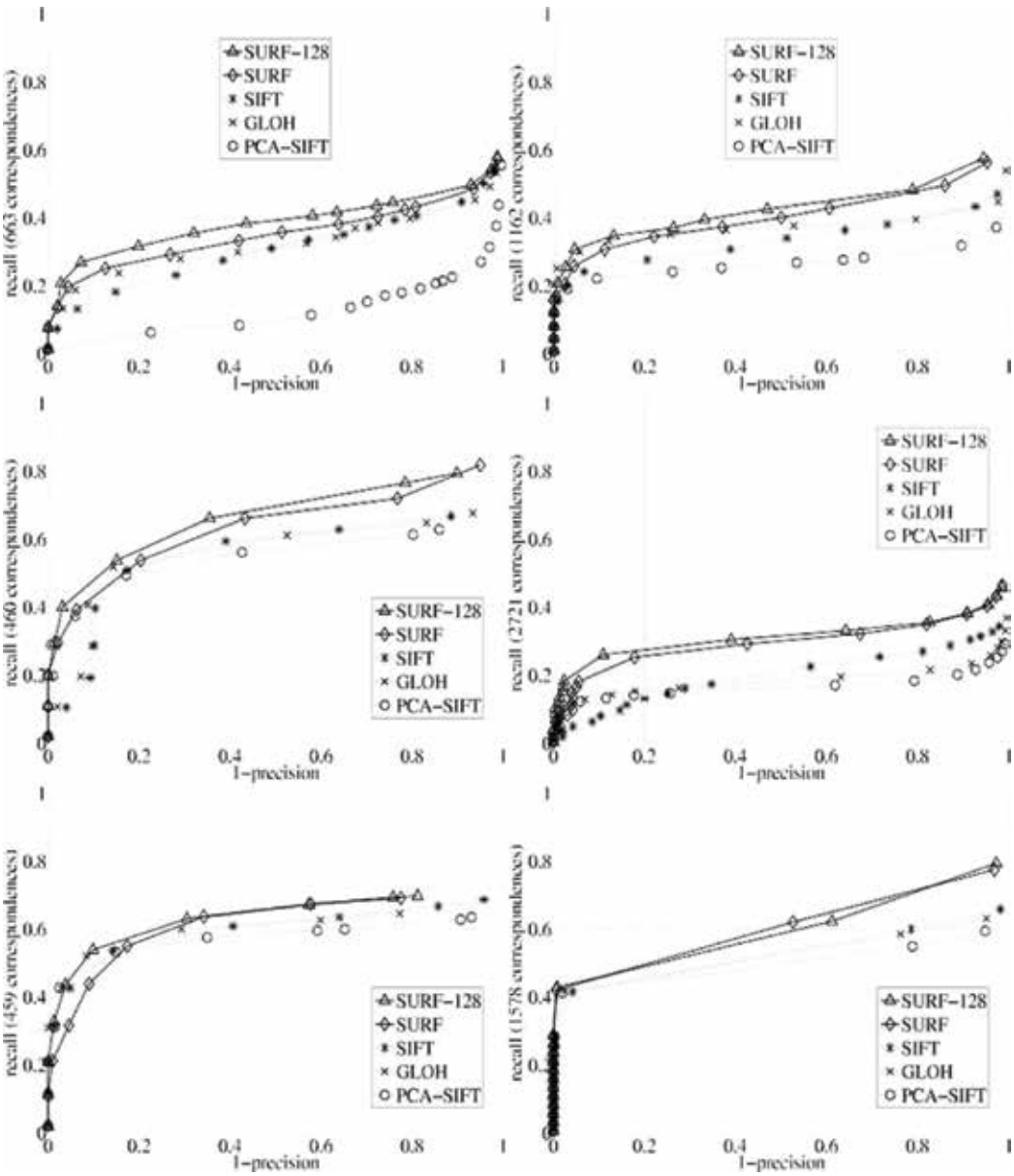

Figure 12. Left to right and top to bottom: graphs of changes in 50 (Walls) grades, descale element 2 (Boats), image blur (Bikes and Trees), illumination level (Leuven), and JPEG compression (Ubc).

the accuracy and performance of different algorithms. Given that detecting counterfeiting is still in its early stages, considerable work remains to be performed, and other ideas can be derived or borrowed from other fields, such as object recognition or image analysis (**Figure 12**).

Author details

Haitham Hasan Badi[1]*, Bassam Sabbri[2] and Fitian Ajeel[2]

*Address all correspondence to: haitham@uoitc.edu.iq

1 Information of Computer Science and Information Technology, University of Malaysia, Kuala Lumpur, Malaysia

2 University of Information Technology and Communication, Baghdad, Iraq

References

[1] Ho A, Shi Y, Kim H, Barni M, Wang W, Dong J, Tan T. A survey of passive image tampering detection. In: Digital Watermarking. Vol. 5703. Berlin/Heidel-berg: Springer; 2009. pp. 308-322

[2] Liu G, Wang J, Lian S, Wang Z. A passive image authentication scheme for detecting region-duplication forgery with rotation. Journal of Network and Computer Applications. 2010;**34**(5):1557-1565

[3] Sebe N, Liu Y, Zhuang Y, Huang T, Chang S-F. Blind passive media forensics: Motivation and opportunity. In: Multimedia Content Analysis and Mining. Vol. 4577. Berlin/Heidelberg: Springer; 2007. pp. 57-59

[4] Hu J, Zhang H, Gao Q, Huang H. An improved lexicographical sort algorithm of copy-move forgery detection. In: Proceedings—2nd International Conference on Networking and Distributed Computing, ICNDC 2011. 2011. pp. 23-27

[5] Bo X, Junwen W, Guangjie L, Yuewei D. Image copy-move forgery detection based on SURF. In: International Conference on Multimedia Information Networking and Security (MINES). 2010. pp. 889-892

[6] Lian S, Kanellopoulos D. Recent advances in multimedia information system security. Informatica. 2009;**33**:3-24

[7] Rey C, Dugelay J-L. A survey of watermarking algorithms for image authentication. EURASIP Journal on Applied Signal Processing. 2002;**2002**(1):613-621

[8] Kundur D, Hatzinakos D. Digital watermarking for telltale tamper proofing and authentication. In: Proceedings of the IEEE. Vol. 87. 1999. pp. 1167-1180

[9] Zhou L, Wang D, Guo Y, Zhang J. Blur detection of digital forgery using mathematical morphology. In: Proceedings of the 1st KES International Symposium on Agent and Multi-Agent Systems: Technologies and Applications. Wroclaw, Poland: Springer-Verlag; 2007

[10] Redi JA, Taktak W, Dugelay JL. Digital image forensics: A booklet for beginners. Multimedia Tools and Applications. 2011;**51**(1):133-162

[11] Ardizzone E, Bruno A, Mazzola G. Copy-move forgery detection via texture description. In: MiFor'10—Proceedings of the 2010 ACM Workshop on Multimedia in Forensics, Security and Intelligence, Co-located with ACM Multimedia 2010. 2010. pp. 59-64

[12] Kang L, Cheng XP, Li K, Xiao-ping C. Copy-move forgery detection in digital image. In: Image and Signal Processing (CISP). 2010 3rd International Congress. Vol. 5. 2010. pp. 2419-2421

[13] Ryu SJ, Lee MJ, Lee HK. Detection of copy-rotate-move forgery using zernike moments. In: Lecture Notes in Computer Science (Including Subseries Lecture Notes in Artificial Intelligence and Lecture Notes in Bioinformatics). LNCS. Vol. 6387. 2010. pp. 51-65

[14] Lowe DG. Object recognition from local scale-invariant features. In: Proceedings of the IEEE International Conference on Computer Vision. Vol. 2. 1999. pp. 1150-1157

[15] Bay H, Tuytelaars T, Van Gool L. SURF: Speeded up robust features. In: Lecture Notes in Computer Science (Including Subseries Lecture Notes in Artificial Intelligence and Lecture Notes in Bioinformatics). LNCS. Vol. 3951. 2006. pp. 404-417

[16] Huang H, Guo W, Zhang Y. Detection of copy-move forgery in digital images using sift algorithm. In: Proceedings—2008 Pacific-Asia Workshop on Computational Intelligence and Industrial Application. PACIIA 2008. Vol. 2. 2008. pp. 272-276

[17] Ardizzone E, Bruno A, Mazzola G. Detecting multiple copies in tampered images. In: Proceedings—International Conference on Image Processing, ICIP. 2011. pp. 2117-2120

[18] Zhang C, Guo X, Cao X. Duplication localization and segmentation. In: Lecture Notes in Computer Science (Including Subseries Lecture Notes in Artificial Intelligence and Lecture Notes in Bioinformatics). LNCS No. Part 1. Vol. 6297. 2010. pp. 578-589

[19] Amerini I, Ballan L, Caldelli R, Del Bimbo A, Serra G. A SIFT-based forensic method for copy-move attack detection and transformation recovery. Information Forensics and Security, IEEE Trans. 2011;**6**(3):1099

[20] Pan X, Lyu S. Detecting image region duplication using SIFT features. In: Acoustics Speech and Signal Processing (ICASSP), 2010 IEEE International Conference. 2010. pp. 1706-1709

[21] Pan X, Lyu S. Region duplication detection using image feature matching. IEEE Transactions on Information Forensics and Security. 2010;**5**(4):857-867

[22] Shivakumar BL, Baboo S. Automated forensic method for copy-move forgery detection based on Harris interest points and SIFT descriptors. International Journal of Computer Applications. 2011;**27**(3):9-17

[23] Shamshiri F. Rotten Gods [Online]. 2008. Available: http://www.rottengods.com/2008/07/missles-forgery.html [Accessed 01.03.12]

[24] Ng T-T, Chang S-F. A model for image splicing. In: International Conference on Image Processing (ICIP 04). Vol. 2. 2004. pp. 1169-1172

[25] Dong J, Wang W, Tan T, Shi YQ. Run-length and edge statistics based approach for image splicing detection. In: Lecture Notes in Computer Science (Including Subseries Lecture Notes in Artificial Intelligence and Lecture Notes in Bioinformatics). LNCS. Vol. 5450. 2009. pp. 76-87

[26] Zhen F, Shuozhong W, Xinpeng Z. Image splicing detection using color edge inconsistency. In: Multimedia Information Networking and Security (MINES), 2010 International Conference. 2010. pp. 923-926

[27] Christlein V, Riess C, Angelopoulou E. On rotation invariance in copy-move forgery detection. In: IEEE International Workshop on Information Forensics and Security, WIFS. 2010

[28] Wang X, Zhang X, Li Z, Wang S. A DWT-DCT based passive forensics method for copy-move attacks. In: 2011 Third International Conference on Multimedia Information Networking and Security. 2011. pp. 304-308

[29] Cao Y, Gao T, Fan L, Yang Q. A robust detection algorithm for region duplication in digital images. International Journal of Digital Content Technology and its Applications. 2011; **5**(6):95-103

[30] Cao Y, Gao T, Fan L, Yang Q. A robust detection algorithm for copy-move forgery in digital images. Forensic Science International. 2011

[31] Huang Y, Lu W, Sun W, Long D. Improved DCT-based detection of copy-move forgery in images. Forensic Science International. 2011;**3**:178-184

[32] Myrna AN, Venkateshmurthy MG, Patil CG. Detection of region duplication forgery in digital images using wavelets and log-polar mapping. In: Conference on Computational Intelligence and Multimedia Applications, 2007, International Conference. Vol. 3. 2007. pp. 371-377

[33] Bravo-Solorio S, Nandi AK. Automated detection and localisation of duplicated regions affected by reflection, rotation and scaling in image forensics. Signal Processing. 2011; **91**(8):1759-1770

[34] Bravo-Solorio S, Nandi AK. Passive forensic method for detecting duplicated regions affected by reflection, rotation and scaling. In: 17th European Signal Processing Conference (EUSIPCO 2009). 2009. pp. 824-828

[35] Bayram S, Sencar HT, Memon N. An efficient and robust method for detecting copy-move forgery. In: Proceedings of IEEE International Conference on Acoustics, Speech and Signal Processing. 2009. pp. 1053-1056

[36] Li W, Yu N. Rotation robust detection of copy-move forgery. In: Proceedings—International Conference on Image Processing, ICIP. 2010. pp. 2113-2116

[37] Lin H-J, Wang C-W, Kao Y-T. Fast copy-move forgery detection. WSEAS Transactions on. Signal Processing. 2009;**5**(5):188-197

[38] Ardizzone E, Mazzola G. Detection of duplicated regions in tampered digital images by bit-plane analysis. In: Lecture Notes in Computer Science (Including Subseries Lecture

Notes in Artificial Intelligence and Lecture Notes in Bioinformatics). LNCS. Vol. 5716. 2009. pp. 893-901

[39] Tamura H, Mori S, Yamawaki T. Textural features corresponding to visual perception. IEEE Transactions on Systems, Man, and Cybernetics. 1978;**8**(6):460-473

[40] Jain AK, Farrokhnia F. Unsupervised texture segmentation using Gabor filters. Pattern Recognition. 1991;**24**(12):1167-1186

[41] Haralick RM. Statistical and structural approaches to texture. Proceedings of the IEEE. 1979;**67**(5):786-804

[42] Fridrich J, Soukal D, Lukáš J. Detection of copy-move forgery in digital images. In: Proceedings of DFRWS 2003. USA: Cleveland, OH; 2003

[43] Wu Q, Wang S, Zhang X. Detection of image region-duplication with rotation and scaling tolerance. In: Lecture Notes in Computer Science (Including Subseries Lecture Notes in Artificial Intelligence and Lecture Notes in Bioinformatics). LNAI. Vol. 6421. 2010. pp. 100-108

[44] Wu Q, Wang S, Zhang X. Log-polar based scheme for revealing duplicated regions in digital images. IEEE Signal Processing Letters. 2011;**18**(10):559-562

[45] Penatti OAB, Valle E, da R, Torres S. Comparative study of global color and texture descriptors for web image retrieval. Journal of Visual Communication and Image Representation. 2012;**23**(2):359-380

[46] Van De Sande K, Gevers T, Snoek C. Evaluating color descriptors for object and scene recognition. IEEE Transactions on Pattern Analysis and Machine Intelligence. 2010; **32**(9):1582-1596

[47] Langille A, Minglun G. An efficient match-based duplication detection algorithm. In: Computer and Robot Vision, 2006. The 3rd Canadian Conference. 2006. p. 64

[48] Luo W, Huang J, Qiu G, Weiqi L, Jiwu H, Guoping Q. Robust detection of regionduplication forgery in digital image. In: Proceedings of the 18th International Conference on Pattern Recognition. Vol. 04. 2006. pp. 746-749

[49] Zimba M, Xingming S. Fast and robust image cloning detection using block characteristics of DWT coefficients. International Journal of Digital Content Technology and its Applications. 2011;**5**(7):359-367

[50] Won CS, Park DK, Park S-J. Efficient use of MPEG-7 edge histogram descriptor. ETRI Journal. 2002;**24**(1):23-30

Section 3

The Motor Image: Reconstructing Semantic Output

Chapter 4

The Application of Motor Imagery to Neurorehabilitation

Yoshibumi Bunno

Additional information is available at the end of the chapter

http://dx.doi.org/10.5772/intechopen.75411

Abstract

We investigated the influence of the imagined muscle contraction strength on the spinal motor neural excitability and sympathetic nerve activity by using the F-wave and heart rate variability analysis. Motor imagery of isometric thenar muscle activity increased the spinal motor neuron excitability and sympathetic nerve activity. The imagined muscle contraction strength did not affect changes of the spinal motor neuron excitability and sympathetic nerve activity. Therefore, Motor imagery at slight imagined muscle contraction strength can facilitate the spinal motor neuron excitability without physical load. Motor imagery-based Brain-machine interface is widely used for neurorehabilitation. To achieve better outcomes in neurorehabilitation used Brain-machine interface, performing trained motor imagery would be required, and the F-wave may be exploited an index of motor imagery training effect.

Keywords: motor imagery, F-wave, imagined muscle contraction strength, autonomic nervous system, neurorehabilitation

1. Introduction

Motor imagery (MI) is defined as an active process during which a specific motor action is reproduced within working memory without any overt movement [1]. MI is considered a potential tool for improvement of motor function in rehabilitation. Indeed, MI has been shown to improve various motor functions. Yue and Cole [2] reported that muscle strength of little finger abduction was significantly increased after MI training for 4 weeks. Additionally, muscle strength of ankle dorsiflexion was significantly increased after MI training for 4 weeks [3]. Also, Guillot et al. [4] reported that muscle flexibility was improved after MI of stretching for 5 weeks.

Immediate enrollment in rehabilitation programs for functional reorganization should be important to obtain better outcomes [5]. Specifically, Motor-evoked potentials (MEPs) amplitude, an index of corticospinal excitability, was decreased in post-stroke [6]. However, MEPs amplitude was increased in patients who have functional motor recovery [7]. Additionally, spinal motor neuron excitability was significantly reduced in the post-stroke acute phase [8]. Thus, facilitating the corticospinal excitability, including the spinal motor neuron excitability, should be needed for post-stroke patients whom have motor impairment.

Numerous neurophysiological studies using positron emission tomography (PET), functional magnetic resonance imaging (fMRI), and near infrared spectroscopy (NIRS) have demonstrated that MI and motor execution activate similar brain activation patterns [9–13]. Specifically, primary motor cortex, supplementary motor area, premotor area, somatosensory area, prefrontal cortex, parietal lobule, cingulate area, cerebellum, and basal ganglia were activated during MI and motor execution. Thus, MI shares common neural substrates with motor execution. When transcranial magnetic stimulation (TMS) was delivered over the primary motor cortex during MI, MEPs amplitude obtained from corresponding muscle was significantly increased relative to rest level [14–16]. The increase of MEPs amplitude during MI indicates that MI facilitates corticospinal excitability. Thus, MI can facilitate the central neural function.

However, previous studies have shown various patterns in the spinal motor neuron excitability during MI using the F-wave and H-reflex as indices of spinal reflex excitability [17–19]. Taniguchi et al. [17] reported that the F-wave amplitude was significantly decreased after volitional relaxation for 3 h. When subjects did MI of thumb abduction during volitional relaxation simultaneously, the F-wave amplitude was maintained at before volitional relaxation level. Whereas, Kasai et al. [18] reported that the H-reflex amplitude was unchanged during MI of wrist flexion movement. Oishi et al. [19] also reported that there was decline of H-reflex amplitude during MI of speed skating. Our laboratory previously investigated the spinal motor neuron excitability during MI of isometric thenar muscle activity at 50% maximal voluntary contraction (MVC) for 1 min using the F-wave [20]. The F-wave is a compound action potential resulting from re-excitation ("backfiring") of an antidromic impulse following distal electrical stimulation of motor nerve fibers at the anterior horn cells [21–23]. The F-wave measured during MI at 50% MVC for 1 min was significantly increased than that at rest. Thus, we concluded that MI of isometric thenar muscle activity can increase the spinal motor neuron excitability.

We are aiming to find the way of MI obtained most beneficial effect. In order to do that, it is important to assess the spinal motor neuron excitability concurrent with the central nervous system. We think that facilitating the spinal motor neuron excitability will be required for improvement of motor function. Because, described above, the facilitation of the corticospinal excitability including the spinal motor neuron excitability is needed for recovery of motor function. In this chapter, we would like to introduce our previous works about the spinal motor neuron excitability during MI of isometric thenar muscle activity. In the first half of this chapter, we described about the spinal motor neuron excitability during MI of isometric thenar muscle activity at various imagined muscle contraction strengths. In the second half of this chapter, we described about the autonomic nervous system during MI. At the end of chapter, we discuss about how apply MI to neurorehabilitation using brain-machine interface (BMI).

http://dx.doi.org/10.5772/intechopen.75411

2. The spinal motor neuron excitability during MI at various imagined muscle contraction strengths

2.1. The spinal motor neuron excitability during MI at 10, 30, 50, and 70% MVC

2.1.1. Purpose

We previously reported that when the subject performed MI of isomeric thenar muscle activity at 50% MVC, the spinal motor neuron excitability was significantly increased than at rest [20]. In actual motion, Suzuki et al. [27] reported the spinal motor neuron excitability was increased linearly with muscle contraction strength. If MI and motor execution share common neural networks, the spinal motor neuron excitability will be increased linearly with imagined muscle contraction strength. Then, we investigated the spinal motor neuron excitability during MI at various imagined muscle contraction strengths. Specifically, we adopted the 10, 30, 50, and 70% MVC for imagined muscle contraction strength. In this research, we assessed the spinal motor neuron excitability during MI by using the F-wave [24–26].

2.1.2. Materials

Ten healthy volunteers were participated in this research (5 males, 5 females; mean age = 28.7 ± 4.5 years). All participants provided informed consent before the study commenced. This research was approved by the Research Ethics Committee at Kansai University of Health Sciences. All recordings were conducted in accordance with the Declaration of Helsinki.

2.1.3. F-wave recording procedure

Participants were in supine position on a bed and instructed to fix one's eye on a pinch meter (Digital indicator F304A, Unipulse Corp., Japan) display throughout the F-wave recording. A Viking Quest electromyography machine ver. 9.0 (Natus Medical Inc., USA) was used for the F-wave recordings. The room temperature was kept at 25°C. The skin was cleaned with an abrasive gel to keep impedance below 5 kΩ. F-waves were recorded from left thenar muscle after stimulating the left median nerve at the wrist. A pair of 10 mm silver EEG cup electrodes (Natus Medical Inc., USA) were placed over the ventral surface of the thumb and base of the first dorsal metacarpal bone. The simulating electrodes comprised a cathode placed over the left median nerve 3 cm proximal to the palmar crease and an anode was placed 2 cm more proximally. Before the F-wave recording, maximal intensity of electrical stimulation was determined by delivering 0.2-ms square-wave pulses of increasing intensity from 0 to 50 mA until eliciting the largest compound muscle action potential (M-wave). Supramaximal electrical stimuli (20% above maximal stimulus intensity) were delivered at 0.5 Hz in each trial. The sensitivity for the F-wave was set at 200 μV/division and a sweep of 5 ms/division. Filter bandwidth was ranged from 20 Hz to 3 kHz.

2.1.4. Experimental protocol

For the rest trial (rest), F-waves were recorded during relaxation for 1 min. Subsequently, for the motor task, participants learned the isometric thenar muscle activity at 50% MVC (i.e.,

participants press the sensor of pinch meter by left thumb and index finger at 50% MVC) for 1 min. They were instructed to keep the 50% MVC value (kgf) measured numerically on the display of pinch meter. For the MI trial, participants performed MI of isometric thenar muscle activity at 50% MVC for 1 min. F-waves were recorded during MI (50% MI). Immediately after 50% MI trial (post), F-waves were recorded during relaxation for 1 min. The above process was defined as the MI at 50% MVC condition (50% MI condition). This protocol was repeated for 10, 30, and 70% MI conditions. Each condition was performed randomly on different days.

2.1.5. F-wave data analysis

All recorded F-wave data were analyzed for the persistence, F/M amplitude ratio, and latency in each trial. The minimum of F-wave peak-to-peak amplitude was at least 20 μV [21]. The persistence was defined as the number of detected F-wave responses divided by 30 supramaximal electrical stimuli. The F/M amplitude ratio was defined as the mean amplitude of all responses divided by the M-wave amplitude. The amplitude measured individually for each F-wave and then the mean calculated. The latency was defined as the mean latency from the time of electrical stimulation to onset of detected F-waves. The persistence reflects the number of backfiring spinal anterior horn cells [22, 23]. The F/M amplitude ratio reflects the number of backfiring spinal anterior horn cells and the individual cells excitability [22, 23]. Thus, these parameters are considered the indices of the spinal motor neuron excitability.

2.1.6. Statistical analysis

The normality of F-wave data was not confirmed by using the Kolmogorov-Smirnov and Shapiro-Wilk tests. We used a nonparametric method in this research. The persistence, F/M amplitude ratio, and latency among three trials (rest, MI, post) under each MI conditions (10% MI, 30% MI, 50% MI, and 70% MI conditions) were compared using the Friedman test and Scheffe's post hoc test.

We also calculated the relative value obtained by dividing F-wave data during MI under four MI conditions by that at rest. The relative values among four MI conditions were compared using the Friedman test. We used SPSS statistics ver. 19 (IBM Corp., USA) for statistical analysis. The threshold for statistical significance was set to $p = 0.05$.

2.1.7. Results

The persistence during MI under all MI conditions was significantly greater than that at rest (10% MI vs. Rest, 70% MI vs. Rest, $^{**}p < 0.01$; 30% MI vs. Rest, 50% MI vs. Rest, $^{*}p < 0.05$) (**Tables 1–4**). The persistence immediately after MI under all MI conditions was reduced to rest level (**Tables 1–4**).

The F/M amplitude ratio during MI under 10, 30, and 50% MI conditions was significantly greater than that at rest (10% MI vs. Rest, 50% MI vs. Rest, $^{**}p < 0.01$; 30% MI vs. Rest, $^{*}p < 0.05$) (**Tables 1–3**). The F/M amplitude ratio during MI under 70% MI condition was tended to be increased than that at rest ($p \fallingdotseq 0.082$) (**Table 4**). The F/M amplitude ratio immediately after MI under all MI conditions was reduced to rest level (**Tables 1–4**).

	Rest	10% MI	post
Persistence (%)	61.8 ± 12.6	91.9 ± 9.70**	73.1 ± 20.7
F/M amplitude ratio (%)	0.90 ± 0.35	2.46 ± 2.61**	1.18 ± 0.67
Latency (ms)	25.3 ± 0.98	25.2 ± 1.25	25.5 ± 0.99

**$p < 0.01$; significant difference between rest and 10% MI trial.

Table 1. Changes in F-wave under 10% MI condition.

	Rest	30% MI	post
Persistence (%)	61.2 ± 19.5	88.0 ± 12.2**	60.0 ± 18.7
F/M amplitude ratio (%)	1.00 ± 0.94	2.92 ± 2.95**	1.11 ± 0.52
Latency (ms)	24.9 ± 1.16	24.6 ± 0.99	24.9 ± 1.14

**$p < 0.05$; significant difference between rest and 30% MI trial.

Table 2. Changes in F-wave under 30% MI condition.

	Rest	50% MI	post
Persistence (%)	62.7 ± 22.3	94.0 ± 9.40*	65.5 ± 27.0
F/M amplitude ratio (%)	1.08 ± 0.28	2.60 ± 2.30**	0.98 ± 0.40
Latency (ms)	24.5 ± 1.61	24.3 ± 1.82	24.5 ± 1.58

*$p < 0.05$; significant difference between rest and 50% MI trial.
**$p < 0.01$; significant difference between rest and 50% MI trial.

Table 3. Changes in F-wave under 50% MI condition.

	Rest	70% MI	post
Persistence (%)	55.9 ± 17.6	88.1 ± 10.8**	65.3 ± 19.9
F/M amplitude ratio (%)	0.94 ± 0.33	1.79 ± 1.23	1.11 ± 0.44
Latency (ms)	24.4 ± 1.37	24.1 ± 1.27	24.3 ± 1.15

**$p < 0.01$; significant difference between rest and 70% MI trial.

Table 4. Changes in F-wave under 70% MI condition.

No significantly differences in the latency were observed among three trials (rest, MI, post) under all MI conditions (**Tables 1–4**).

The relative values of the persistence, F/M amplitude ratio, and latency did not exhibit significant differences among all MI conditions (**Table 5**).

	10% MI condition	30% MI condition	50% MI condition	70% MI condition
Relative values of persistence	1.53 ± 0.31	1.58 ± 0.61	1.78 ± 0.93	1.69 ± 0.45
Relative values of F/M amplitude ratio	2.40 ± 1.38	3.31 ± 0.56	2.52 ± 1.96	2.10 ± 1.37
Relative values of latency	0.99 ± 0.02	0.99 ± 0.02	0.99 ± 0.03	0.99 ± 0.02

Table 5. Comparison of F-wave among 10% MI, 30% MI, 50% MI, and 70% MI condition.

2.2. The spinal motor neuron excitability during MI at 50 and 100% MVC

2.2.1. Purpose

Our previous works [24–26] suggested that MI of isometric thenar muscle activity at 10, 30, 50, and 70% MVC can facilitate the spinal motor neuron excitability. However, the imagined muscle contraction strength did not influence on change of the spinal motor neuron excitability. Whereas, Cowley et al. [29] previously reported that the amplitude of H-reflex during MI of ankle plantar flexion at 100% MVC was significantly greater than that at 50% MVC. Then, we hypothesized the MI of isometric thenar muscle activity at 100% MVC will be greater than that at 50% MVC. In this research, we compared the spinal motor neuron excitability between 50% MI and 100% MI condition [28].

2.2.2. Materials

Fifteen healthy volunteers were participated in this research (13 males, 2 females; mean age = 25.3 ± 5.0 years). All participants provided informed consent before the study commenced. This research was approved by the Research Ethics Committee at Kansai University of Health Sciences. All recordings were conducted in accordance with the Declaration of Helsinki.

2.2.3. F-wave recording procedure

The environment and F-wave recording condition was set as previous works [24, 25].

2.2.4. Experimental protocol

For the rest trial (rest), F-waves were recorded during relaxation for 1 min. Subsequently, for the motor task, participants learned the isometric thenar muscle activity at 50% MVC (i.e., participants press the sensor of pinch meter by left thumb and index finger at 50% MVC) for 1 min. They were instructed to keep the 50% MVC value (kgf) measured numerically on the display of pinch meter. For the MI trial, participants performed MI of isometric thenar muscle activity at 50% MVC for 1 min. F-waves were recorded during MI (50% MI) and immediately after 50% MI trial (post) for 1 min respectively. The above process was defined as the MI at 50% MVC condition (50% MI condition). F-wave recording under 100% MI condition was performed using the same protocol as 50% MI condition. These conditions were performed randomly on different days.

After all F-wave recordings, F-wave data was analyzed with respect to the persistence, F/M amplitude ratio, and latency.

2.2.5. Statistical analysis

The normality of F-wave data was not confirmed by using the Kolmogorov-Smirnov and Shapiro-Wilk tests. We used a nonparametric method in this research. The persistence, F/M amplitude ratio, and latency among three trials (rest, MI, post) under two MI conditions (50% MI and 100% MI conditions) were compared using the Friedman test and Scheffe's post hoc test.

We also calculated the relative value obtained by dividing F-wave data during MI under four MI conditions by that at rest. The relative values among two MI conditions were compared using the Wilcoxon signed rank test. We used SPSS statistics ver. 19 (IBM Corp., USA) for statistical analysis. The threshold for statistical significance was set to $p = 0.05$.

2.2.6. Results

The persistence during MI under two MI conditions was significantly greater than that at rest (50% MI vs. Rest, 100% MI vs. Rest, $^{**}p < 0.01$) (**Tables 6**, **7**). The persistence immediately after MI under two MI conditions was reduced to rest level (**Tables 6**, **7**).

The F/M amplitude ratio during MI under two MI conditions was significantly greater than that at rest (50% MI vs. Rest, 100% MI vs. Rest, $^{**}p < 0.01$) (**Tables 6**, **7**). The F/M amplitude ratio immediately after MI under two MI conditions was reduced to rest level (**Tables 6**, **7**).

No significantly differences in the latency were observed among three trials (rest, MI, post) under two MI conditions (**Tables 6**, **7**).

The relative values of the persistence, F/M amplitude ratio, and latency did not exhibit significant differences between two MI conditions (**Table 8**).

2.3. Discussion

2.3.1. The spinal motor neuron excitability during MI of isometric thenar muscle activity

From results of our previous works, it is suggested that MI of isometric thenar muscle activity at 10, 30, 50, 70, and 100% can facilitate the spinal motor neuron excitability. About this, it is considered to be influence of descending pathways corresponding to thenar muscle. Previous researches have demonstrated the activation of diverse brain area contribute to motor preparation and planning during MI [9–13]. The excitatory and inhibitory inputs modulate the spinal motor neuron excitability via the corticospinal and/or extrapyramidal tract [30]. Thus, it is plausibly that the activation of central nervous system contributes to motor preparation and planning during MI facilitated the spinal motor neuron excitability via the corticospinal and/or extrapyramidal tract.

Furthermore, all subjects participated in our previous works were instructed to perform MI with holding the sensor of a pinch meter. Mizuguchi et al. [31] reported that corticospinal excitability during MI utilizing an object was modulated by a combination of tactile and proprioceptive inputs while holding an object. We previously reported that the spinal motor neuron

	Rest	50% MI	post
Persistence (%)	50.8 ± 21.7	88.2 ± 13.2**	48.3 ± 19.9
F/M amplitude ratio (%)	1.71 ± 0.89	3.96 ± 4.56**	1.29 ± 0.56
Latency (ms)	25.5 ± 1.40	24.9 ± 1.91	25.3 ± 1.29

**$p < 0.01$; significant difference between rest and 50% MI trial.

Table 6. Changes in F-wave parameters under 50% MI condition.

	Rest	100% MI	post
Persistence (%)	60.8 ± 24.9	91.9 ± 7.58**	60.7 ± 21.5
F/M amplitude ratio (%)	1.32 ± 1.12	3.57 ± 4.67**	1.39 ± 1.25
Latency (ms)	25.2 ± 1.32	24.8 ± 1.31	25.2 ± 1.40

**$p < 0.01$; significant difference between rest and 100% MI trial.

Table 7. Changes in F-wave parameters under 100% MI condition.

	50% MI condition	100% MI condition
Relative values of persistence	2.04 ± 1.17	2.06 ± 1.71
Relative values of F/M amplitude ratio	2.75 ± 2.04	2.53 ± 1.76
Relative values of latency	0.98 ± 0.06	0.99 ± 0.03

Table 8. Comparison of F-wave parameters between 50% MI and 100% MI condition.

excitability during MI with holding the sensor of a pinch meter was significantly greater than that during MI without holding the sensor [20]. Consequently, it is suggested that tactile and proprioceptive perceptions during MI while holding the sensor facilitated the spinal motor neuron excitability cooperatively with MI-activated pathways.

2.3.2. Influence of the imagined muscle contraction strength on the spinal motor neuron excitability

In our previous works, the relative value of the persistence, F/M amplitude, and latency were similar among all MI conditions. It is suggested that the imagined muscle contraction strength may not affect the spinal motor neuron excitability. There are several previous researches investigated the spinal motor neuron excitability during MI at different imagined muscle contraction strengths. Bonnet et al. [32] reported that the amplitude of H-reflex was significantly greater during MI of ankle plantar flexion at 2 and 10% than that at rest. Additionally, the amplitude of H-reflex during MI was similar between 2% MI and 10% MI condition. Hale et al. [33] also reported that the amplitude of H-reflex during MI of ankle plantar flexion was similar among five (i.e., 20, 40, 60, 80, and 100% MVC) MI conditions.

Similarly, Aoyama and Kaneko [34] reported that the amplitude of H-reflex during MI was similar between 50% MI and 100% MI condition. In actual motion, the spinal motor neuron excitability was increased linearly with the muscle contraction strength [27]. Described in the introduction, MI is the mental rehearsal of a movement without any overt movement [1]. One possibility is the contribution of neural mechanism which inhibits actual movement and muscle contraction during MI. Park and Li [35] reported that the amplitude of MEPs during MI of finger flexion and extension at 10, 20, 30, 40, 50, and 60% MVC was significantly greater than that at rest. However, the amplitude of MEPs during MI was similar among all six MI conditions. Further, in an event-related potential study, the magnitude of primary motor cortex activity during MI did not correlate with the imagined muscle contraction strength, although activities of the supplementary motor and premotor area during MI were strongly correlated with it [36]. The supplementary motor and premotor area have crucial roles in larger force generation [37], motor planning, preparation, and inhibition [38, 39]. Thus, the supplementary motor and premotor area may inhibit the actual muscle activity depending on the muscle contraction strength. Because these areas also are connected directly to primary motor cortex, inhibitory inputs from the supplementary motor and premotor area may suppress any additional excitation of primary motor cortex conferred by MI with high imagined contraction strength. Furthermore, the spinal motor neuron excitability during MI is thought to be affected by central nervous system via the corticospinal and/or extrapyramidal tract. The degree of the spinal motor neuron excitability during MI at various imagined muscle contraction strengths may be modulated by both excitatory and inhibitory inputs from the central nervous system.

2.4. Conclusion

Our previous woks showed significant increase of the spinal motor neuron excitability during MI of isometric thenar muscle activity. However, the imagined muscle contraction strength was not involved in change of the spinal motor neuron excitability.

3. The autonomic nervous system during MI of isometric thenar muscle activity

3.1. The autonomic nervous system during MI of isometric thenar muscle activity at 10 and 50% MVC

3.1.1. Purpose

We previously suggested that MI can facilitate the spinal motor neuron excitability. Sympathetic nerve activity was increased during actual isometric muscle contraction [41]. If MI shares common neural substrates with motor execution, it would be expected to observe the similar pattern in autonomic nervous system (ANS) activity during MI would be observed. In previous research, the heart rate during MI was significantly increased than that at rest [42]. Thus, MI can regulate sympathetic nerve activity without any overt movement. However, whether the imagined muscle contraction strength affects the ANS activity is still unclear.

Then, this research aimed to investigate the ANS activity during MI of isometric thenar activity at 10 and 50% MVC [40].

3.1.2. Materials

Nine healthy volunteers were participated in this research (7 males, 2 females; mean age = 25.3 ± 5.3 years). All participants provided informed consent before the study commenced. This research was approved by the Research Ethics Committee at Kansai University of Health Sciences. All recordings were conducted in accordance with the Declaration of Helsinki.

3.1.3. The ANS activity recording procedure

The ANS activity was recorded using a heart rhythm scanner PE (Biocom Technologies, USA). The pulse wave from the photoplethysmography sensor attached on earlobe was measured. The low frequency/high frequency (LF/HF) ratio was calculated by analyzing measured the pulse wave. The LF/HF ratio is considered to be an index of the sympathetic nerve activity.

3.1.4. Experimental protocol

For the rest trial (rest), the ANS activity was recorded during relaxation for 5 min. The European Society of Cardiology and the North American Society of Pacing and Electrophysiology recommend 5 min recordings for heart rate variability analysis [43]. Subsequently, for the motor task, participants learned the isometric thenar muscle activity at 50% MVC (i.e., participants press the sensor of pinch meter by left thumb and index finger at 50% MVC) for 1 min. They were instructed to keep the 50% MVC value (kgf) measured numerically on the display of pinch meter. For the MI trial, participants performed MI of isometric thenar muscle activity at 10% MVC for 5 min. The ANS activity was recorded during MI (10% MI) and immediately after 10% MI trial (post) for 5 min respectively. The above process was defined as the MI at 10% MVC condition (10% MI condition). The ANS activity recording under 50% MI condition was performed using the same protocol as 10% MI condition. These conditions were performed randomly on different days.

3.1.5. Statistical analysis

The normality of the ANS activity data was not confirmed by using the Kolmogorov-Smirnov and Shapiro-Wilk tests. We used a nonparametric method in this research. The LF/HF ratio among three trials (rest, MI, post) under two MI conditions (10% MI and 50% MI conditions) were compared using the Friedman test and Scheffe's post hoc test.

We also calculated the relative value obtained by dividing the LF/HF ratio during MI under four MI conditions by that at rest. The relative values among two MI conditions were compared using the Wilcoxon signed rank test. We used SPSS statistics ver. 19 (IBM Corp., USA) for statistical analysis. The threshold for statistical significance was set to $p = 0.05$.

3.1.6. Results

The LF/HF ratio during MI under two MI conditions was greater than that at rest (50% MI vs. Rest, $*p < 0.05$) (**Tables 9**, **10**). The LF/HF ratio immediately after MI under two MI conditions was reduced to rest level (**Tables 9**, **10**).

	Rest	10% MI	post
LF/HF ratio (%)	1.23 ± 0.75	2.73 ± 3.68	1.54 ± 0.52

Table 9. Changes in ANS activity under 10% MI condition.

	Rest	50% MI	post
LF/HF ratio (%)	1.74 ± 1.16	2.92 ± 2.17*	2.07 ± 1.42

*$p < 0.05$; significant difference between rest and 50% MI trial.

Table 10. Changes in ANS activity under 50% MI condition.

The relative values of the LF/HF ratio did not exhibit significant differences between two MI conditions (**Table 11**).

3.2. The autonomic nervous system during MI of isometric thenar muscle activity at 50 and 100% MVC

Firstly, about purpose, the ANS recording procedure, experimental protocol, and statistical analysis, please refer to our previous research [40].

3.2.1. Materials

Ten healthy volunteers were participated in this research (8 males, 2 females; mean age = 25.3 ± 5.3 years). All participants provided informed consent before the study commenced. This research was approved by the Research Ethics Committee at Kansai University of Health Sciences. All recordings were conducted in accordance with the Declaration of Helsinki.

3.2.2. Results

The LF/HF ratio during MI under two MI conditions was significantly greater than that at rest (50% MI vs. Rest, 100% MI vs. Rest, *$p < 0.05$) (**Tables 12**, **13**). The LF/HF ratio immediately after MI under two MI conditions was reduced to rest level (**Tables 12**, **13**).

The relative values of the LF/HF ratio did not exhibit significant differences between two MI conditions (**Table 14**).

3.3. Discussion

Our previous works demonstrated significant increase of the LF/HF ratio during MI at various imagined muscle contraction strengths (i.e., 10% MVC, 50% MVC, and 100% MVC) [40, 44]. Thus, MI of isometric thenar muscle activity can increase the sympathetic nerve activity as with previous researches [42]. The central command is defined as a feed-forward mechanism by which activation of cardiovascular and respiratory centers is accomplished by descending signals from central nervous system [45]. TMS delivered over the primary motor cortex

	50% MI condition	10% MI condition
Relative value of LF/HF ratio	2.64 ± 3.35	1.75 ± 1.14

Table 11. Comparison of ANS activity between 10% MI and 50% MI condition.

	Rest	50% MI	post
LF/HF ratio (%)	2.04 ± 1.44	3.40 ± 2.55*	2.33 ± 1.58

*$p < 0.05$; significant difference between rest and 50% MI trial.

Table 12. Changes in LF/HF ratio under 50% MI condition.

	rest	100% MI	post
LF/HF ratio (%)	1.86 ± 1.21	4.60 ± 5.48*	2.29 ± 1.12

*$p < 0.05$; significant difference between rest and 50% MI trial.

Table 13. Changes in LF/HF ratio under 100% MI condition.

	50% MI condition	100% MI condition
Relative value of LF/HF ratio	2.69 ± 3.32	2.14 ± 1.15

Table 14. Comparison of ANS activity between 50% MI and 100% MI condition.

increased the skin sympathetic nerve activity [46]. Furthermore, transcranial direct current stimulation (tDCS) delivered over the primary motor cortex increased the LF/HF ratio [47]. Thus, the corticospinal pathway including the primary motor cortex may affect the sympathetic nerve activity. The rostral ventromedial medulla is also part of the reticulospinal tract [48]. The activation of central nervous system during MI may increase the sympathetic nerve activity via the corticospinal and reticulospinal tracts.

The imagined muscle contraction did not affect the change of the sympathetic nerve activity. This is very similar with the result of the spinal motor neuron excitability during MI at various imagined muscle contraction strengths [24–26, 28]. If central command during MI affects the sympathetic nerve activity via the corticospinal pathway, the imagined muscle contraction strength may affect the sympathetic nerve activity. Park and Li [35] reported that the imagined muscle contraction strength did not affect the corticospinal excitability. Thus, it considered that the imagined muscle contraction strength might not be involved in change of the sympathetic nerve activity.

3.4. Conclusion

Our previous woks showed significant increase of the sympathetic nerve activity during MI of isometric thenar muscle activity. However, the imagined muscle contraction strength was not involved in change of the sympathetic nerve activity.

http://dx.doi.org/10.5772/intechopen.75411

4. The application of MI to neurorehabilitation

30–60% of patients have difficulty in using their affected upper limb after stroke [49]. Nakayama et al. [50] reported that recovery of upper limb function related activity of daily living mainly took place within the first 2 months after stroke. Further they reported that 79% of patients with mild upper limb paresis could achieve full upper limb function, whereas, in case with severe upper limb paresis, only 18% of patients who could achieve full upper limb function.

Depending on alteration of peripheral and central inputs, cortical connections and responses are continuously reorganized [51]. Motor cortex excitability will be decreased in post-stroke due to the damage of neural substrates, loss of sensory inputs, and disuse of the affected limb [52]. Described in introduction of this chapter, various brain areas including primary motor cortex corresponding to motor planning, preparation and execution were activated during MI [9–13]. Pascual-Leon et al. [53] employed TMS in the healthy subjects to map the primary motor cortex targeting the contralateral hand muscles pre- and post-MI training. Cortical representation of hand muscles in contralateral the primary motor cortex increased after MI training. Similarly, MI induced an enhancement of hand muscle cortical representation in post-stroke [54]. Thus, MI can induce the cortical plasticity after neural damage. Additionally, Wrigley et al. [55] reported that the corticospinal excitability was decreased following the significant decline of both size and number of the corticospinal neurons. Also, the spinal motor neuron excitability was significantly reduced in the post-stroke acute phase [8]. Ruffino et al. [56] indicated that neural adaptation following MI training, such as cortical reorganization, the reinforcement of synapse conductivity, and the decline of pre-synaptic inhibition, would be occurred at cortical and spinal level. Thus, in post-stroke patients, facilitating the corticospinal excitability, including the spinal motor neuron excitability should be important for improvement motor function. MI can increase the corticospinal excitability [14–16]. Further, Grosprêtre et al. [57] reported that during MI, the amplitude of cervico-medullar-evoked potentials (CMEPs) can measure directly pyramido-motoneuronal junction was significantly increased. The H-reflex amplitude, however, was unchanged. Conversely, the H-reflex amplitude was increased during MI [29]. Further, we showed significant increase the F-wave during MI [24–26, 28]. In regard to difference between two techniques, the H-reflex size can be influenced by pre-synaptic interneuron, whereas the F-wave is solely dependent on the spinal motor neuron excitability [58]. Although effect of MI on the spinal motor neuron excitability is still under debate, MI can be considered to be an effective method for improvement upper limb function in post-stroke.

Brain-machine interface (BMI) is thought to be a potentially useful technology in neurorehabilitation. BMI can supplement for the lost motor function by bypassing disabled neuromuscular system, and improve brain plasticity and restoration of motor function by using external feedback [59, 60]. Various neurophysiological technologies, such as electroencephalography (EEG), magnetencephalography (MEG), and NIRS, have been used to measure and analyze brain activities. Among, the mu (μ) rhythm (ranged from 10-12 Hz) has been commonly used to monitor brain activities [61]. The event-related desynchronization (ERD) of the μ-rhythm was observed during MI. MI plays an important role in neurorehabilitation using EEG triggered-BMI. However, many people have difficulty in performing MI. Especially MI ability was significantly decreased in post-stroke patients [62]. They have no feedback about whether MI did perform correctly, because MI is a mental rehearsal of movement without any overt

motor outputs [1]. Thus, MI training should be needed with providing appropriate feedback. Actually, kinesthetic feedback provided better hand motor recovery in MI-based BCI combined with exoskeleton [63].

From the result of our previous works [24–26, 28], we propose the spinal motor neuron excitability may be one of useful index of MI training effect, because Takemi et al. [64] suggested that the degree of ERD was significantly correlated with the spinal motor neuron excitability. Actually, Hale et al. [33] reported that the spinal motor neuron excitability was more facilitated with each MI practice. Thus, the spinal motor neuron excitability during MI may be altered depending on MI learning status. However, Oishi et al. [19] also reported that the spinal motor neuron excitability was decreased during MI in athlete of speed skating. About alteration of the spinal motor neuron excitability during MI in various learning status, further research will be required.

Conflict of interest

None declared.

Author details

Yoshibumi Bunno[1,2]*

*Address all correspondence to: bunno@kansai.ac.jp

1 Graduate School of Health Sciences, Graduate School of Kansai University of Health Sciences, Kumatori, Sennan, Osaka, Japan

2 Clinical Physical Therapy Laboratory, Faculty of Health Sciences, Kansai University of Health Sciences, Osaka, Japan

References

[1] Guillot A, Di Rienzo F, Maclntyre T, Moran A, Collet C. Imagining is not doing but involves specific motor commands: A review of experimental data related to motor inhibition. Frontiers in Human Neuroscience. 2012;**6**:247. DOI: 10.3389/fnhum.2012.00247

[2] Yue G, Cole KJ. Strength increases from the motor program: Comparison of training with maximal voluntary and imagined muscle contractions. Journal of Neurophysiology. 1992;**67**(5):1114-1123. DOI: 10.1152/jn.1992.67.5.1114

[3] Sidaway B, Trzaska AR. Can mental practice increase ankle dorsiflexor torque? Physical Therapy. 2005;**85**(10):1053-1060. DOI: 10.1093/ptj/85.10.1053

[4] Guillot A, Tolleron C, Collet C. Does motor imagery enhance stretching and flexibility? Journal of Sports Sciences. 2010;**28**(3):291-298. DOI: 10.1080/02640410903473828

[5] Pantano P, Formisano R, Ricci M, Di Piero V, Sabatini U, Di Pofi B, et al. Motor recovery after stroke. Morphological and functional brain alterations. Brain. 1996;**119**(6):1849-1857. DOI: 10.1093/brain/119.6.1849

[6] Foltys H, Krings T, Meister IG, Sparing R, Boroojerdi B, Thron A, et al. Motor representation in patients rapidly recovering after stroke: A functional magnetic resonance imaging and transcranial magnetic stimulation study. Clinical Neurophysiology. 2003; **114**(12):2404-2015. DOI: 10.1016/S1388-2457(03)00263-3

[7] Triggs WJ, Calvanio R, Levine M. Transcranial magnetic stimulation reveals a hemispheric asymmetry correlate intermanual differences in motor performance. Neuropsychologia. 1997;**35**(10):1335-1363. DOI: 10.1016/S0028-3932(97)00077-8

[8] Drory VE, Neufeld MY, Korczyn AD. F-wave characteristics following acute and chronic upper motor neuron lesions. Electromyography and Clinical Neurophysiology. 1993;**33**(7):441-446

[9] Stephan KM, Fink GR, Rassingham RE, Silbersweiq D, Ceballos-Baumann AO, Frith CD, et al. Functional anatomy of the mental representation of upper extremity movements in healthy subjects. Journal of Neurophysiology. 1995;**73**(1):373-386. DOI: 10.1152/jn.1995.73.1.373

[10] Porro CA, Fancescato MP, Cettolo V, Diamond ME, Baraldi P, Zuiani C, et al. Primary motor and sensory cortex activation during motor performance and motor imagery: A functional magnetic resonance imaging study. The Journal of Neuroscience. 1996; **16**(23):7688-7698

[11] Luft AR, Skalej M, Stefanou A, Klose U, Voiqt K. Comparing motion- and imagery-related activation in the human cerebellum: A functional MRI study. Human Brain Mapping. 1998;**6**(2):105-113. DOI: 10.1002/(SICI)1097-0193(1998)6:2<105::AID-HBM3>3.3.CO;2-R

[12] Lotze M, Montoya P, Erb M, Hülsmann E. Activation of cortical and cerebellar motor areas during executed and imagined hand movements: An fMRI study. Journal of Cognitive Neuroscience. 1999;**11**(5):491-501. DOI: 10.1162/089892999563553

[13] Nakano H, Ueta K, Osumi M, Morioka S. Brain activity during the observation, imagery, and execution of tool use: An fNIRS/EEG study. Journal of Novel Physiotherapies. 2012;**S1**:009. DOI: 10.4172/2165-7025.S1-009

[14] Fourkas AD, Ionta S, Aglioti SM. Influence of imagined posture and imagery modality on corticospinal excitability. Behavioural Brain Research. 2006;**168**(2):190-196. DOI: 10.1016/j.bbr.2005.10.015

[15] Fadiga L, Buccino G, Craighero L, Fogassi L, Gallese V, Pavesi G. Corticospinal excitability is specifically modulated by motor imagery: A magnetic stimulation study. Neuropsychologia. 1998;**37**(2):147-158. DOI: 10.1016/S0028-3932(98)00089-X

[16] Stinear CM, Byblow WD. Modulation of corticospinal excitability and intracortical inhibition during motor imagery is task-dependent. Experimental Brain Research. 2004;**157**(3):351-358. DOI: 10.1007/s00221-004-1851-z

[17] Taniguchi S, Kimura J, Yamada T, Ichikawa H, Hara M, Fujisawa R, et al. Effect of motion imagery to counter rest-induced suppression of F-wave as a measure of anterior horn cell excitability. Clinical Neurophysiology. 2008;**119**(6):1346-1352. DOI: 10.1016/j.clinph.2007.11.179

[18] Kasai T, Kawai S, Kawanishi M, Yahagi S. Evidence for facilitation of motor evoked potentials (MEPs) induced by motor imagery. Brain Research. 1997;**744**(1):147-150. DOI: 10.1016/S0006-8993(96)01101-8

[19] Oishi K, Kimura M, Yasukawa M, Yoneda T, Maeshima T. Amplitude reduction of H-reflex during mental movement simulation in elite athletes. Behavioural Brain Research. 1994;**62**(1):55-61. DOI: 10.1016/0166-4328(94)90037-X

[20] Suzuki T, Bunno Y, Onigata C, Tani M, Uragami S. Excitability of spinal neural function during several motor imagery tasks involving isometric opponens pollicis activity. NeuroRehabilitation. 2013;**33**(1):171-176. DOI: 10.3233/NRE-130942

[21] Fisher MA. F-waves-physiology and clinical uses. The Scientific World Journal. 2007; **7**(1):144-160. DOI: 10.1100/tsw.2007.49

[22] Kimura J. F-wave velocity in the central segment of the median and ulnar nerves. A study in normal subjects and in patients with Charcot-Marie-tooth disease. Neurology. 1974;**24**(6):539-546. DOI: 10.1212/WNL.24.6.539

[23] Mesrati F, Vecchierini MF. F-waves neurophysiology and clinical value. Neurophysiologie Clinique. 2004;**34**(5):217-243. DOI: 10.1016/j.neucli.2004.09.005

[24] Bunno Y, Yurugi Y, Onigata C, Suzuki T, Iwatsuki H. Influence of motor imagery of isometric opponens pollicis activity on the excitability of spinal motor neurons: A comparison using different muscle contraction strengths. Journal of Physical Therapy Science. 2014;**26**(7):1069-1073. DOI: 10.1589/jpts.26.1069

[25] Bunno Y, Onigata C, Suzuki T. The imagined muscle contraction strengths did not affect the changes of spinal motor neurons excitability. Journal of Novel Physiotherapies. 2016;**S3**:008. DOI: 10.4172/2165-7025.S3-008

[26] Bunno Y, Fukumoto Y, Todo M, Onigata C. The effect of motor imagery on spinal motor neuron excitability and its clinical use in physical therapy. In: Suzuki T, editor. Neurological Physical Therapy. Rijeka: Intech; 2017. pp. 29-50. DOI: 10.5772/67471

[27] Suzuki T, Fujiwara T, Takeda I. Excitability of the spinal motor neuron pool and F-waves during isometric ipsilateral and contralateral contraction. Physiotherapy Theory and Practice. 1993;**9**(1):19-24. DOI: 10.3109/09593989309036482

[28] Bunno Y, Onigata C, Suzuki T. Excitability of spinal motor neurons excitability during motor imagery of thenar muscle activity under maximal voluntary contractions of 50% and 100%. Journal of Physical Therapy Science. 2015;**27**(9):2775-2778. DOI: 10.1589/jpts.27.2775

[29] Cowley PM, Clark BC, Ploutz-Snyder LL. Kinesthetic motor imagery and spinal excitability: The effect of contraction intensity and spatial localization. Clinical Neurophysiology. 2008;**119**(8):1849-1856. DOI: 10.1016/j.clinph.2008.04.004

[30] Lemon RN. Descending pathways in motor control. Annual Review of Neuroscience. 2008;**31**(1):195-218. DOI: 10.1146/annurev.neuro.31.060407.125547

[31] Mizuguchi N, Sakamoto M, Muraoka T, Nakagawa K, Kanazawa S, Nakata H, et al. The modulation of corticospinal excitability during motor imagery of action with objects. PLoS One. 2011;**6**(10):e26006. DOI: 10.1371/journal.pone.0026006

[32] Bonnet M, Decety J, Jeannerod M, Requina J. Mental simulation of an action modulates the excitability of spinal reflex pathways in man. Cognitive Brain Research. 1997;**5**(3):221-228. DOI: 10.1016/S0926-6410(96)00072-9

[33] Hale BS, Raglin JS, Koceja DM. Effect of mental imagery of a motor task on the Hoffmann reflex. Behavioural Brain Research. 2003;**142**(1-2):81-87. DOI: 10.1016/S0166-4328(02)00397-2

[34] Aoyama T, Kaneko F. The effect of motor imagery on gain modulation of the spinal reflex. Brain Research. 2011;**1372**(1):41-48. DOI: 10.1016/j.brainres.2010.11.023

[35] Park WH, Li S. No graded responses of finger muscles to TMS during motor imagery of isometric finger forces. Neuroscience Letters. 2011;**494**(3):255-259. DOI: 10.1016/j.neulet.2011.03.027

[36] Romero DH, Lacourse MG, Lawrence KE, Schandler S, Cohen MJ. Event-related potentials as a function of movement parameter variations during motor imagery and isometric action. Behavioural Brain Research. 2000;**117**(1-2):83-96. DOI: 10.1016/S0166-4328(00)00297-7

[37] Oda S, Shibata M, Moritani T. Force-dependent changes in movement-related cortical potentials. Journal of Electromyography and Kinesiology. 1996;**6**(4):247-252. DOI: 10.1016/S1050-6411(96)00010-7

[38] Nakata H, Sakamoto K, Ferretti A, Perrucci MG, Gratta CD, Kakigi R, et al. Somato-motor inhibitory processing in humans: An event-related functional MRI study. NeuroImage. 2008;**39**(4):1858-1866. DOI: 10.1016/j.neuroimage.2007.10.041

[39] Watanabe J, Sugiura M, Sato K, Sato Y, Maeda Y, Matsue Y, et al. The human prefrontal and parietal association cortices are involved in NO-GO performances: An event-related fMRI study. NeuroImage. 2002;**17**(3):1207-1216. DOI: 10.1006/nimg.2002.1198

[40] Bunno Y, Suzuki T, Iwatsuki H. Motor imagery muscle contraction strength influences spinal motor neuron excitability cardiac sympathetic nerve activity. Journal of Physical Therapy Science. 2015;**27**(12):3793-3798. DOI: 10.1589/jpts.27.3793

[41] Seals DR. Influence of force on muscle and skin sympathetic nerve activity during sustained isometric contractions in humans. The Journal of Physiology. 1993;**462**(1):147-159. DOI: 10.1113/jphysiol.1993.sp019548

[42] Decety J, Jeannerod M, Germain M, Pastene J. Vegetative response during imagined movement is proportional to mental effort. Behavioural Brain Research. 1991;**42**(1):1-5. DOI: 10.1016/S0166-4328(05)80033-6

[43] Malik M, Bigger JT, Camm AJ, Kleiger RE, Malliani A, Moss AJ, et al. Heart rate variability. Standards of measurement, physiological interpretation, and clinical use. Task force of the European Society of Cardiology and the north American Society of Pacing and Electrophysiology. European Heart Journal. 1996;**17**(1):354-381

[44] Bunno Y, Suzuki T, Iwatsuki H. Influence of motor imagery of isometric thenar muscle activity under different muscle contraction strengths on spinal motor neurons' excitability and cardiac sympathetic nerve activity. Rigakuryoho Kagaku. 2016;**31**(1):117-125. (In Japanese). DOI: 10.1589/rika.31.117

[45] Hajduczok G, Hade JS, Mark AL, Williams JL, Felder RB. Central command increases sympathetic nerve activity during spontaneous locomotion in cats. Circulation Research. 1991;**69**(1):66-75. DOI: 10.1161/01.RES.69.1.66

[46] Silber DH, Sinoway LI, Leuenberger UA, Amassian VE. Magnetic stimulation of the human motor cortex evokes skin sympathetic nerve activity. Journal of Applied Physiology. 2000;**88**(1):126-134. DOI: 10.1152/jappl.2000.88.1.126

[47] Clancy JA, Johnson R, Raw R, Deuchars SA, Deuchars J. Anodal transcranial direct current stimulation (tDCS) over the motor cortex increases sympathetic nerve activity. Brain Stimulation. 2014;**7**(1):97-104. DOI: 10.1016/j.brs.2013.08.005

[48] Allen GV, Cechetto DF. Serotoninergic and nonserotoninergic neurons in the medullary raphe system have axon collateral projections to autonomic and somatic cell groups in the medulla and spinal cord. The Journal of Comparative Neurology. 1994;**350**(3):357-366. DOI: 10.1002/cne.903500303

[49] Kwakkel G, Kollen BJ, Wagenaar RC. Therapy impact on functional recovery in stroke rehabilitation: A critical review of the literature. Physiotherapy. 1999;**85**(7):377-391. DOI: 10.1016/S0031-9406(05)67198-2

[50] Nakayama H, Jørgensen HS, Raaschou HO, Olsen TS. Recovery of upper extremity function in stroke patients: The Copenhagen stroke study. Archives of Physical Medicine and Rehabilitation. 1994;**75**(4):394-398. DOI: 10.1016/0003-9993(94)90161-9

[51] Mulder T. Motor imagery and action observation: Cognitive tools for rehabilitation. Journal of Neural Transmission. 2007;**114**(10):1265-1278. DOI: 10.1007/s00702-007-0763-z

[52] Liepert J, Bauder H, Wolfgang HR, Miltner WH, Taub E, Weiller C. Treatment-induced cortical reorganization after stroke in humans. Stroke. 2000;**31**(6):1210-1216. DOI: 10.1161/01.STR.31.6.1210

[53] Pascual-Leon A, Nguyet D, Cohen LG, Brasil-Neto JP, Cammarota A, Hallett M. Modulation of muscle responses evoked by transcranial magnetic stimulation during the acquisition of new fine motor skills. Journal of Neurophysiology. 1995;**74**(3):1037-1045. DOI: 10.1152/jn.1995.74.3.1037

[54] Cicinelli P, Marconi B, Zaccagnini M, Pasqualetti P, Filippi MM, Rossini PM. Imagery-induced cortical excitability changes in stroke: A transcranial magnetic stimulation study. Cerebral Cortex. 2006;**16**(2):247-253. DOI: 10.1093/cercor/bhi103

[55] Wrigley PJ, Gustin SM, Macey PM, Nash PG, Gandevia SC, Macefield VG, et al. Anatomical changes in human motor cortex and motor pathways following complete thoracic spinal cord injury. Cerebral Cortex. 2008;**19**(1):224-232. DOI: 10.1093/cercor/bhn072

[56] Ruffino C, Papaxanthis C, Lebon F. Neural plasticity during motor learning with motor imagery practice: Review and perspectives. Neuroscience. 2017;**347**(1):61-78. DOI: 10.1016/j.neuroscience.2016.11.023

[57] Grosprêtre S, Lebon F, Papaxanthis C, Martin A. New evidence of corticospinal network modulation induced by motor imagery. Journal of Neurophysiology. 2016;**115**(3):1279-1288. DOI: 10.1152/jn.00952.2015

[58] Mercuri B, Wassemann EM, Manqanotti P, Ikoma K, Samii A, Hallett M. Cortical modulation of spinal excitability: An F-wave study. Electroencephalography and Clinical Neurophysiology. 1996;**101**(1):16-24. DOI: 10.1016/0013-4694(95)00164-6

[59] Liu M, Fujiwara T, Shindo K, Kasashima Y, Otaka Y, Tsuji T, et al. Newer challenges to restore hemiparetic upper extremity after stroke: HANDS therapy and BMI neurorehabilitation. Hong Kong Physiotherapy Journal. 2012;**30**(2):83-92. DOI: 10.1016/j.hkpj.2012.05.001

[60] Kaiser V, Kreilinger A, Müller-Putz GR, Neuper C. First steps toward a motor imagery based stroke BCI: New strategy to set up a classifier. Frontiers in Neuroscience. 2011;**5**:86. DOI: 10.3389/fnins.2011.00086

[61] Hwang HJ, Kwon K, Im CH. Neurofeedback-based motor imagery training for brain-computer interface (BCI). Journal of Neuroscience Methods. 2009;**179**(1):150-156. DOI: 10.1016/j.jneumeth.2009.01.015

[62] Oostra KM, Vereecke A, Jones K, Vanderstraeten G, Vingerhoets G. Motor imagery ability in patients with traumatic brain injury. Archives of Physical Medicine and Rehabilitation. 2012;**93**(5):828-833. DOI: 10.1016/j.apmr.2011.11.018

[63] Frolov A, Mokienko O, Lyukmanov R, Biryukova E, Kotov S, Turbina L, et al. Post-stroke rehabilitation training with a motor-imagery-based brain-computer interface (BCI)-controlled hand exoskeleton: A randomized controlled multiceter trial. Frontiers in Neuroscience. 2017;**11**(1):400. DOI: 10.3389/fnins.2017.00400

[64] Takemi M, Masakado Y, Liu M, Ushiba J. Sensorimotor event-related desynchronization represents the excitability of human spinal motoneurons. Neuroscience. 2015;**297**(1):58-67. DOI: 10.1016/j.neuroscience.2015.03.045

Chapter 5

Brain-Computer Interface and Motor Imagery Training: The Role of Visual Feedback and Embodiment

Maryam Alimardani, Shuichi Nishio and Hiroshi Ishiguro

Additional information is available at the end of the chapter

http://dx.doi.org/10.5772/intechopen.78695

Abstract

Controlling a brain-computer interface (BCI) is a difficult task that requires extensive training. Particularly in the case of motor imagery BCIs, users may need several training sessions before they learn how to generate desired brain activity and reach an acceptable performance. A typical training protocol for such BCIs includes execution of a motor imagery task by the user, followed by presentation of an extending bar or a moving object on a computer screen. In this chapter, we discuss the importance of a visual feedback that resembles human actions, the effect of human factors such as confidence and motivation, and the role of embodiment in the learning process of a motor imagery task. Our results from a series of experiments in which users BCI-operated a humanlike android robot confirm that realistic visual feedback can induce a sense of embodiment, which promotes a significant learning of the motor imagery task in a short amount of time. We review the impact of humanlike visual feedback in optimized modulation of brain activity by the BCI users.

Keywords: motor imagery, BCI training, visual feedback, android robot, positive bias, embodiment, performance, neurorehabilitation

1. Introduction

Brain-computer interfaces (BCIs) have been considered for years as a new method of control and communication with the outside world not only for disabled patients who have lost motor control [1, 2] or speech abilities [3], but also for healthy users who are seeking new ways of interaction with virtual reality (VR) environments [4] and gaming applications [5].

However, despite their popularity and potentials, BCIs still remain mostly used inside laboratories and barely commercialized for real-world applications. The main reason behind this slow progress is the lack of reliability and poor performance of the BCI systems [6]. Even the finest BCI classifiers developed to date are not yet able to extract the relevant features from brain activity with high accuracy and robustness, particularly if the activity is recorded with electroencephalography (EEG) and contains noise. Many BCI researchers have made it a quest of their life to develop systems and algorithms that can decode EEG activity with high accuracy [7]. However, beside the algorithms, there is another element in the BCI loop that often gets neglected and that is the human user who is the source of the input signals [6, 8]. Although it has been previously shown that not every user is capable of controlling a BCI, the so-called BCI illiteracy [9], most users can obtain a decent level of "skill" with a few sessions of training.

Motor imagery-based BCIs demand particularly longer training time compared to ERP-based BCIs (such as P300 speller) or BCIs that use steady-state visual-evoked potentials (SSVEPs). This is due to the fact that motor imagery task, the mental rehearsal of a movement without actually performing it, is a counterintuitive task for the majority of individuals. Most users cannot visualize a vivid picture of the movement and its kinesthetic experience. Hwang et al. refer to this as the unknown "feel of motor imagery" [10]. An imaginary action can range from the visualization of a self-performed movement from a first-person perspective, to a third-person view of the self-body movement, to the manipulation of an external object that is either physical or imaginary [11]. Although these types of motor imagery all involve voluntary actions, they may not involve similar cognitive processes. For novice BCI users, the instruction about a motor imagery task is normally given verbally by an experimenter, and it is up to the user to find the optimum image, by trial and error, that leads to a high performance.

On the other hand, similar to any other interface, BCI users should receive feedback of their performance in order to close the control loop between them and the interface. Over years, various feedback paradigms for motor imagery training have been proposed, most of which are based on visual and auditory feedback [12, 13]. One of the main issues in the design of visual feedback in most of motor imagery-based BCIs is that the feedback presentation is not congruent with the subject's image of a bodily movement. For example, in the training paradigm introduced by Pfurtscheller and Neuper, subjects imagined either a right- or a left-hand movement and watched a horizontal feedback bar on a computer screen that was extended to the right or to the left based on the classifier output [12]. Blankertz et al. presented a falling ball on the screen that could be horizontally displaced either to the left or right side if the user's left- or right-hand imagery was successfully detected by the classifier [13]. In another study, Nijboer et al. employed two feedback designs: a visual feedback with a cursor on a screen that moved up and down based on the subject's sensorimotor rhythm and an auditory feedback that presented different types of sound in existence or the absence of motor imagery activation [14]. In all of the given examples, the feedback design that was employed had no congruity with the type of image that the subjects held (image of a bodily hand or a foot). Not only the disparity between the visual feedback and the type of image can confuse the subjects during the task, but it also prevents them from obtaining "the feel of motor imagery" and correcting their imagery strategy.

http://dx.doi.org/10.5772/intechopen.78695

To overcome such a deficiency, some studies have employed a double-modality design. For instance, Chatterjee et al. introduced a vibrotactile feedback paradigm that delivered haptic information during BCI control [15]. Every time subjects imagined a hand movement, the classifier result was presented to them in the form of a cursor movement (visual feedback) and a vibration on their corresponding arm (tactile feedback). A design like this can enormously change the interaction a clinical BCI user has with a neuroprosthesis and may facilitate the decoding of sensorimotor rhythm during neurorehabilitation therapy with BCIs [16]; however, in the case of a healthy user, the application of vibration on a part of body that is not involved in the imagination of movement (arm instead of the hand) can again disturb the conduct of the motor imagery task by the user.

Another commonly faced problem in the BCI training protocols is the lack of motivation for novice users. Motor imagery BCI takes a very long training that is often accompanied with unsuccessful and unsatisfying results in the beginning. It has been shown that motivation [17, 18] along with other mental states such as fatigue and frustration [19] can substantially influence BCI performance. To alleviate this problem, some of the previous studies have given their attention to the design of a more interactive feedback environment by means of virtual reality techniques [18, 20]. A few others have tried to improve users' level of confidence and perception of control over the BCI system by intentionally biasing the presented feedback accuracy [21, 22].

What is important, and often neglected in the BCI research, is that the interaction between a user and the interface is the most critical component in the BCI loop, and therefore an inappropriate training design can hinder the user's learning of the task and BCI skills. In this chapter, we address the importance of training and feedback design in the production and control of the EEG components that are required for a motor imagery-based BCI. We first review research on the compatibility of the feedback appearance with a real human body and its impact on learning of the motor imagery task. We then discuss works that have tried to improve the motivation level of a user either by making the environment playful or by positively faking the performance of the user. In the following, we investigate the role of embodiment, the feeling of owning a controlled body, which has long been disregarded in the BCI research. In the final part of this chapter, we introduce our android-based training paradigm that has exhibited a promising potential for improving motor imagery learning in novice BCI users.

2. Motor imagery and action observation

It has been shown that mental imagery of a motor action can produce cortical activation similar to that of the same action executed [23, 24]. For instance, the execution of a hand movement results in the suppression of mu rhythm (8–12 Hz) in sensorimotor regions and so does the motor imagery of the corresponding hand [25]. By monitoring single-trial EEG signals and measuring event-related desynchronization (ERD), it is even possible to detect whether the imagined hand was the right or the left one [26]. However, previous studies suggest that the detection of hand imagery can only achieve a high rate when the user has employed a kinesthetic motor imagery strategy (first-person process) [27]. In the same study, Neuper et al.

report that the observation of a left- or a right-hand movement could also lead to high classification accuracies at parieto-occipital regions [27]. Many neuroimaging studies have found empirical evidences that combining motor imagery with action observation could induce a stronger cortical activation compared to either condition alone [28]. This has been associated with the firing of mirror neurons [29] that become active during the observation of a motion and represent high-level information about goals and intentions [28]. It also indicates a shared neurocognitive process between motor imagery and action observation that could be utilized in BCI training and control. Particularly, if the action is congruent with the motor imagery, the observed image is a simulation of one's own action, the combination of the two conditions can lead to a "sense of effort," a sense of agency, and imagined kinesthetic sensations that would arise during one's own motor execution [30].

Ono et al. examined the effect of visual feedback on ERD during a motor imagery task [31]. In a series of training sessions, they hired different groups of subjects and trained them on different types of visual feedback, including a conventional feedback bar, a human hand that was shown on a screen in front of the subject and a human hand that was shown on a screen as the extension of one's own arm. They found that by the end of the training, the group that was presented anatomically congruent feedback produced the highest ERD value and classification accuracy. Neuper et al. have also investigated the impact of a visual feedback presentation on sensorimotor EEG rhythms and BCI performance [32]. They trained two groups of subjects on a motor imagery-based BCI using two feedback designs: a realistic feedback (a video of a moving hand that grasped a glass) and an abstract feedback (a moving bar that extended horizontally). Their results, however, showed no difference between the two feedback groups in terms of motor imagery learning and ERD changes. An explanation for this, as authors have indicated in their discussion, could be the short training period and few number of feedback sessions.

With recent advancement in videogames and VR technology, a more rich, realistic, and engaging visual presentation of the BCI output has become possible. Pineda et al. designed a three-dimensional first-person shooter game that enabled BCI users to make navigational movements by left and right motor imageries [33]. Their results indicated that subjects could learn to control levels of mu rhythm very quickly, within approximately 3–10 hours of training that was scheduled over a course of five weeks. Leeb et al. also reported a case study with a tetraplegic patient who was able to navigate through VR by imagination of his feet movements that was translated into movements of an avatar [34]. The most obvious benefits of VR in the construction of visual feedback are the richness of details that could be incorporated, the sense of embodiment it induces (see Section 4), and a relatively low cost. Particularly, in terms of detailed feedback, it can involve different types of movement and inclusion of goal-oriented tasks. Past studies have shown that motor cortex is sensitive to different forms of observed motor behavior [35] and subjective perspective [30, 36]. Muthukumaraswamy et al. have shown that the observation of an object-directed precision grip produces more mu suppression than the observation of a non-object-directed grip [35]. In our previous study, we compared motor imagery learning between two groups of BCI users who operated either a pair of robotic gripper or a pair of humanlike robotic hands [8]. We found a more robust learning of the BCI task for the second group who were trained with a pair of humanlike robotic hands. This result provides evidence that visual

feedback with a more detailed appearance and compatible action to one's real hand can extend larger effect on neural plasticity and reinforcement of motor imagery learning.

It is worth noting that BCI training along with visual feedback of a body movement (action observation) has been employed in neurorehabilitation studies and with stroke patients as well [37–42]. It is suggested that providing anthropomorphic feedback during motor imagery works in a similar way as does mirror therapy for phantom limb patients [39]. That is, providing feedback of a bodily movement can activate neural networks associated with action observation system and induce a "motor resonance" [40]. Thereby by directly matching the observed or imagined action onto the internal simulation of that action, motor resonance can further facilitate the relearning of the impaired motor functions [41]. For instance, Foldes et al. trained spinal cord injury patients with hand paralysis on a motor imagery-based BCI combined with a virtual hand feedback. Results showed that all patients could successfully modulate their brain activity in order to grasp the virtual hand and two of three participants could improve their sensorimotor rhythms in only one session of feedback training [39]. Kim et al. also combined an action observation training with a motor imagery-based BCI and found promising results in terms of actual functional improvements in the upper arm movement of stroke patients [42].

The above review shows that a neurofeedback paradigm that merges motor imagery with the observation of a bodily action has the potential to promote plastic changes in somatosensory activation, the recovery of motor functions, and the improvement of motor performance [43]. In a very similar way, such combination can bring significant benefits to BCI training, by helping the user to activate motor-related cortical areas and generate brain signals that are easily detectable by the BCI classifier.

3. Human factors and BCI learning

To control a BCI, the user has to perform a mental imagery task and generate distinguishable brain activity for signal-processing algorithms. Modulation of one's own brain signals is not an intuitive task, and therefore the user needs to practice and learn the BCI "skill." However, an efficient learning of a skill requires optimized training protocols that consider the user's psychological states (such as motivation, attention, confidence, and satisfaction) in order to ensure more effort and better performance from the user's side [44]. Kleih et al. have shown that in the control of a P300 BCI, the level of P300 amplitude was significantly correlated with the level of self-rated motivation, that is, highly motivated subjects were able to communicate through BCI faster than less motivated subjects [45]. In another BCI study with ALS patients, Nijboer et al. reported that motivational factors, specifically challenge and confidence, were positively correlated with BCI performance, whereas fear had a negative influence [46]. It is suggested that even with highly motivated subjects, users can experience a low level of satisfaction if they do not succeed in accomplishing the BCI-control task [47].

In order to overcome such issues, many researchers have explored alternative BCI training protocols. Leeb et al. suggested employment of VR environments in designing attractive BCI

training paradigms that increase user's engagement [18]. Their results show that users are likely to perform better in a VR navigation task compared to the conventional training with cue-based feedback. Lotte et al. proposed improvement of engagement and motivation in a social context by the application of a BCI game between two users [44]. Users could either participate in a collaborative game, where the sum of the BCI outputs from both users was used to direct a ball on a screen, or in a competitive version, where the users had to push the ball toward the opposite direction. They observed that multiplayer version of the games could effectively improve BCI performance compared to its single player version.

Multimodality and closing the sensorimotor loop has also been suggested as another method to increase user's engagement and performance. Jeunet et al. compared users' performances in a motor imagery-based multi-task BCI with different feedback modalities (visual vs. tactile) and found a significant improvement when subjects received continuous tactile feedback compared to an equivalent visual feedback [48]. This is consistent with the study in [16] where haptic feedback, provided in a synchronized manner with the subject's execution of a motor imagery task, could facilitate decoding of movement intentions and increase classification accuracy for both healthy and stroke patients.

In addition to the above strategies, some studies have proposed manipulation of the feedback either by biasing the feedback accuracy (i.e., giving the user a perception that he/she did better/worse than what he/she actually did) or by error-ignoring (i.e., presenting feedback only when the user performed the task correctly) [21, 22, 49, 50]. Barbero et al. investigated the influence of a biased feedback on BCI performance when subjects navigated a falling ball on a screen by right- and left-hand imageries. They found that subjects with a poor performance benefitted from positive biasing of their performance level, whereas for those already capable of the BCI task, the bias of feedback impeded the results [21]. This is while Gonzalez-Franco et al. found larger learning effects for negative feedback than for positive feedback [49]. In our previous studies with BCI operation of a pair of humanlike robotic hands, we found a general improving effect, both when subjects received a positively biased feedback of their BCI performance and when their mistakes were not presented to them, that is, error ignoring [22]. This improvement could have been associated with the higher sense of embodiment that users experienced during operation of the hands (see Section 4).

Overall, previous research demonstrates that human psychological factors play a significant role in the process of BCI training. It is even suggested that parameters such as personality, motivation, and attention span could predict performance in a single session of motor imagery-based BCI control [51]. Future training environments should take these parameters into account in order to enhance learning of the BCI task as well as to address the problem of "BCI inefficiency" that concerns users who are unable to learn BCI control.

4. The role of embodiment

Recent view of cognitive development suggests that our cognitive skills are dynamically shaped through our bodily interaction with the environment and thus are grounded in

sensory and motor experiences [52, 53]. Under this view, the mind (mental images, thoughts, representation) is created from processes that are closely related to brain representations of the body and the way it interacts with the real world [54]. This fosters the notion of neural plasticity during the learning of new motor skills and tool use that might lead to temporary or long-term incorporation of new objects and augmented cognition [55]. When extended to external body parts (dummy limbs), the experience of embodiment is often described by the two senses of body ownership (to what extent the seen body part was perceived as one's own body) and agency (to what extent the motions of the seen body were attributed to one's own movements) [56]. Although there are some counter arguments [57], embodiment is generally conceived as an important component in establishing interaction between a patient and medical BCIs (such as neural prostheses) for better incorporation of the artificial limb [58]. However, with the recent advancements in VR and robotic technology, the concept of embodiment has also been proposed as a reinforcing factor for immersive experience of healthy users.

The first question, however, is whether BCI control of a non-body object would evoke a sense of embodiment for the operator. Here, we mainly focus on the sense of embodiment that is induced over a humanlike body shape rather than embodiment in physical space and for general objects as it is reported in [59]. Perez-Marcos et al. combined virtual reality and a motor imagery-based BCI in order to induce a sense of ownership for a virtual hand [60]. Although they did not assess motor-related features of the collected EEG signals in this study, they showed that BCI control of a virtual hand could induce an illusion of body ownership and trigger an electromyogram (EMG) response when the virtual hand suddenly fell down. Using a real-time fMRI setup, Cohen et al. also proposed a robotic embodiment for a humanoid robot in France that was remotely controlled by subjects performing motor imagery in Israel [61]. While they did not perform a systematic evaluation of the sense of embodiment and the number of subjects was limited, post-experiment interviews indicated a high level of tele-presence and embodiment for at least two of the four subjects who participated in this study.

In a similar direction, the authors of this chapter have reported an illusion of body ownership for a pair of humanlike robotic hands that were controlled by a BCI system [62]. In this experiment, subjects watched robot's hands from a first-person perspective in a head-mounted display and performed a right or a left motor imagery in order to grasp a lighted ball inside the robot's hands (**Figure 1**). Our subjective (questionnaire) and physiological measurements (skin conductance response) revealed that the subjects experienced a feeling of owning the robot's hands, and this feeling had a significant correlation with their BCI performance [22].

In addition to the enhancement of the immersive experience, the feeling of embodiment has been shown to have a positive impact on neurofeedback training and motor imagery learning at the neural level. Braun et al. reported a sense of ownership for an anthropomorphic robotic hand that was placed in front of the subjects and was controlled by a right motor imagery task [63]. Interestingly, their results indicated a stronger ERD in alpha and beta frequency bands when the robotic hand was in a congruent position (higher embodiment) compared to

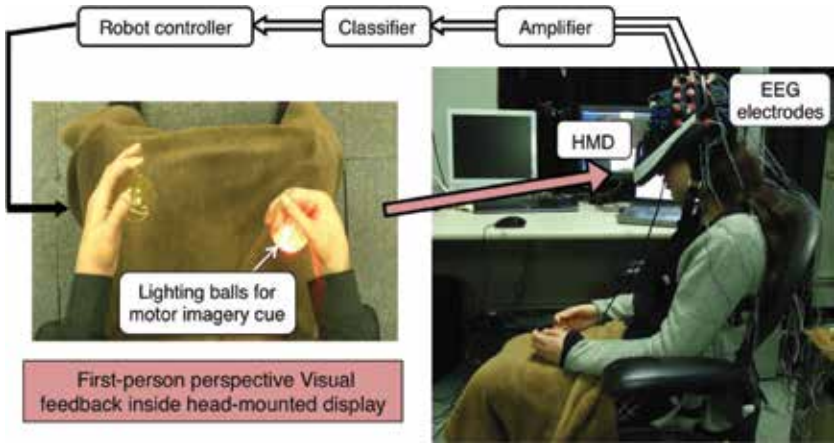

Figure 1. Users controlled a pair of humanlike robotic hands by performing right- and left-hand imageries while watching first-person perspective images of the robot's body.

an incongruent condition. Leeb et al. also compared the influence of feedback types on the motor imagery performance and BCI classification accuracy. They found that an immersive feedback (walking inside a VR environment) resulted in a better task performance by the subjects than a simple BCI feedback (bar presented on a computer screen), although this did not seem to affect the BCI classification accuracy [64].

The results obtained from the above studies are all consistent with our previously reported findings in [8] where subjects practiced motor imagery task in a BCI-control session with two types of feedback (**Figure 2A**). As mentioned earlier in this chapter, subjects who were trained with a more humanlike android robot could perform better on the motor imagery task in the final BCI-control session than those who were trained with a pair of metallic gripper (**Figure 2B**). In this study, "motor imagery performance" was defined as how well subjects could generate discriminant brain patterns for the two classes of right and left motor imageries and it was obtained by the Fisher's discriminant criterion in a linear discriminant analysis that observed the distribution of EEG features [8]. The ΔMotor imagery performance in **Figure 2B** represents the ratio of this criterion between the two evaluations and training sessions (for more details, refer to [8]). In another study, we also reported that in comparison with a classical feedback bar, motor imagery training with a humanlike android feedback that induces a sense of embodiment could lead to a stronger mu suppression in the sensorimotor areas and eventually improved subjects' online BCI performance [65].

Research suggests that cortical connections mediating motor activation are formed through experience [66], making perception-action coupling an important functional factor in the learning of new motor skills [67]. Under this view, a procedural memory of motor programs together with their sensory concomitants is stored during motor learning which gives rise to anticipatory mechanisms that predict sensorimotor outcomes of planned actions in real time

http://dx.doi.org/10.5772/intechopen.78695

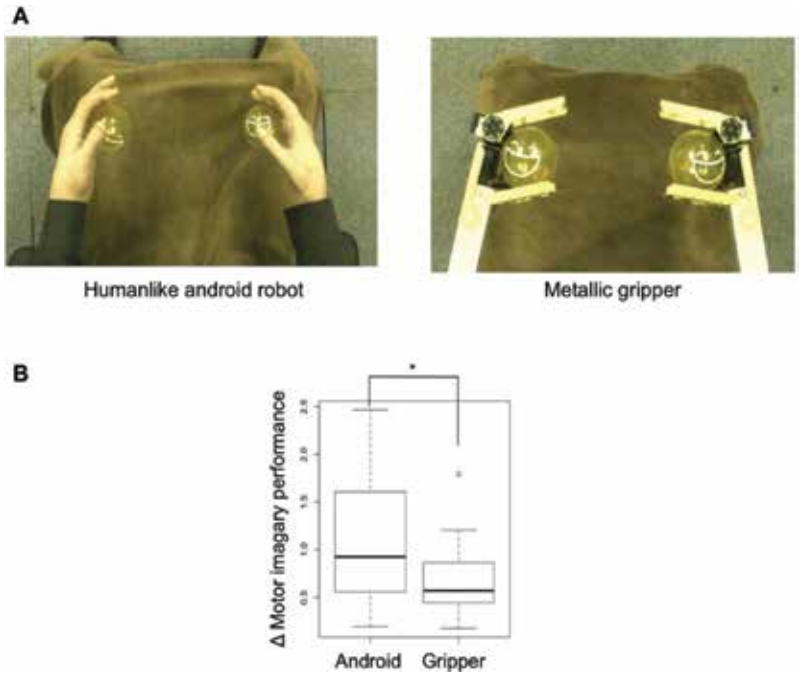

Figure 2. Effect of embodiment on motor imagery learning. (A) Two groups of subjects practiced motor imagery task while receiving visual feedback from a humanlike android robot and a pair of metallic gripper. (B) Subjects who were trained with the android robot demonstrated a significantly more robust learning of the motor imagery task compared to the group who were trained with the non-humanlike gripper.

[11]. The usage of a humanlike android in our studies could have influenced motor imagery learning twofold. First, it is speculated that the visual feedback provided from the android's body resembled a self-body action—as we experience it in our daily activities—and therefore matched with the visual anticipations of the motor intentions. Second, a more detailed and compatible visual feedback from the android's body (in terms of appearance and motion) could have excited motor memories more intensely, and therefore subjects trained with a humanlike android recalled more vivid and explicit images of the movement during the imagery task [8].

Not only that embodiment can reinforce learning of the motor imagery and BCI task, it has also been shown that the two share spectral and anatomical mechanisms [68]. In the study of [68], subjects watched either a pair of virtual arms or a pair of non-body objects projecting out from their body inside a head-mounted display. For both visual feedbacks, they first received a visuotactile stimulation to experience a body ownership illusion similar to rubber hand illusion (RHI) [69], and then they were instructed to perform a motor imagery for either their right or left hand. Their overall results demonstrated that both illusory hand ownership and motor imagery were associated with a mu-band modulation, and more importantly, there was an overlap between the areas that were activated during illusory hand ownership and motor

imagery conditions. This finding suggests that multisensory mechanisms related to the sense of body ownership and embodiment share neural processes with motor imagery and thus could be used in the activation and classification of EEG patterns in BCIs. Indeed, the two processes have been shown to go hand in hand as in [70], we demonstrated that the BCI control of a pair of humanlike robotic hands by means of motor imagery induces a higher sense of body ownership and agency compared to a direct control by means of motor execution. It could be speculated that because of the shared mechanism between embodiment and motor imagery, there is a positive loop effect: motor imagery of the hands induces a strong sense of embodiment and embodiment activates more motor-related neurons detectable by the BCI classifier.

5. Our proposed model

Based on our review in this chapter, we summarize three elements that should be considered in the design of a BCI training protocol:

- Feedback should be realistic and compatible with the task content. Particularly, in a motor imagery-based BCI, users would benefit from observation of movements that are consistent with their mental images.
- Human factors such as motivation, confidence, and fatigue can significantly affect user's interaction with the BCI system and subsequently influence their performance in the BCI task. Employment of interactive environments such as VR and providing positively biased feedback are two techniques that can enhance motor imagery learning particularly for novice BCI users.
- The sense of embodiment and body ownership establishes a positive interaction with subjects' motor imagery performance, and therefore, it is important to provide a realistic visual feedback that resembles a human body in terms of appearance, movement, and perspective.

By integrating the knowledge we obtained in our previous experiments [8, 22, 62] and the abovementioned points, we proposed an android-based training protocol in [65]. In this study, two groups of novice participants practiced hand grasp imagery either by a classical cue-based feedback (arrow and feedback bar) or by watching first-person perspective images of a humanlike android robot that made hand grasps based on the subject's EEG patterns (**Figure 3**). In addition, subjects' performance was positively biased during the training phase in order to boost their confidence and motivation for the motor imagery task. More importantly, we added a pre-training phase for the android group, where subjects could practice motor imagery, followed by kinesthetic motor actions. Results from this study revealed that participants who were trained with an android-based BCI achieved a significantly higher mu suppression in the sensorimotor areas (C3/C4 scalp positions) as well as a significantly better online BCI performance in the final evaluation phase compared to the participants who were trained with a classical training paradigm. We believe that the improved modulation of the sensorimotor rhythms in the proposed

Figure 3. Subjects who were trained with a humanlike android robot and experienced a high sense of embodiment revealed a stronger mu suppression in the sensorimotor areas and showed better BCI performance compared to subjects who were trained with a classical feedback bar.

training protocol is highly influenced by the sense of embodiment that participants perceived during BCI control of the robot's hands.

6. Conclusion

In this chapter, we highlighted the importance of a human user in the BCI loop and addressed some of the deficiencies in the training and feedback design of the classical motor imagery-based BCI systems. We provided empirical evidence that a careful training design that views BCI experience from the user's perspective and considers such factors as task-feedback compatibility, motivation, and embodiment could reinforce users' learning of the motor imagery task and consequently improve their BCI performance in a very short amount of time. We believe that our results are of importance to the BCI community and should be taken into account for future design of BCI systems that are employed in real-world applications outside of laboratories.

Acknowledgements

This research was supported by Grants-in-Aid for Scientific Research 25220004, 26540109, and 15F15046.

Conflict of interest

The authors declare no conflicts of interest.

Author details

Maryam Alimardani[1,2]*, Shuichi Nishio[2] and Hiroshi Ishiguro[2,3]

*Address all correspondence to: m.alimardani@uvt.nl

1 Department of Cognitive Science and Artificial Intelligence, Tilburg University, Tilburg, The Netherlands

2 Advanced Telecommunications Research Institute International (ATR), Kyoto, Japan

3 Department of Systems Innovation, Osaka University, Osaka, Japan

References

[1] Wolpaw JR, Birbaumer N, McFarland DJ, Pfurtscheller G, Vaughan TM. Brain-computer interfaces for communication and control. Clinical Neurophysiology. 2002;**113**(6):767-791

[2] Neuper C, Müller GR, Kübler A, Birbaumer N, Pfurtscheller G. Clinical application of an EEG-based brain-computer interface: A case study in a patient with severe motor impairment. Clinical Neurophysiology. 2003;**114**(3):399-409

[3] Brumberg JS, Nieto-Castanon A, Kennedy PR, Guenther FH. Brain-computer interfaces for speech communication. Speech Communication. 2010;**52**(4):367-379

[4] Lécuyer A, Lotte F, Reilly RB, Leeb R, Hirose M, Slater M. Brain-computer interfaces, virtual reality, and videogames. Computer. 2008;**41**(10):66-72

[5] Nijholt A, Bos DPO, Reuderink B. Turning shortcomings into challenges: Brain-computer interfaces for games. Entertainment Computing. 2009;**1**(2):85-94

[6] Lotte F, Larrue F, Mühl C. Flaws in current human training protocols for spontaneous brain-computer interfaces: Lessons learned from instructional design. Frontiers in Human Neuroscience. 2013;**7**:568

[7] Lotte F, Congedo M, Lécuyer A, Lamarche F, Arnaldi B. A review of classification algorithms for EEG-based brain-computer interfaces. Journal of Neural Engineering. 2007;**4**(2):R1

[8] Alimardani M, Nishio S, Ishiguro H. The importance of visual feedback design in BCIs: From embodiment to motor imagery learning. PLoS One. 2016;**11**(9):e0161945

[9] Guger C, Edlinger G, Harkam W, Niedermayer I, Pfurtscheller G. How many people are able to operate an EEG-based brain-computer interface (BCI)? IEEE Transactions on Neural Systems and Rehabilitation Engineering. 2003;**11**(2):145-147

[10] Hwang HJ, Kwon K, Im CH. Neurofeedback-based motor imagery training for brain-computer interface (BCI). Journal of Neuroscience Methods. 2009;**179**(1):150-156

[11] Annett J. Motor imagery: Perception or action? Neuropsychologia. 1995;**33**(11):1395-1417

[12] Pfurtscheller G, Neuper C. Motor imagery and direct brain-computer communication. Proceedings of the IEEE. 2001;**89**(7):1123-1134

[13] Blankertz B, Dornhege G, Krauledat M, Müller KR, Curio G. The non-invasive Berlin brain-computer interface: Fast acquisition of effective performance in untrained subjects. NeuroImage. 2007;**37**(2):539-550

[14] Nijboer F, Furdea A, Gunst I, Mellinger J, McFarland DJ, Birbaumer N, Kübler A. An auditory brain-computer interface (BCI). Journal of Neuroscience Methods. 2008;**167**(1):43-50

[15] Chatterjee A, Aggarwal V, Ramos A, Acharya S, Thakor NV. A brain-computer interface with vibrotactile biofeedback for haptic information. Journal of Neuroengineering and Rehabilitation. 2007;**4**(1):40

[16] Gomez-Rodriguez M, Peters J, Hill J, Schölkopf B, Gharabaghi A, Grosse-Wentrup M. Closing the sensorimotor loop: Haptic feedback facilitates decoding of motor imagery. Journal of Neural Engineering. 2011;**8**(3):036005

[17] Kleih SC, Riccio A, Mattia D, Kaiser V, Friedrich EVC, Scherer R, Kübler A. et al. Motivation influences performance in SMR-BCI. na. In: Proceeding of the 5th International Brain-Computer Interface Conference. 2011:108-111

[18] Leeb R, Lee F, Keinrath C, Scherer R, Bischof H, Pfurtscheller G. Brain-computer communication: Motivation, aim, and impact of exploring a virtual apartment. IEEE Transactions on Neural Systems and Rehabilitation Engineering. 2007;**15**(4):473-482

[19] Myrden A, Chau T. Effects of user mental state on EEG-BCI performance. Frontiers in Human Neuroscience. 2015;**9**:308

[20] Ron-Angevin R, Díaz-Estrella A. Brain-computer interface: Changes in performance using virtual reality techniques. Neuroscience Letters. 2009;**449**(2):123-127

[21] Barbero Á, Grosse-Wentrup M. Biased feedback in brain-computer interfaces. Journal of Neuroengineering and Rehabilitation. 2010;**7**(1):34

[22] Alimardani M, Nishio S, Ishiguro H. Effect of biased feedback on motor imagery learning in BCI-teleoperation system. Frontiers in Systems Neuroscience. 2014;**8**:52

[23] Jeannerod M, Frak V. Mental imaging of motor activity in humans. Current Opinion in Neurobiology. 1999;**9**(6):735-739

[24] Jeannerod M. The representing brain: Neural correlates of motor intention and imagery. Behavioral and Brain Sciences. 1994;**17**(2):187-202

[25] Pfurtscheller G, Neuper C. Motor imagery activates primary sensorimotor area in humans. Neuroscience Letters. 1997;**239**(2-3):65-68

[26] Pfurtscheller G, Brunner C, Schlögl A, Da Silva FL. Mu rhythm (de) synchronization and EEG single-trial classification of different motor imagery tasks. NeuroImage. 2006;**31**(1):153-159

[27] Neuper C, Scherer R, Reiner M, Pfurtscheller G. Imagery of motor actions: Differential effects of kinesthetic and visual-motor mode of imagery in single-trial EEG. Cognitive Brain Research. 2005;**25**(3):668-677

[28] Sale P, Franceschini M. Action observation and mirror neuron network: A tool for motor stroke rehabilitation. European Journal of Physical and Rehabilitation Medicine. 2012;**48**(2):313-318

[29] Rizzolatti G, Fadiga L, Gallese V, Fogassi L. Premotor cortex and the recognition of motor actions. Cognitive Brain Research. 1996;**3**(2):131-141

[30] Vogt S, Di Rienzo F, Collet C, Collins A, Guillot A. Multiple roles of motor imagery during action observation. Frontiers in Human Neuroscience. 2013;**7**:807

[31] Ono T, Kimura A, Ushiba J. Daily training with realistic visual feedback improves reproducibility of event-related desynchronisation following hand motor imagery. Clinical Neurophysiology. 2013;**124**(9):1779-1786

[32] Neuper C, Scherer R, Wriessnegger S, Pfurtscheller G. Motor imagery and action observation: Modulation of sensorimotor brain rhythms during mental control of a brain-computer interface. Clinical Neurophysiology. 2009;**120**(2):239-247

[33] Pineda JA, Silverman DS, Vankov A, Hestenes J. Learning to control brain rhythms: Making a brain-computer interface possible. IEEE Transactions on Neural Systems and Rehabilitation Engineering. 2003;**11**(2):181-184

[34] Leeb R, Friedman D, Müller-Putz GR, Scherer R, Slater M, Pfurtscheller G. Self-paced (asynchronous) BCI control of a wheelchair in virtual environments: A case study with a tetraplegic. Computational Intelligence and Neuroscience. 2007;**2007**:7

[35] Muthukumaraswamy SD, Johnson BW, McNair NA. Mu rhythm modulation during observation of an object-directed grasp. Cognitive Brain Research. 2004;**19**(2):195-201

[36] Ruby P, Decety J. Effect of subjective perspective taking during simulation of action: A PET investigation of agency. Nature Neuroscience. 2001;**4**(5):546

[37] i Badia SB, Morgade AG, Samaha H, Verschure PFMJ. Using a hybrid brain computer interface and virtual reality system to monitor and promote cortical reorganization through motor activity and motor imagery training. IEEE Transactions on Neural Systems and Rehabilitation Engineering. 2013;**21**(2):174-181

[38] Machado S, Araújo F, Paes F, Velasques B, Cunha M, Budde H, Piedade R, et al. EEG-based brain-computer interfaces: An overview of basic concepts and clinical applications in neurorehabilitation. Reviews in the Neurosciences. 2010;**21**(6):451-468

[39] Foldes ST, Weber DJ, Collinger JL. MEG-based neurofeedback for hand rehabilitation. Journal of Neuroengineering and Rehabilitation. 2015;**12**(1):85

[40] Van Dokkum LEH, Ward T, Laffont I. Brain computer interfaces for neurorehabilitation—Its current status as a rehabilitation strategy post-stroke. Annals of Physical and Rehabilitation Medicine. 2015;**58**(1):3-8

[41] Holper L, Muehlemann T, Scholkmann F, Eng K, Kiper D, Wolf M. Testing the potential of a virtual reality neurorehabilitation system during performance of observation,

imagery and imitation of motor actions recorded by wireless functional near-infrared spectroscopy (fNIRS). Journal of Neuroengineering and Rehabilitation. 2010;**7**(1):57

[42] Kim T, Kim S, Lee B. Effects of action observational training plus brain-computer interface-based functional electrical stimulation on paretic arm motor recovery in patient with stroke: A randomized controlled trial. Occupational Therapy International. 2016;**23**(1):39-47

[43] Wang W, Collinger JL, Perez MA, Tyler-Kabara EC, Cohen LG, Birbaumer N, Weber DJ, et al. Neural interface technology for rehabilitation: Exploiting and promoting neuroplasticity. Physical Medicine and Rehabilitation Clinics. 2010;**21**(1):157-178

[44] Lotte F, Jeunet C. Towards improved BCI based on human learning principles. In: 2015 3rd International Winter Conference on Brain-Computer Interface (BCI). Sabuk, South Korea: IEEE; January 2015. pp. 1-4

[45] Kleih SC, Nijboer F, Halder S, Kübler A. Motivation modulates the P300 amplitude during brain-computer interface use. Clinical Neurophysiology. 2010;**121**(7):1023-1031

[46] Nijboer F, Birbaumer N, Kubler A. The influence of psychological state and motivation on brain-computer interface performance in patients with amyotrophic lateral sclerosis – A longitudinal study. Frontiers in Neuroscience. 2010;**4**:55

[47] Spataro R, Chella A, Allison B, Giardina M, Sorbello R, Tramonte S, La Bella V, et al. Reaching and grasping a glass of water by locked-In ALS patients through a BCI-controlled humanoid robot. Frontiers in Human Neuroscience. 2017;**11**:68

[48] Jeunet C, Vi C, Spelmezan D, N'Kaoua B, Lotte F, Subramanian S. Continuous tactile feedback for motor-imagery based brain-computer interaction in a multitasking context. In: Human-Computer Interaction. Cham: Springer; September 2015. pp. 488-505

[49] Gonzalez-Franco M, Yuan P, Zhang D, Hong B, Gao S. Motor imagery based brain-computer interface: A study of the effect of positive and negative feedback. In: Engineering in Medicine and Biology Society, EMBC, 2011 Annual International Conference of the IEEE; Boston, MA, USA: IEEE; August 2011. pp. 6323-6326

[50] Yu T, Xiao J, Wang F, Zhang R, Gu Z, Cichocki A, Li Y. Enhanced motor imagery training using a hybrid BCI with feedback. IEEE Transactions on Biomedical Engineering. 2015;**62**(7):1706-1717

[51] Hammer EM, Halder S, Blankertz B, Sannelli C, Dickhaus T, Kleih S, Kübler A, et al. Psychological predictors of SMR-BCI performance. Biological Psychology. 2012;**89**(1): 80-86

[52] Schöner G. Dynamical systems approaches to cognition. In: Cambridge Handbook of Computational Psychology (Cambridge Handbooks in Psychology). Cambridge: Cambridge University Press; 2008. pp. 101-126

[53] Smith LB. Movement matters: The contributions of Esther Thelen. Biological Theory. 2006;**1**(1):87-89

[54] Gibbs RW Jr. Embodiment and Cognitive Science. Cambridge: Cambridge University Press; 2005

[55] Clark A. Re-inventing ourselves: The plasticity of embodiment, sensing, and mind. Journal of Medicine and Philosophy. 2007;**32**(3):263-282

[56] Tsakiris M. My body in the brain: A neurocognitive model of body-ownership. Neuropsychologia. 2010;**48**(3):703-712

[57] Aas S, Wasserman D. Brain-computer interfaces and disability: Extending embodiment, reducing stigma? Journal of Medical Ethics. 2016;**42**(1):37-40

[58] Tyler DJ. Neural interfaces for somatosensory feedback: Bringing life to a prosthesis. Current Opinion in Neurology. 2015;**28**(6):574

[59] LaFleur K, Cassady K, Doud A, Shades K, Rogin E, He B. Quadcopter control in three-dimensional space using a noninvasive motor imagery-based brain-computer interface. Journal of Neural Engineering. 2013;**10**(4):046003

[60] Perez-Marcos D, Slater M, Sanchez-Vives MV. Inducing a virtual hand ownership illusion through a brain-computer interface. Neuroreport. 2009;**20**(6):589-594

[61] Cohen O, Druon S, Lengagne S, Mendelsohn A, Malach R, Kheddar A, Friedman D. fMRI-based robotic embodiment: Controlling a humanoid robot by thought using real-time fMRI. Presence Teleoperators and Virtual Environments. 2014;**23**(3):229-241

[62] Alimardani M, Nishio S, Ishiguro H. Humanlike robot hands controlled by brain activity arouse illusion of ownership in operators. Scientific Reports. 2013;**3**:2396

[63] Braun N, Emkes R, Thorne JD, Debener S. Embodied neurofeedback with an anthropomorphic robotic hand. Scientific Reports. 2016;**6**:37696

[64] Leeb R, Keinrath C, Friedman D, Guger C, Scherer R, Neuper C, Pfurtscheller G, et al. Walking by thinking: The brainwaves are crucial, not the muscles! Presence Teleoperators and Virtual Environments. 2006;**15**(5):500-514

[65] Penaloza CI, Alimardani M, Nishio S. Android feedback-based training modulates sensorimotor rhythms during motor imagery. IEEE Transactions on Neural Systems and Rehabilitation Engineering. 2018;**26**(3):666-674

[66] Heyes C, Bird G, Johnson H, Haggard P. Experience modulates automatic imitation. Cognitive Brain Research. 2005;**22**(2):233-240

[67] Thelen E. Motor development: A new synthesis. American Psychologist. 1995;**50**(2):79

[68] Evans N, Blanke O. Shared electrophysiology mechanisms of body ownership and motor imagery. NeuroImage. 2013;**64**:216-228

[69] Botvinick M, Cohen J. Rubber hands 'feel' touch that eyes see. Nature. 1998;**391**(6669):756

[70] Alimardani M, Nishio S, Ishiguro H. Removal of proprioception by BCI raises a stronger body ownership illusion in control of a humanlike robot. Scientific Reports. 2016;**6**:33514

Section 4

Advancing Syntactical Options in BCI Therapy

Chapter 6

SSVEP-Based BCIs

Rajesh Singla

Additional information is available at the end of the chapter

http://dx.doi.org/10.5772/intechopen.75693

Abstract

This chapter describes the method of flickering targets, eliciting fundamental frequency changes in the EEG signal of the subject, used to drive machine commands after interpretation of user's intentions. The steady-state response of the changes in the EEG caused by events such as visual stimulus applied to the subject via a computer screen is called steady-state visually evoked potential (SSVEP). This feature of the EEG signal can be used to form a basis of input to assistive devices for locked in patients to improve their quality of life, as well as for performance enhancing devices for healthy subjects. The contents of this chapter describe the SSVEP stimuli; feature extraction techniques, feature classification techniques and a few applications based on SSVEP based BCI.

Keywords: EEG, SSVEP, BCI, BCI-wheelchair, ITR, evoked potential, EEG assistive devices

1. Introduction

1.1. Evoked potential

Evoked potentials (EP) are the electrical signals measured from the scalp after the stimulation rendered by some external stimulus. Corresponding to various stimuli, evoked potentials are distinguished as visual, auditory and somatosensory evoked potentials.

Event related potential (ERP) implies both EP and brain responses prompted by cognitive processes evolved by external stimuli or precursory mechanisms for motor action [1, 2].

1.2. Visual evoked potential

Visual evoked potentials (VEPs) are the brain activity modulations occurring in the visual cortex after encountering visual stimulus [3]. They are easy to detect as the movement of stimulus closer to the central visual field immensely enhances the amplitude of VEPs [4].

Based on following criteria, VEPs are classified into different categories [5]:

i. Morphology of the optical stimuli

- **a.** VEPs caused by flash stimulation
- **b.** VEPs caused by graphic patterns like checkerboard lattice, gate

ii. Frequency of visual stimulation

- **a.** Transient VEPs (TVEPs): VEPs with visual stimulation frequency below 6 Hz
- **b.** Steady-state VEPs (SSVEPs): VEPs with visual stimulation frequency above 6 Hz [3, 6]

iii. Field stimulation

- **a.** Whole field VEPs
- **b.** Half field VEPs
- **c.** Part field VEPs

While the user needs to gaze at the screen and keep his eyes fixed on one particular point. These exogenous signals are not suitable while dealing with advanced level amyotrophic lateral sclerosis (ALS) patients or users with uncontrollable eye or neck movements [7].

1.3. Steady-state visual evoked potential

Regan experimented with long trains of stimuli that comprised of sinusoidally modulated monochromatic light [8]. Small amplitude stable VEP were generated which were entitled "steady-state" visually evoked potentials (SSVEPs) of the human visionary system. There hence, steady-state visual evoked potentials (SSVEPs) are defined as the potential elicited by the change in the visual field with the frequency higher than 6 Hz.

When a user is presented with some periodic stimuli, SSVEP is generated strongly at the occipital areas of the brain [10]. SSVEP is usually acquired from various electrode sites like Oz, O1, O2, Pz, P3, P4, and some surrounding locations to occipital region. While the most commonly used SSVEP frequency range is 4–60 Hz, the resonance phenomenon is generally observed around 10, 20, 40 and 80 Hz [11].

1.4. Feature extraction

Various features are procured from the properties of the brain signals that have discriminative information embedded in them. Various feature extraction techniques are used to extract such features when overlapped in time and space by several brain signals.

The feature extraction in SSVEP signals was often done with the study of amplitude in the target frequency [12–14], followed by independent component analysis (ICA) [16], the fast Fourier transform (FFT) [15], continuous wavelet transform (CWT) [17, 18], Hilbert-Huang transform (HHT) [19, 20] or the PSD [21] can be used.

1.4.1. Independent component analysis (ICA)

ICA follows a statistical procedure for separating a set of mixed signals into its sources without any presumptuous information regarding the nature of the signal. The only criteria that need to be followed are that the unspecified underlying sources must be statistically mutually independent. ICA can express an EEG signal as following:

$$x(t) = f(s(t)) + n(t) \tag{1}$$

where, f is some unknown mixer function, s(t) is the source vector, n(t) is the additive arbitrary noisy vector and x(t) is the resultant EEG signal. ICA mainly follows two approaches: spatial ICA that extricates out independent spatial maps and temporal ICA that extricates out independent time courses.

EEG over the visual cortex was fragmented into SSVEP signals and background noise using ICA in the study by Wang et al. [16].

1.4.2. Fast Fourier transform (FFT)

Fourier transform (FT) comprises fast Fourier transform (FFT) and fiscrete Fourier transform (DFT). Wang et al. used 256-point FFT for transforming EEG signals to corresponding frequency domain representation. This was represented in terms of five frequencies: 9, 11, 13, 15 and 17 Hz [21]. Mouli et al. considered the maximum amplitudes of the FFT as the prime parameter for differentiating various target stimuli of 7, 8, 9 and 10 Hz [22].

1.4.3. Spatial filtering

The most commonly endorsed EEG recording methods emanated monopolar signals or Laplacian filtered signals. For example, channel Oz consisted as follows:

$$\text{Monopolar: } y^{M}_{Ox} = y_{Ox} - y_{A2}$$

$$\text{Laplacian: } y^{L}_{Ox} = y^{M}_{Ox} - \frac{y^{M}_{O1} + y^{M}_{O2}}{2}$$

Laplacian signals are extracted considering both the sides (like Cz utilizes C3 and C4) [23].

1.4.4. Continuous wavelet transform (CWT)

Wavelet transform (WT) is best suited to extract information from nonstationary signals as it extends a versatile method for representation of time-frequency of a signal [24]. CWT is basically the convolution of signal with the wavelet function [25]:

$$w(s, \tau) = \int_{-\infty}^{\infty} x(t)\psi * (t)dt \tag{2}$$

where, ψ*(t) is the complex conjugate wavelet function, x(t) is the particular function and w(s,τ) is the wavelet coefficient corresponding to frequency related with scale s and time τ of the involved wavelet function. CWT works like template matching just like matched filter where cross variance is calculated for the signal and some predefined waveform [26].

Zhang et al. established the use of CWT technique for extracting features and classifying them in SSVEP-based BCI [16]. Kumari et al. transformed the CWT coefficients into feature vectors for tracing out the site of high frequency SSVEP components [17].

1.4.5. Hilbert-Huang transform (HHT)

HHT is a self-adaptive data analysis technique comprising empirical mode decomposition (EMD) and Hilbert spectral analysis (HAS) [27]. It can opt stationary and non-stationary signals analysis. An intrinsic mode function (IMF) is an oscillator function with time-varying frequencies capable of depicting the local properties of non-stationary signals [28].

Huang et al. identified high frequency SSVEP signals using HHT in SSVEP-based BCI [18]. HHT remodeled the original signals into 11-order IMF with the help of EMD.

1.5. Feature classification

The classification algorithms designate boundaries between various targets in the feature space on the basis of feature vectors involved considering the as independent variables.

The classification methods for SSVEP signals are heterogeneous in nature, like Bayesian classifier [14], linear discriminant classifier (LDA) [29–31], support vector machine (SVM) [32–35], k-nearest neighbor (k-NNC) [31, 36].

1.5.1. Bayesian classifier

Bayesian statistical classifier obtains the posterior probability P(y | x) as per prior probability of a feature vector for belonging to some particular class. The class that has got the maximum probability is the one to which the particular feature vector belongs.

$$P(y \mid x) = \frac{P(y)P(x \mid y)}{P(x)} \tag{3}$$

1.5.2. Linear discriminant classifier (LDA)

LDA or Fisher's LDA (FLDA) classifies the data into various classes using hyper planes [36]. This classifier is successfully applied in BCI community despite of high computational time involvement. This classifier traces out an optimal projection that maximizes the distance

between the classes. The decision hyper plane that divides the feature space into various classes is perpendicular to the projection direction [37]. The hyper plane is expressed as:

$$m(x) = w^{T}x + w_o \quad (4)$$

where, w, x and w_o implies the weight vector, the input feature vector and the threshold, respectively.

1.5.3. Support vector machine (SVM)

SVM classifies the feature vectors into various classes by the concept of construction of one or more hyper planes. This classifier differs from LDA, as in this, the decision boundary or hyper plane escalates the margins that implies, the distance between the decision boundary and the training sample nearest to it [38]. While the hyper plane separates the training data set with maximal margin, it also maps them to a higher dimensional space [39]. The decision boundary followed up in SVM may be linear as well as non-linear depending upon the choice of kernel function (linear, cubic, polynomial, Gaussian or radial basis (RBF)) [40].

1.6. k-Nearest neighbor (k-NNC)

The classification principle of k-NNC is that the features belonging to different classes get flocked up in different clusters while keeping the adjacent neighbors in one cluster. It considers k metric distances between the testing dataset features and those of the nearest classes for classifying a test feature vector. Although classification with k-NNC reduces the error probability in the decision but still it is not so commonly used in BCI community [41].

2. SSVEP in BCIs

A BCI is an artificial intelligence system that has the ability to identify particular set of patterns in the brain signals to provide an additional output channel for the control of artificial devices like restoring motor function, robot arm, communication program, etc. [43, 44]. SSVEPs based BCIs are classified into following categories:

- **i.** Time modulated VEP (t-VEP) BCI: In this BCI, the follow up of flash sequences of various stimuli are orthogonal in time, that is, they are strictly non overlapping or stochastic in nature.
- **ii.** Frequency modulated VEP (f-VEP) BCI: In this BCI, stimuli are made to flash at some exclusive frequency and the potential evoked is generated with the fundamental frequency same as that of the stimuli as it harmonics.

iii. Pseudorandom code modulated (c-VEP) BCI: In this BCI, a pseudorandom sequence defines the duration of ON and OFF states of each stimulus. This mode yields highest communication speed.

2.1. Stimulus types

In SSVEP-based experiments, the user is asked to identify the target with eye-gaze. The attention of the user is supposed to be visually fixed on the target and the target is identified by feature extraction and its analysis [42]. In case of single graphic stimuli, stimulus appears and disappears at some particular rate just like displayed in **Figure 1**. In case of pattern reversal stimuli, at least two graphical patterns are displayed by alternative oscillations like shown in **Figure 2**. Such stimulus maybe of checkerboard or grating type.

With flashing stimulus, SSVEP appears as a sinusoidal-like waveform with fundamental frequency as that of blinking frequency of the stimulus. With graphic pattern stimulus, SSVEP appears at the reversal rate and their harmonics [8]. The SSVEP discrete frequency components stay intently constant in terms of amplitude and phase for long time [9].

2.2. Applications of SSVEP in BCI's

2.2.1. SSVEP for BCI based wheelchair

Singla in 2014 spearheaded the research on the effects of stimuli color, of the flickering targets, on the accuracy of decision making to drive a wheelchair. In the study, SSVEPs were selected as compared to VEP because they are less vulnerable to artifacts produced by the eye blinks, eye movements as well as EMG noise [44].

SSVEP data was acquired, which originated due to four different flickering target frequencies, from the occipital region of the brain. The frequency features of the data were extracted using fast Fourier transform (FFT) and wavelet transform (WT). Three different classification methods were tried, two based on ANN with back propagation algorithm and one based on

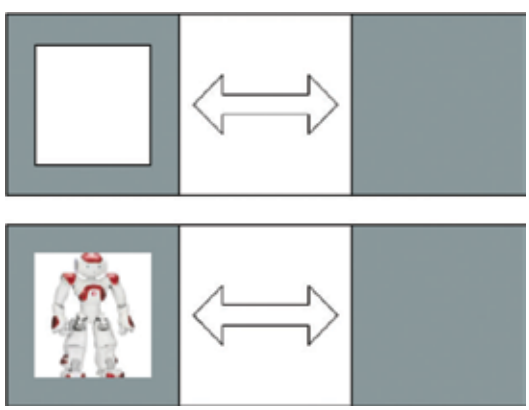

Figure 1. Single graphic stimuli.

http://dx.doi.org/10.5772/intechopen.75693

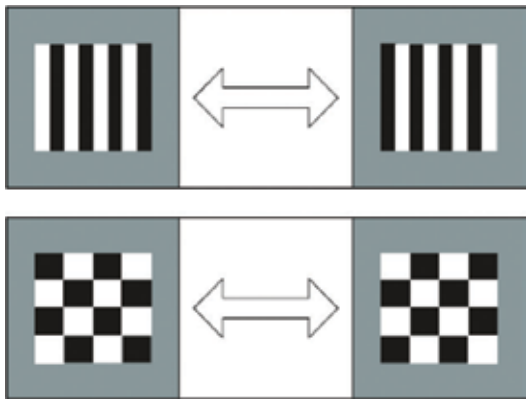

Figure 2. Pattern reversal stimuli.

SVM with One against All (OAA) strategy. The control signals were assigned for each of the five classes detected (7, 9, 11, 13 and rest signal). Corresponding to five classes, five movement positions such as forward (F), backward (B), left (L), right (R) and stop (S) were obtained.

The SSVEP stimulus produces a response in the EEG signal, which is characterized by oscillations of the order of the stimulation frequency and sometimes at harmonics or sub harmonics of it. The visual system can be divided into three subsystems [45].

(i) Low frequency subsystem (near 10 Hz). It gives the greatest SSVEP amplitudes.

(ii) Medium frequency subsystem (16–18 Hz). It gives medium amplitude.

(iii) High frequency subsystem (40–50 Hz). It shows the smallest response.

The ability of the human eye to distinguish colors is based upon the varying sensitivity of cone cells to the light of different wavelengths [46]. There are three kinds of cone cells and are conventionally labeled as short (S), medium (M), and long (L) cones according to the wavelengths of the peaks of their spectral sensitivities. S, M and L cone cells are therefore sensitive to blue (short-wavelength), green (medium-wavelength) and red (long-wavelength) light respectively. The brain combines the information from each cone cells to give different perceptions for different colors and as a result the SSVEP strength elicited with different colors of the stimuli will be different [46]. In this work blue, green, red and violet were selected as stimuli colors to explore how different colors influence the elicited SSVEPs and the performance of SSVEP based system.

The research used, repetitive visual stimuli (RVS) with four different flickering frequencies was designed by using LabVIEW software (National Instrument Inc., USA). The front panel of RVS is shown in **Figure 3**. RVS with violet, red, green and blue flickering bars were designed as four different sets. The back ground color of the RVS was selected as black. The visual stimuli were square (4 × 4 cm) in shape and were placed on the four corners of the LCD screen. Four frequencies 7, 9, 11 and 13 Hz, i.e., in the low frequency range were selected by considering 60 Hz refreshing rate of LCD monitor [45]. In order to select any particular stimuli the four visual stimuli were separated in pair of two each, i.e., 7, 11 and 9, 13. Further in an interval of

Figure 3. Visual stimuli with four different flickering frequencies.

2 s if eye blink once then first pair is selected, i.e., 7, 11 and if eye is blinked twice then the next pair is selected, i.e., 9, 13. Once a pair of stimuli is selected then again in next interval of 2 s if eye blink once then upper stimuli is selected and if it is blinked twice then the lower stimuli is selected in that pair of stimuli.

The research used, repetitive visual stimuli (RVS) with four different flickering frequencies was designed by using LabVIEW software (National Instrument Inc., USA). The front panel of RVS is shown in **Figure 3**. RVS with violet, red, green and blue flickering bars were designed as four different sets. The back ground color of the RVS was selected as black. The visual stimuli were square (4 × 4 cm) in shape and were placed on the four corners of the LCD screen. Four frequencies 7, 9, 11 and 13 Hz, i.e., in the low frequency range were selected by considering 60 Hz refreshing rate of LCD monitor [45].

In order to select any particular stimuli the four visual stimuli were separated in pair of two each, i.e., 7, 11 and 9, 13. Further in an interval of 2 s if eye blink once then first pair is selected, i.e., 7, 11 and if eye is blinked twice then the next pair is selected, i.e., 9, 13. Once a pair of stimuli is selected then again in next interval of 2 s if eye blink once then upper stimuli is selected and if it is blinked twice then the lower stimuli is selected in that pair of stimuli.

The EEG signals recorded from each channel were digitized and segmented into 1-s time window in every 0.25 s. The coefficients of first (fundamental frequency) and second harmonic of all the four target frequencies were considered as the feature vector for classification. It can be seen from **Table 1** that for SSVEP input of 7 Hz, maximum values of amplitude exists at 7, followed by 14.

In case of ANN, there were total eight parameters (first and second harmonics of all the four frequencies) so the input vector contains eight rows. Another set of Q target vectors (the correct output vectors in four digits for each of the input vectors) formed a second matrix. They developed wheelchair prototype to control in forward, backward, left, right and stop positions. The schematic representation of the BCI wheelchair control is shown in **Figure 4**. The wheelchair prototype is shown in **Figure 5**. Motor driver IC, L293D (www.instructables.com)

7	14	9	18	11	22	13	26	Stimulus frequency (Hz)
27.62	8.01	9.2	5.25	5.50	1.81	4.61	1.40	7
18.21	7.40	6.97	1.42	7.92	2.34	0.99	2.38	7
2.65	4.17	23.02	9.91	9.2	1.15	1.00	2.22	9
3.57	6.02	20.4	7.83	4.04	2.52	0.70	1.13	9
11.72	3.62	2.25	2.92	19.91	5.20	3.91	2.24	11
6.83	4.60	4.7	2.40	14.22	3.40	1.42	1.40	11
3.27	6.82	11.83	4.85	9.19	2.02	16.63	4.83	13
8.81	3.82	12.7	5.25	3.62	0.91	14.22	5.66	13
4.75	6.60	5.00	1.09	2.55	1.42	6.48	1.53	Relax
2.44	3.14	5.06	2.34	3.62	1.65	6.36	3.11	Relax

Table 1. Samples of extracted feature components of different frequencies and relax state for two subjects.

was used. By changing the polarity of the signal given to the motors, it moves each of the motors in both forward and backward directions [32].

2.2.2. SSVEP based BCI as independent application for locked-in syndrome

Lesenfants et al. in [47] conducted studies with a basic aim of developing independent SSVEP based BCI applications for locked in patients. Lesenfants et al. used the covert attention of healthy as well as locked-in patients by developing an independent, covert two-class paradigm of flashing targets. The study was divided over two groups of subjects. Group A consisted of 12 healthy subjects and Group B consisted of 12 healthy and 6 Locked-in Syndrome (LIS) patients. For both the groups 12 channels of EEG were recorded (P3, P1, P2, P4, PO7, PO3, POz, PO4, PO8, O1, Oz, and O2).

The visual stimulation was delivered via a custom made stimulus device, which had two subsystems: a control unit and a stimulation panel, based on the paradigm introduced in [48].

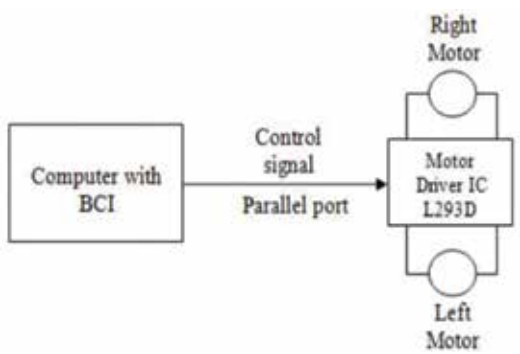

Figure 4. Schematic representation of BCI-based wheelchair control.

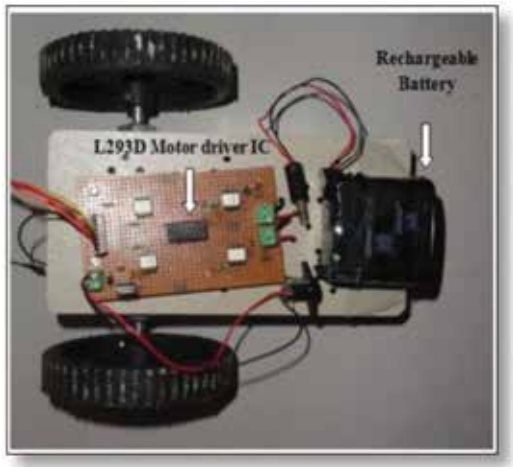

Figure 5. Wheelchair prototype for SSVEP-based BCI control.

The panel, placed at 30 cm from subject's head, was a 7 × 7 cm^2 "interlaced square" made of red and yellow 1 × 1 cm^2 light emitting diode (LED) - squares with a white fixation cross in the middle (**Figure 6**).

The yellow squares (represented by white squares here) flicker at the frequency of 10 Hz. The red squares (represented by grey squares here) flash at 14 Hz.

The interlaced square pattern showed a 10% improvement in accuracy in comparison with a "line" pattern [49]. The control unit was designed to precisely control the red and yellow flickering frequencies independently between 1 and 99 Hz by microcontroller based circuit.

Figure 6. Electronic visual stimulation unit.

The yellow and red squares were programmed to flicker at 10 and 14 Hz, respectively. The pattern was composed of two 2 × 2 cm^2 blocks made of 1 × 1 cm^2 LED squares separated by 12 cm with a white fixation cross in between (**Figure 7**).

The subjects were asked 33 yes/no questions (e.g., "is your name Paul?"). To answer "yes," the subjects had to focus their attention over yellow flashes for 7 s or over the red for "no." Epochs of 7 s were used as a unique window, where after four different feature extraction algorithms like DFT, multitaper spectral analysis (PMTM) [53, 54], CCA, lock-in analyser system (LAS) [49–51]. A automatic channel selection algorithm (ACSA) based on distinction sensitive learning vector quantization (DSLVQ) [52] selected an optimal channel set specific to each subject out of the 12 available channels. Classification was performed using LDA or a SVM (linear kernel), and assessed with a 10 × 10 fold cross validation.

PMTM obtained maximum accuracy of 77.0 ± 3.4% averaged over subject population, while LAS produced a similar mean accuracy of 74.4 ± 3.2% (**Tables 2** and **3**). DFT and CCA gave worse results as compared to PMTM and LAS (respectively, 69.4 ± 3.4% and 58.4 ± 3.9%).

Another comparison was done with the results obtained from the feature extraction methods using the ACSA as well as a single harmonic. PMTM and LAS produced significantly greater accuracy than DFT and CCA, with an accuracy of 84.7 ± 2.0 and 83.1 ± 2.3%, respectively. DFT obtained a 79.3 ± 2.7% accuracy and CCA was able to attain 72.4 ± 1.6% but in only five out of the 10 subjects. The performance with and without ACSA could therefore not be compared with CCA. For a single harmonic, a significant mean accuracy increase of 7.8% for PMTM, 7.9% for LAS and 7.6% for DFT was obtained.

2.2.3. SSVEP based virtual gaming application

Martišius and Damaševičius in 2016 [55] proposed an SSVEP based BCI gaming system. The researchers developed a 3-class BCI system based on SSVEP and emotive EPOC Headset. The game involved target shooting developed in the OpenVIBE environment which provided the user feedback. Emotive EPOC, a 16 electrode based gaming headset, was used in combination with the SSVEP paradigm. Raw EEG data from the head set was acquired with internal sampling of 2048 Hz. Signals from the O1, O2, P7, and P8 were taken.

At first, data was split into three groups, according to their corresponding class labels, LEFT, RIGHT, and CENTER. Each group of signals was subjected to band-pass filter centered on the target frequency of interest: for the LEFT class, 29.5–30.5 Hz; CENTER, 19.5–20.5 Hz; RIGHT, 11.5–12.5 Hz.

Figure 7. Overt block pattern.

Subject (Group A)	Nharm = 1		Nharm = 2		Nharm = 3	
	AC	ACSA	AC	ACSA	AC	ACSA
Subject 1	78.4 ± 3.4	85.7 ± 1.8	73.9 ± 4.7	94.3 ± 1.8	—	94.4 ± 2.2
Subject 2	92.3 ± 2.4	94.8 ± 1.0	76.5 ± 4.9	91.3 ± 1.6	—	92.6 ± 1.1
Subject 3	78.4 ± 3.4	84.4 ± 2.1	73.9 ± 4.7	84.9 ± 2.6	—	80.6 ± 3.0
Subject 4	67.8 ± 3.5	76.0 ± 2.3	51.7 ± 4.7	76.7 ± 3.7	—	78.6 ± 3.2
Subject 5	62.4 ± 3.9	78.9 ± 2.3	51.6 ± 4.8	77.4 ± 2.4	—	70.5 ± 3.2
Subject 6	71.6 ± 3.8	85.8 ± 2.6	62.6 ± 5.0	81.9 ± 3.3	—	85.6 ± 2.9
Subject 7	89.5 ± 2.4	94.5 ± 1.4	76.0 ± 3.9	92.8 ± 2.4	—	92.6 ± 1.9
Subject 8	82.7 ± 3.3	89.2 ± 2.3	77.3 ± 4.3	94.4 ± 1.9	—	87.2 ± 1.7
Subject 9	91.1 ± 2.3	94.6 ± 1.6	84.0 ± 4.3	91.7 ± 1.1	—	91.8 ± 1.3
Subject 10	56.6 ± 4.4	63.5 ± 1.8	58.3 ± 4.7	67.5 ± 3.0	—	68.4 ± 2.4
Subject 11	57.0 ± 3.8	—	43.1 ± 5.0	—	—	—
Subject 12	44.5 ± 3.8	—	43.2 ± 5.8	—	—	—
Total	77.0 ± 3.4	84.7 ± 2.0	68.6 ± 4.6	85.3 ± 2.5	—	84.2 ± 2.4

Table 2. Mean and standard deviation of classification accuracy (in percent) obtained with the Thomson multitaper method (PMTM) for different numbers of harmonics with (ACSA) and without (AC) the use of automatic channel selection algorithm.

There have been studies [46] that analyzed how different colors of the targets influence classification quality. The user was presented with an LCD display, containing three blinking targets on a black background and a yellow arrow. On cue, the targets start blinking at different frequencies as shown in **Figure 8(a)**.

After classifier training, subjects were invited to participate in the game experiment. During the game, the subjects were presented with an interface from **Figure 8(b)**. The "spaceship" with two "engines," represented by two rectangles, and a "cannon," represented by the triangle. The subject could rotate the spaceship by focusing his/her attention on one of the rectangular targets.

By focusing attention on the middle triangle, the user was able to fire the spaceship cannon. The aim of the game is to rotate the spaceship and fire its canon to hit the red target. Once the target was hit, it disappeared to reappear in another position.

An evaluation of the system was performed using two subjects, named S1 and S2, unfamiliar with the BCI technology. The first algorithm used was wave atom transform (WAT) coefficients and the second algorithm used the band power (BP) in the stimulation frequency bands.

The accuracy was measured for each subject, while performing classification with 4 different classifiers (LDA, sparse LDA (sLDA), SVM with linear kernel, and SVM with RBF kernel (with parameter values, gamma = 10)). The results are depicted in **Table 4**.

Subject (Group A)	Nharm = 1		Nharm = 2		Nharm = 3	
	AC	ACSA	AC	ACSA	AC	ACSA
Subject 1	76.7 ± 3.1	85.0 ± 1.9	73.2 ± 4.9	93.9 ± 1.8	—	94.7 ± 1.2
Subject 2	86.5 ± 2.1	93.5 ± 0.8	74.8 ± 5.2	95.4 ± 0.9	—	95.0 ± 1.7
Subject 3	76.7 ± 3.1	82.5 ± 2.7	73.2 ± 4.9	79.4 ± 2.7	—	74.6 ± 2.6
Subject 4	61.0 ± 4.2	73.6 ± 3.5	58.3 ± 4.5	73.6 ± 2.2	—	77.6 ± 1.9
Subject 5	69.7 ± 2.9	80.2 ± 2.4	54.2 ± 4.6	76.1 ± 2.8	—	72.8 ± 1.9
Subject 6	61.4 ± 3.6	76.2 ± 2.0	60.8 ± 4.7	79.0 ± 2.2	—	77.7 ± 3.3
Subject 7	85.2 ± 2.8	90.0 ± 2.2	76.5 ± 4.7	91.2 ± 2.4	—	94.0 ± 2.4
Subject 8	83.0 ± 2.9	87.4 ± 2.2	75.9 ± 4.4	94.3 ± 2.2	—	91.5 ± 2.6
Subject 9	90.5 ± 2.4	92.9 ± 1.7	75.9 ± 4.2	90.9 ± 2.1	—	91.5 ± 1.8
Subject 10	53.7 ± 3.8	70.1 ± 2.4	61.7 ± 4.7	70.9 ± 3.0	—	71.4 ± 2.9
Subject 11	57.8 ± 4.3	—	48.5 ± 5.1	—	—	—
Subject 12	49.7 ± 4.3	—	54.0 ± 5.0	—	—	—
Total	74.4 ± 3.2	83.1 ± 2.8	68.4 ± 4.7	84.5 ± 2.3	—	84.1 ± 2.3

Table 3. Mean and standard deviation of classification accuracy (in per cent) obtained with the lock-in analyzer system (LAS) for different numbers of harmonics with (ACSA) and without (AC) the use of automatic channel selection algorithm.

2.2.4. SSVEP based communicator/speller enhancement

Nakanishi et al. in [56] designed a high speed speller based on SSVEP stimulus. The study was aimed at exploring the feasibility of mixed frequency and phase coding to form a high speed speller using a TFT monitor. A frequency and phase approximation approach was deployed to remove the limitation of the number of targets caused by the monitor refresh rate, resulting in a speller comprising 32 flickers specified by eight frequencies (8–15 Hz at an interval of 1 Hz) and four phases (0, 90, 180, and 270°).

Wang et al. [57] proposed an approach that generates visual flickers at a flexible frequency by approximating the frequency with variable number of frames in a stimulation cycle. For instance, a flicker at 11 Hz under a 60 Hz refresh rate can be realized by bridging five and six frames in a stimulation cycle as "11100011100111000111001111…" Based on this technique we can generate flicker frequencies up to 50% of the screen refresh rate, hence increasing the number of stimuli that can be presented. Generally, to render a visual flicker at frequency f with an initial phase ϕ, a stimulus sequence s(f, ϕ,i) can be generated by:

$$s(f, \phi, i) = \text{square}\left[2\pi f\left(\frac{i}{\text{refesh rate}}\right) + \phi\right] \quad (5)$$

where the function square [] generates a square wave of 50% duty cycle with levels 0 and 1, and i indicates the frame index. Nakanishi et al. used quad-phase coded flickering signals at

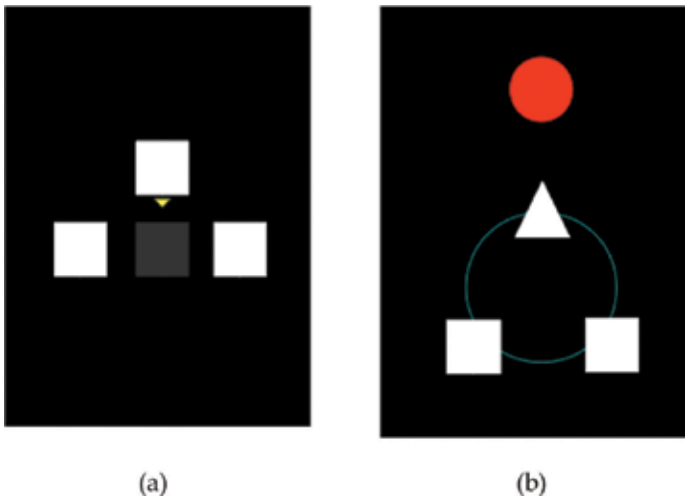

Figure 8. SSVEP BCI game interface: (a) training and (b) playing.

Classifier	Features	Accuracy, %		F1 Score	
		S1	S2	S1	S2
LDA	WAT	71.5	78.2	0.64	0.67
	BP	66.2	73.2	0.56	0.62
sLDA	WAT	70.6	77.4	0.64	0.68
	BP	68.4	73.5	0.59	0.61
SVM, linear kernel	WAT	75.5	79.3	0.64	0.68
	BP	74.3	75.1	0.64	071
SVM, RBF kernel	WAT	78.7	82.2	0.68	0.71
	BP	74.0	77.4	0.63	0.67

S1: subject number 1, S2: subject number 2, LDA: linear discriminant analysis, sLDA: sparse LDA, SVM: support vector machine, RBF: radial basis function, WAT: wave atom transform, and BP: band power.

Table 4. Comparison of classification accuracy.

phases or 0, 90, 180, and 270, for frequencies 8–15 Hz with an interval of 1 Hz, hence providing 32 unique targets instead of just 8 as indicated in **Figure 8**.

The subjects were instructed to gaze at one out of the 32 visual stimuli (a target stimulus) for 4 s, and the other 31 targets were indicated in a random order in a run. At the beginning of each trial, a red rectangle marker (**Figure 9**) appeared for half a second highlighting the target stimulus. Subjects were asked to shift their gaze to the target within the same duration. After which, all the stimuli started to flicker simultaneously for 4 seconds. Seven runs were carried out for each subject EEG data were recorded by 16 electrodes over the

http://dx.doi.org/10.5772/intechopen.75693

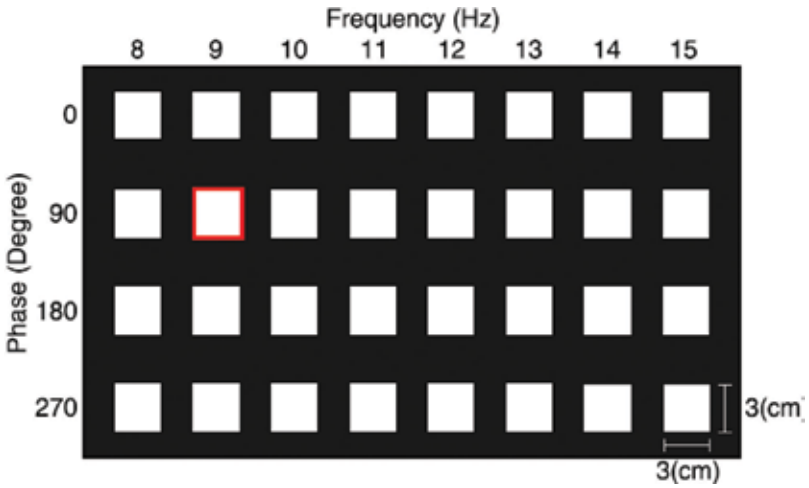

Figure 9. Presentation of the 32-target visual stimuli using mixed frequency and phase coding.

parietal and occipital areas (FPz, F3, F4, Fz, Cz, P1, P2, Pz, PO3, PO4, PO7, PO8, POz, O1, O2, and Oz).

The entire data epochs were correlated using common average reference (CAR) and then subjected to a band-pass filter with cut off frequencies 7–50 Hz with an infinite impulse response (IIR) filter. Zero-phase forward and reverse IIR filtering were implemented.

Canonical correlation analysis (CCA) was used for target identification which used the reference from the SSVEP training data ($\hat{X}_k$) to identify the user's intention. The study developed an ensemble classifier that correlates the test (X) and training ($\hat{X}_k$) set signals with sine-cosine reference signals Y. A correlation vector ρ is defined as follows:

$$\rho = \begin{bmatrix} \rho_1 \\ \rho_2 \\ \rho_3 \\ \rho_4 \end{bmatrix} = \begin{bmatrix} \rho \\ \rho\left(X^T W_{X\hat{X}}, \hat{X}^T W_{X\hat{X}}\right) \\ \rho\left(X^T W_{XY}, \hat{X}^T W_{XY}\right) \\ \rho\left(X^T W_{\hat{X}Y}, \hat{X}^T W_{\hat{X}Y}\right) \end{bmatrix} \quad (6)$$

To validate the efficiency of the combined method, this study compared classification performance of the following five methods: (M1) a standard CCA-based method; (M2) a correlation analysis using a spatial filter derived from test set and training reference signals; (M3) a correlation analysis using a spatial filter derived from test set and since-cosine reference signals; (M4) a correlation analysis using a spatial filter derived from training reference signals and sine-cosine reference signals; and (M5) the combined method using the ensemble classifier described in Eq. (6).

Figure 10 shows the averaged accuracy (**Figure 10(a)**) and ITR (**Figure 10(b)**) across all subjects for the offline experiments. Results for different CCA-based methods were calculated with different data lengths from 1 to 4 s. It is evident that the four methods (M2, M3, M4, and M5) outperformed M1 under all conditions with different data lengths.

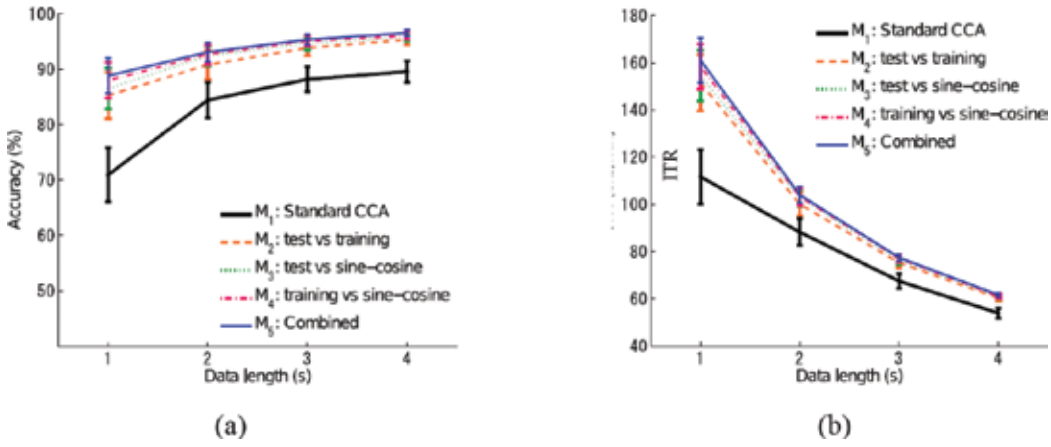

Figure 10. (a) Target identification accuracy, (b) ITRs as functions of data length (from 1 to 4 s) calculated by different methods.

2.3. Information transfer rate (ITR)

The dynamic performance of any BCI can be evaluated by the information transfer rate (ITR) as introduced in [58]. This parameter depends upon three factors regarding the BCI

- Speed
- Accuracy
- Number of unique commands

ITR (B) is defined as

$$B = V\left[\log_2 N + P\log_2 P + (1-P)\log_2\left(\frac{1-P}{N-1}\right)\right] \quad (7)$$

where, V = application speed in trials per second.

P = classifier accuracy, i.e., how accurately the thoughts are translated into command.

N = number of mental tasks used in the BCI application under consideration.

3. Conclusion

SSVEP proves to be the most widely used paradigm for BCI used for various different application for healthy as well as locked in patients due to the fact that SSVEP-BCI's require minimum user training. This is because the subject does not have to regulate his/her own brain activity to provide controlling input for the task at hand. The subjects have to merely focus their attention towards the flickering targets which is then converted to machine command by a trained classifier.

The accuracy of SSVEP based BCI's is fairly high for most subjects with substantial amount of visual capabilities. However some subjects were not able to produce a significant change in the EEG with respect to the SSVEP stimuli. This condition is termed as BCI illiteracy [59]. This phenomena cause the failure of BCI for such subjects as the task is not performed due to minimal EEG activity. To counter this problem a novel approach of hybrid brain computer interfacing (hBCI) was proposed [60, 61]. The hBCI combines a standard BCI paradigm (SSVEP, P300, slow cortical potential (SCP) or event related synchronisation/de-synchronisation (ERS/ERD)), with another BCI signal or some other physiological signal. hBCI's are an emerging area of research where all possible combinations are being explored to increase system accuracy as well as eliminate the phenomena of BCI illiteracy. The hBCI's also address the problem of subject fatigue due to fixing of gaze at flickering targets for a longer duration, this fatigue is known to reduce the accuracy of the BCI due increase in the number of False Positive (FP) outcomes.

Author details

Rajesh Singla

Address all correspondence to: singlar@nitj.ac.in

Associate Professor, Dr. BR Ambedkar NIT, Jalandhar, Punjab, India

References

[1] Kolodziej M, Majkowski A, Rak R. A new method of EEG classification for BCI with feature extraction based on higher order statistics of wavelet components and selection with generic algorithms. In: Adaptive and Natural Computing Algorithms. Lecture Notes in Computer Science. Warsaw, Poland: Warsaw University of Technology; 2011;**6593**:280-289

[2] Donchin E, Ritter W, McCallu C. Cognitive Psychophysiology: The Endogenous Components of the ERP. Brain-Event Related Potentials in Man. New York: Academic; 1978

[3] Regan D. Human Brain Electrophysiology: Evoked Potentials and Evoked Magnetic Fields in Science and Medicine. New York, NY, USA: Elsevier; 1989

[4] Yijun W, Ruiping W, Xiaorong G, Bo H, Shangkai G. A practical VEP-based brain-computer interface. IEEE Transactions on Neural Systems and Rehabilitation Engineering. 2006;**14**:234-240

[5] Jinghai Y, Derong J, Jianfeng H. Design and application of brain-computer InterfaceWeb browser based on VEP. In: Proceedings of the International Conference on Future Biomedical Information Engineering (FBIE'09); Sanya, China; 13-14 December, 2009. pp. 77-80

[6] Xiaorong G, Dingfeng X, Ming C, Shangkai G. A BCI-based environment controller for the motion-disabled. IEEE Transactions on Neural Systems and Rehabilitation Engineering. 2003;**11**:137-140

[7] Dan Z, Alexander M, Xiaorong G, Bo H, Andreas KE, Shangkai G. An independent brain-computer interface using convert non-spatial visual selective attention. Journal of Neural Engineering. 2010;**7**:016010

[8] Regan D. Some characteristics of average steady-state and transient responses evoked by modulated light. Electroencehalography & Clinical Neurophysiology. 1966;**20**(3):238-248

[9] Zhu D, Bieger J, Garcia Molina G, Aarts RM. A survey of stimulation methods used in SSVEP-based BCIs. Computational Intelligence and Neuroscience. 2010;**2010**:1-12. DOI: 10.1155/2010/702357

[10] Jasper HH. The ten twenty electrode system of the international federation. Electroen cephalography and Clinical Neurophysiology. 1958;**10**:371-375

[11] Herrmann CS, Human EEG. Responses to 1-100 Hz flicker: Resonance phenomenon in visual cortex and their potential correlation to cognitive phenomena. Experimental Brain Research. 2001;**137**(3-4):346-353

[12] Mandel C, Lüth L, Laue T, Röfer T, Gräser A, Krieg-Brückner B. Navigating a smart wheelchair with a brain-computer interface interpreting steady-state visual evoked potentials. In: IEEE/RSJ International Conference on Intelligent Robotics Systems (IROS); 2009. pp. 1118-1125

[13] Muller SMT, Bastos TF, Filho MS. Proposal of a SSVEP-BCI to command robotic wheelchair. Journal of Control, Automation and Electrical Systems. 2013;**24**:97-105

[14] Ng DWK, Soh YW, Goh SY. Development of an autonomous BCI wheelchair. In: IEEE Symposium on Computational Intelligence Brain Computer Interfaces; 2014. pp. 1-4

[15] Wang Y, Zhang Z, Gao X. Lead selection for SSVEP-based brain-computer interface. In: International Conference of the IEEE Engineering in Medicine & Biology Society, IEEE Engineering in Medicine & Biology Society Conference; 2004. pp. 4507-4510

[16] Zhang Z, Li X, Deng Z. A CWT-based SSVEP classification method for brain-computer interface system. In: International Conference on Intelligent Control and Information Processing. IEEE; 2010. pp. 43-48

[17] Kumari M, Somani SB. Enhancing the classification accuracy of SSVEP based BCI using CWT method along with ANN. International Journal of Advanced Research in Engineering & Management. 2015;**01**:81-89

[18] Huang M, Wu P, Liu Y. Application and contrast in brain-computer interface between Hilbert-Huang transform and wavelet transform. In: international Conference for Young Computer Scientists. IEEE Computer Society; 2008. pp. 1706-1710

[19] Ruan XG, Kuc K, Li M. Feature extraction of SSVEP-based brain-computer interface with ICA and HHT method. In: Intelligent Control and Automation. IEEE; 2014. pp. 2418-2423

[20] Diez PF, SMT M, Mut VA, Laciar E, Avila E, Basto-Filho TF, Sarcinelli-Filho MM. Commanding a robotic wheelchair with a high-frequency steady-state visual evoked potential based brain-computer interface medical engineering and physics. Elsevier; 2013;**35**(8):1155-1164. DOI: 35-1155-64

[21] Wang H, Lu T, Huang Z. Remote control of an electric car with SSVEP-based BCI. In: IEEE International Conference on Information Theory and Information Security. IEEE; 2010. pp. 837-840

[22] Mouli S, Palaniappan R, Sillitoe IP. Performance analysis of multi-frequency SSVEP-BCI using clear and frosted colour LED stimuli. In: IEEE International Conference on Bioinformatics and Bioengineering; 2013. pp. 1-4

[23] Yamaguchi T, Omori K, Irie J, Inoue K. Feature extraction from EEG signals in SSVEP spelling system. In: SICE Annual Conference; 2010. pp. 58-62

[24] Ghanbari AA, Kousarrizi MRN, Teshnehlab M, Aliyari M. Wavelet and Hilbert transform-based Brain Computer Interface. In: Proceedings of the International Conference on Advances in Computational Tools for Engineering Applications (ACTEA '09); Beirut, Lebanon; July 2009. pp. 438-442

[25] Samar VJ, Bopardikar A, Rao R, Swartz K. Wavelet analysis of neuroelectric waveforms: A conceptual tutorial. Brain and Language. 1999;**66**:7-60

[26] Krusienski DJ, Schalk G, McFarland DJ, Wolpaw JR. A mu-rhytm matched filter for continuous control of a brain-computer interface. IEEE Transactions on Biomedical Engineering. 2007;**54**:273-280

[27] Huang NE, Long SR, Shen Z. The mechanism for frequency downshift in nonlinear wave evolution. Advances in Applied Mechanics. 1996;**32**(08):59-117

[28] Lee PL, Chnag HC, Hseih TY. A brain-wave-Actuauted small robot car using ensemble empirical mode decomposition-based approach. IEEE Transactions on Systems Man and Cybernetics – Part A Systems and Humans. 2012;**42**(5):1053-1064

[29] Chu Y, Zhao X, Han J. SSVEP based brain-computer interface controlled functional electrical stimulation system for upper extremity rehabilitation. In: IEEE International Conference on Robotics and Biometrics. IEEE; 2015. pp. 2244-2249

[30] Bi L, Li Y, Jie K. A new SSVEP brain-computer interface based on a head up display, In: ICME International Conference on Complex Medical Engineering; 2013. pp. 201-204

[31] Oikonomou VP, Liaros G, Georgiadis K. Comparative Evaluation of State-of-the-Art Algorithms for SSVEP-Based BCIs. Beijing, China: International Conference, BI 2017; 2016

[32] Singla R, Haseena BA. BCI based wheelchair control using steady state visual evoked potentials and support vector machines. International Journal of Soft Computing Engineering. Beijing, China: International Conference; 2013;**3**(3):46-52

[33] Bi L, Fan X, Jie K. Using a head-up display-based steady-state visually evoked potential brain-computer Interface to control a stimulated vehicle. IEEE Transactions on Intelligent Transportation Systems. 2014;**15**(3):959-966

[34] Sakurada T, Kawase T, Takano K. A BMI-based occupational therapy assist suit: Asynchronous control by SSVEP. Frontiers in Neuroscience;**213**(7):172

[35] Jian HL, Tang KT. Improving classification accuracy of SSVEP based BCI using RBF SVM with signal quality evaluation. In: International Symposium on Intelligent Signal Processing and Communication Systems. IEEE; 2014

[36] Ko LW, Lin SC, Liang WG. Development of SSVEP-based BCI using common frequency pattern to enhance system performance. In: 2014 IEEE Symposium on Computational Intelligence in Brain Computer Interfaces (CIBCI); Orlando, FL, USA: IEEE; 2014, pp. 30-35

[37] Duda RO, Hart PE, Stork DG. Pattern classification. In: En Broeck the Statistical Mechanics of Learning Rsity. 2nd ed. 2000

[38] Burges CJC. A tutorial on support vector machines for pattern recognition. Data Mining and Knowledge Discovery. 1998;**2**:121-167

[39] Xiang L, Dezhong Y, Wu D, Chaoyi L. Combining spatial filters for the classification of single-trial EEG in a finger movement task. IEEE Transactions on Biomedical Engineering. 2007;**54**:821-831

[40] Schlogl A, Lee F, Bischof H, Pfurtscheller G. Characterization of four-class motor imagery EEG data for the BCI-competition 2005. Journal of Neural Engineering. 2005;**2**:L14

[41] Borisoff JF, Mason SG, Bashashati A, Birch GE. Brain-computer interface design for asynchronous control applications: Improvements to the LF-ASD asynchronous brain switch. IEEE Transactions on Biomedical Engineering. 2004;**51**:985-992

[42] Luis-Fernando NA, Jaime GG. Brain computer interfaces: A review. Sensors. 2012; **12**(2):1211-1279

[43] Kubler A, Muller KR. Towards Brain-Computer Interfacing: An Introduction to Brain-Computer Interfacing. Cambridge, MA, USA: MIT Press; 2007. pp. 1-25. ISBN: 9870-262-04244-4

[44] Nicolas-Alonso LF, Gomez-Gil J. Brain computer interfaces, a review. Basel, Switzerland: International Journal of Sensors. 2012;**12**(2):1211-1279. www.mdpi.com/journal/sensors

[45] Wang YJ, Wang RP, Gao XR, Hong B, Gao SK. A practical VEP-based brain-computer interface. IEEE Transactions on Neural Systems and Rehabiliation Engineering. 2006;**14**(2):234-240

[46] Cao T, Wan F, Mak PU, Mak P, Vai MI, Hu Y. Flashing color on the performance of SSVEP-based brain-computer interfaces. In: 34th Annual International Conference of the IEEE EMBS; California, USA; 2012. pp. 1819-1822

[47] Lesenfants D, Habbal D, Lugo Z, Lebeau M, Horki P, Amico E, Pokorny C, Gomez F, Soddu A, Muller-Putz G, Laureys S, Noirhomme Q. An independent SSVEP-based brain–computer interface in locked-in syndrome. Journal of Neural Engineering. 2014. DOI: 10.1088/1741-2560/11/3/035002

[48] Lesenfants D, Partoune N, Soddu A, Lehembre R, M¨uller-Putz GR, Laureys S, Noirhomme Q. Design of a covert SSVEP-based BCI. In: Proceedings of 5th International Brain-Computer Interface Conference; Graz, Austria; 2011. pp. 216-219

[49] Zhang D, Maye A, Gao X, Hong B, Engel AK, Gao S. An independent brain-computer interface using covert non-spatial visual selective attention. Journal of Neural Engineering. 2010;**7**:16010-16021

[50] Muller-Putz GR, Scherer R, Brauneis C, Pfurtscheller G. Steady-state visual evoked potential (SSVEP)-based communication: Impact of harmonic frequency components. Journal of Neural Engineering. 2005;**2**:123-130

[51] Muller-Putz GR, Eder E, Wriessnegger SC, Pfurtscheller G. Comparison of dft and lock-inamplifier features and search for optimal electrode positions in SSVEP-based BCI. Journal of Neuroscience Methods. 2008;**168**:174-181

[52] Pregenzer M, Pfurtscheller G, Flotzinger D. Automated feature selection with a distinctionsensitive learning vector quantizer. Neurocomputing. 1996;**11**:19-29

[53] Thomson DJ. Spectrum estimation and harmonic analysis. Proceedings of the IEEE. 1982;**70**:1055-1096

[54] Hoogenboom N, Schoffelen JM, Oostenveld R, Parkes LM, Fries P. Localizing human visual gamma-band activity in frequency, time and space. NeuroImage. 2006;**29**:764-773

[55] Martišius I, Damaševičius R. A prototype SSVEP based real time BCI gaming system. Computational Intelligence and Neuroscience. 2016;**2016**:3861425

[56] Nakanishi M, Wang Y, Wang YT, Mitsukura Y, Jung TP. A high-speed brain speller using steady-state visual evoked potentials. International Journal of Neural Systems. 2014;**24**:1450019

[57] Wang Y, Wang YT, Jung TP. Visual stimulus design for high-rate SSVEP BCI. Electronics Letters. 2010;**46**(15):1057-1058. DOI: 1057-1058

[58] Wolpaw R, Ramoser H, McFarland DJ, Pfurtscheller G. EEG-based communication: Improved accuracy by response verification. IEEE Transactions on Neural Systems and Rehabilitation Engineering. 1998;**6**(3):326-333

[59] Fazel-Rezai R, Allison BZ, Guger C, Sellers EW, Kleih SC, Kubler A. P300 brain computer interface: Current challenges and emerging trends. Frontiers in Neuroengineering. 2012;**5**:1-14

[60] Allison BZ, Brunner C, Kaiser V, Müller-Putz GR, Neuper C, Pfurtscheller G. Toward a hybrid brain–computer interface based on imagined movement and visual attention. Journal of Neural Engineering. 2010;**7**(2):026007-026016

[61] Allison BZ, Luth T, Valbuena D, Teymourian A, Volosyak I, Graser A. BCI demographICS: How many (and what kinds of) people can use an SSVEP BCI. IEEE Transactions on Neural Systems and Rehabilitation Engineering. 2010;**18**(2):107-116

Chapter 7

Hybrid Brain-Computer Interface Systems: Approaches, Features, and Trends

Bijay Guragain, Ali Haider and Reza Fazel-Rezai

Additional information is available at the end of the chapter

http://dx.doi.org/10.5772/intechopen.75132

Abstract

Brain-computer interface (BCI) is an emerging field, and an increasing number of BCI research projects are being carried globally to interface computer with human using EEG for useful operations in both healthy and locked persons. Although several methods have been used to enhance the BCI performance in terms of signal processing, noise reduction, accuracy, information transfer rate, and user acceptability, the effective BCI system is still in the verge of development. So far, various modifications on single BCI systems as well as hybrid are done and the hybrid BCIs have shown increased but insufficient performance. Therefore, more efficient hybrid BCI models are still under the investigation by different research groups. In this review chapter, single BCI systems are briefly discussed and more detail discussions on hybrid BCIs, their modifications, operations, and performances with comparisons in terms of signal processing approaches, applications, limitations, and future scopes are presented.

Keywords: BCI, EEG, hybrid, signal processing, P300, SSVEP, MI

1. Introduction

The spontaneous electrical currents in mammalian brain (rabbit and monkey) were first demonstrated by English Physiologist Richard Caton in 1870s, but the human electroencephalogram (EEG) was discovered in 1924 by German Psychiatrist Hans Berger [1]. The brain waves (neural oscillations) can be considered as biomarkers for wide range of applications from therapeutic to cognitive disorders [2]. The neural activities in brain generate voltages in response to external events or stimuli called event potential (EP). However, event-related desynchronization/synchronization (ERD/ERS) does not require such external stimulation.

Interestingly, EP components can be subdivided into steady-state evoked potential (SSEP) and event-related potential (ERP), and ERD/ERS from motor imagination. Eventually, there are three main approaches employed by researchers to study electric signals generated from the brain activities. Following sections will elaborate discussion about these approaches.

1.1. P300 event-related potential

This event-related potential is a function of uncertainty of the external stimuli, and major changes in the positive amplitude of the EEG waveform appears at about 300 ms after the stimulus which is called P300 component of ERP, first used by Sutton et al. [3]. The P300 component of ERP was tested in human by Farwell and Donchin, and their experiment revealed that the rare event elicits P300 which can be used to develop mental prosthesis [4]. Farwell and Donchin proposed alphanumeric BCI speller consisting of 26 alphabets and 10 numbers (0–9) arranged in 6×6 matrix of rows and columns as shown in **Figure 1a** [4]. In this row-column (RC) paradigm, rows and columns are flashed randomly and the subject is asked to count the number of flashings of rows and columns corresponding to the target character. Flashed row/column containing target stimulus elicits P300 from parietal, occipital, and temporal regions (majorly in parietal) of the brain based on Oddball Paradigm, i.e., occurrence of rare (odd ball) event. The higher amplitude P300 is evoked from stimulus with higher strength and low probability (rare event). However, this paradigm suffers from low information transfer rate (ITR) due to multiple trials.

Various changes in visual aspects of RC paradigm in terms of background color, character distance, and character size is done [5] to test the system performance. In this experiment, various visual protocols such as black background, white background, large symbol size, small symbol size, larger inter-symbol distance, and smaller inter-symbol distance are tested to observe the performance in RC BCI speller. Visual protocol with white background outperformed all the other protocols, while small symbol size resulted in poor performance.

A region-based (RB) BCI paradigm was designed by [6] to reduce human perpetual errors such as attentional blink, repetition blindness, habituation, and other spatial errors such as crowding effect and adjacency problems. Human perpetual errors in P300 speller was demonstrated by [7] to show the effect of adjacency problems. RB paradigm shown in **Figure 1b** and **c** uses seven regions flash at two levels instead of rows and columns. The region containing

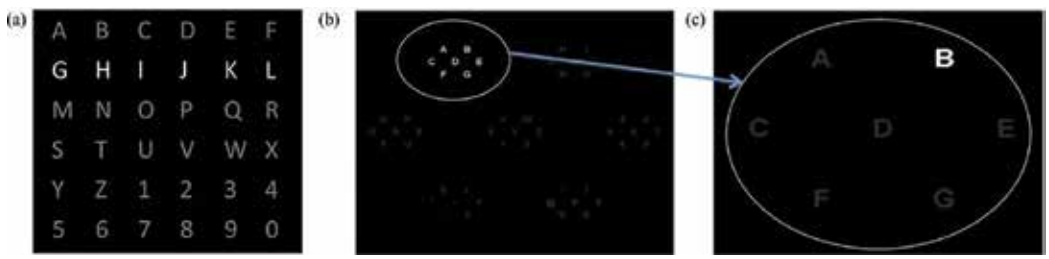

Figure 1. (a) RC paradigm with second row flashing [4]. (b) and (c) RB paradigm where seven sets of characters in level 1 (b) is expanded in level 2 (c) to spell a character "B" [6].

target character is selected at first level and the target is selected at second level which elicits P300. The number of characters in the RB speller is 49 and the probability of hitting a target is 1/7 which evokes higher amplitude of P300. Thus, accuracy, user acceptability, and ITR are enhanced in RB paradigm than traditional RC paradigm [6].

Only one character flashes in single character (SC) paradigm rather than all the six characters in row or column in RC paradigm [8]. In [9], SC paradigm was compared with RC paradigm for 19 subjects and observed that the classification accuracy was better for RC (85.3%) than SC (77.90%). Further, in [10], four P300 BCI spellers: RC, SC and two RB paradigms were compared, in which characters were based on alphabetical order in one and frequency of use in another. It was observed that accuracy of RB with characters in alphabetical order was highest and SC, the least for six subjects to spell two words WATER and LUCAS in three trials. In addition, whereas, user acceptability was highest for both RB paradigms than RC and SC, and region accuracy was least for central character on seven regions [6].

A checker board (CB) paradigm was proposed in [11], having 8×9 matrix of alphanumeric characters and keyboard commands, and compared the performance with traditional RC paradigm. Eighteen healthy subjects were used for the experiment and it was found that mean online accuracy, mean bit rate, and user acceptability were significantly higher for CB than RC but it suffers from adjacency errors. Other various modifications on standard RC paradigm have been done like a constant character flashing and shape changing which enhances the performances of P300 to some extent [12].

1.2. Steady-state visual evoked potential

The concept of visual evoked potential (VEP) was given by [13] using flash light and calculated evoked EEG signal by averaging to measure visual evoked responses from four parietal and occipital regions of scalp with bipolar electrodes. A clear high amplitude plot after 80 and 145 ms of the stimulus was found. VEPs, due to low stimulus rates, are classified as transient VEPs (TVEPs) and the repetitive high stimulations are under steady-state VEPs (SSVEPs). TVEP responses are during brain resting stage and if visual stimuli duration is shorter, evoked responses by each stimulus overlap each other and SSVEP is generated at steady state of brain excitation [14, 15].

SSVEP based on gaze detection falls into dependent BCI and is not suitable for ALS patients who cannot move their eyes. Gaze-independent SSVEP using LED interlaced square pattern for stimulation has been designed by [16]. People can shift attention among visual stimuli without shifting gaze, called as covert attention and overlapping stimuli can evoke changes in SSVEP which is sufficient to control BCI without gaze shifting like two overlapped images. Training for selective attention like playing certain types of computer games can improve SSVEP performance, and SSVEP systems are suitable to operate in challenging environments with distractions and noises like in homes and hospitals [17].

SSVEP visual stimuli are three main types as categorized below among which LED stimulation results in highest bit rate. All visual stimuli have properties like frequency, color, and contrast which affect SSVEP. Stimuli frequency can be divided into low (1–12 Hz),

medium (12–30 Hz), and high (30–60 Hz) bands. Visual fatigues and false positives can occur at low frequency bands, whereas flash and pattern reversal stimuli can provoke epileptic seizures above low frequency bands. Red light has strong SSVEP response at 11 Hz but decreases at other frequency levels. However, the response decreases further for blue and yellow light. The three major types of visual stimuli for SSVEP are categorized as follows [18].

- Light stimuli: light sources are LEDs, fluorescent lamps, Xe lights, etc., and their intensity is measured in candela per sq. meter.
- Single graphics stimuli: rectangle, square, or arrow on computer screen that appear and disappear at specific rate and stimulation rate are the number of full cycles per second called frequency of stimulus.
- Pattern reversal stimuli: periodic alternation of graphical patterns are usually black and white such as line boxes, checkerboards, etc., on computer screen.

The effect of visual distractions in SSVEP is dependent on the level of attention requirement during the task and the nature of distractions. SSVEP amplitude and identification accuracy decreases in dynamic screen condition compared to static condition [19]. Visual stimuli with a frequency resolution of 0.1 Hz were classified with high accuracy sufficient for practical BCI and the factors affecting the SSVEP speller are distance between adjacent stimuli, light source arrangements, stimulating frequencies, electrode arrangements, and visual angles [20].

The frequency response of SSVEP is experimented in [21] using visual stimulation at 14 different frequencies within the range of 5–60 Hz and found that the primary visual cortex follows an activation pattern similar to SSVEP and the SSVEP amplitude peaks at 15 Hz stimulation shown in **Figure 2**.

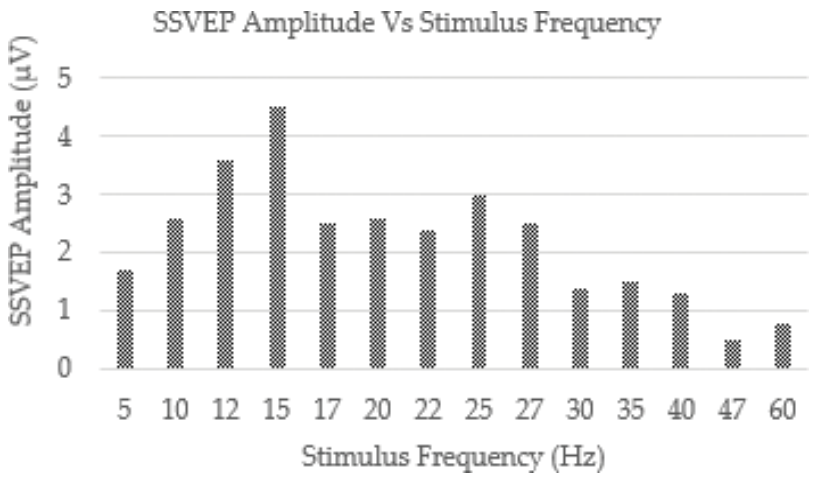

Figure 2. Variation of SSVEP amplitude with respect to stimulus frequency [21].

SSVEP response not only has the same fundamental frequency as stimulus but also includes higher harmonics and use of three SSVEP harmonics has resulted higher classification accuracy than for one or two harmonics [22]. SSVEP-based BCI has many advantages over other EEG-based BCI systems due to the following reasons [16].

- high signal-to-noise ratio
- high information transfer rate
- less susceptibility to eye movements and blink artifacts
- require very little or no training

Asynchronous SSVEP-based BCI using flickering lights was used to control neuro-prosthetic devices for restoration of grasp function in spinal cord injured people [23] and as a functional electrical stimulation for abdominal stimulation to augment respiration in tetraplegia [24]. An emergency call system using SSVEP-based brain switch was developed for ALS patients and they successfully called their guardians by simply starring at stimulus in about 6.56 s, starting the experiment by themselves. This system had fairly good performance when experimented up to 4 weeks. A chromatic visual stimulus with isoluminant red color is used to reduce intensity of the stimulus [25]. SSVEP-based BCI using single flicker stimulus is coded spatially to control four channels for navigation of 2-D computer games. Control channels are coded by their spatial position rather than flickering frequency or phase which may provide alternative route toward a practical SSVEP BCI with reduced visual strain [26]. To reduce visual fatigue from traditional SSVEP using flickering lights, an equal-luminance, ring-shaped, red-green colored checkerboard paradigm is used which produces high SSVEP power around 15 Hz [27]. Most people, despite no prior BCI experience, can use SSVEP BCI system even in a very noisy environment and better performances is observed in young and female subjects [28].

1.3. Motor imagery

Sensorimotor rhythms (SMRs) are synchronized brain waves over sensorimotor cortex in three different frequency bands: μ (8–12 Hz), β (18–30 Hz), and γ (30–200 Hz). EEG recording is mostly limited to μ and β bands. SMR amplitude is higher during idle stage called as event-related synchronization (ERS) and the amplitude decreases when the sensorimotor areas are active due to a certain motor task or even during motor imagery (MI). This decrease in SMR amplitude is called event-related desynchronization (ERD). The ERD signal is used for MI-related BCI. ERS immediately occurs after ERD [29]. For MI tasks, the subjects are instructed to imagine themselves performing a specific motor action without actual motor output and there exists contralateral lateralization of left-hand/right-hand/foot [30].

A novel typewriter "Hex-O-Spell" was presented in [31] using imagined right-hand and right foot movements shown in **Figure 3**. Five letters or symbols are inside six hexagons surrounding a circle having center arrow. Imagination of right-hand movement turns arrow clockwise and imagination of right foot movement stops the rotation and arrow extends to select a character if the imagination persists longer. A synchronous MI-based "Oct-O-Spell" paradigm is designed by [32] using 2-D cursor control with simultaneous MI tasks and claimed to be feasible with higher efficiency.

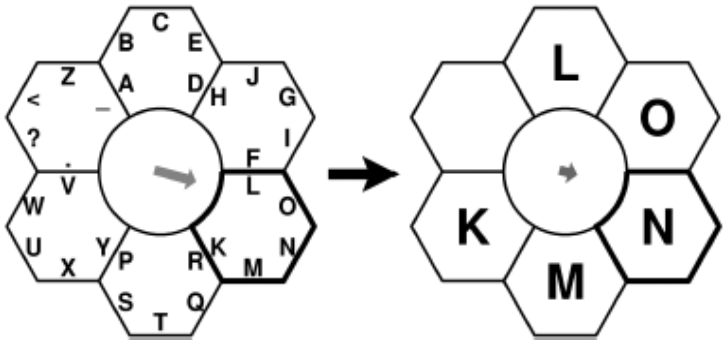

Figure 3. Two states of "Hex-O-Spell" paradigm selecting a character using MI [31].

MI detection is challenging due to low signal-to-noise ratio, but development of advance signal processing enables MI-based BCI to implement various tasks [33]. MI-based BCI was used first time by [34] for stroke rehabilitation in a tetraplegic patient using imagination of foot movement where the patient was able to grasp cylinder with the paralyzed hand.

MI-based BCI is a system that is subject specific and requires data recording and a system training for each new user. Subject-independent MI was developed by training the data acquired from several subjects [35] and a conscious target strengthens ERD in β frequency band [36]. ERD amplitude was higher due to body ownership illusion like moving rubber hand than other visual targets [37].

MI activity acts as a neurofeedback and a feasible part of stroke rehabilitation but may increase moderate fatigue due to external factors like long hours of training session [38]. Neural plasticity can be achieved through neurofeedback [38, 39]. MI-based BCI uses a neurofeedback strategy in poststroke rehabilitation using functional electrical stimulation (FES), robot, and orthosis [40]. Majority of stroke patients can use EEG-based MI [41, 42] for limb rehabilitation [43] and was extended to imagination of tongue movement [44]. MI can be used for a reliable and high performance BCI for both healthy subjects and ALS patients where the user requires less trainings [45]. MI-based BCI can be used for stroke rehabilitation to perform various functions such as controlling computer cursor, processing word, accessing Internet, and controlling environment and entertainment [33]. Without any muscular activities, MI tasks were employed in an experiment to drive a car in 3-D virtual environment [46] and to play video game on virtual ground [47].

There are other methods apart from EEG to measure brain activities such as magnetoencephalography (MEG), electro-corticography (ECoG), functional magnetic resonance imaging (fMRI), and functional near-infrared imaging (fNIR). However, due to noninvasive method, easy experimental setup, low cost, and high efficiency, EEG is most widely used. Although P300, SSVEP, and ERD/ERS are most widely used EEG signals, there are also other brain signals such as slow cortical potentials (SCP) and electrooculogram (EOG) in BCI [29]. Each of these brain signals do not work same for all users. So, a novel approach has been used to combine two or more conventional BCIs to form a hybrid BCI to enhance the overall performance [48].

http://dx.doi.org/10.5772/intechopen.75132

2. Hybrid BCI and modes of operation

The initial concept of hybrid BCI was used in [49] to incorporate electrocardiogram (ECG) with EEG for autonomous BCI switch ON and OFF operation to analyze whether heart bit rate can be used as an additional communication channel in BCI. P300 was combined to μ and β rhythms from sensorimotor cortex to operate a brain-controlled wheelchair [50]. In [51], hybrid P300/SSVEP system was compared with conventional P300 and SSVEP BCI from 10 healthy subjects and observed improved performance relative to single SSVEP system and the user acceptability was higher for the hybrid which suggested the need for efficient future protocols. A continuous simultaneous hybrid BCI for two dimensional cursor control was introduced in [52] using ERD and SSVEP activity, in which vertical position of the cursor was controlled via ERD with imagined movement and the horizontal position with SSVEP from visual attention, and the overall result suggested that further research is needed to optimize hybrid BCI.

In [53], hybrid BCI systems were reviewed and different possibilities to combine their advantages and disadvantages were discussed. Hybrid P300/SSVEP was used by [54] for GO/STOP command in wheelchair control at simultaneous asynchronous mode and obtained improved performance in terms of detection accuracy and response time. A novel hybrid P300/SSVEP was designed by [55] integrating random flashing and periodic flickering to reduce adjacency problem and habitual repetition, and obtained an online classification accuracy of 93.85% and information transfer rate of 56.44 bit/min from 12 healthy subjects in a single trial. A new hybrid P300/SSVEP was proposed in [56] based on visual approach of shape changing instead of existing color changing and compared the performances with traditional P300, SSVEP, and normal P300/SSVEP hybrid. The new hybrid BCI was compared with normal hybrid and each traditional BCIs, and found better performance with 100% accuracy and 30 bit/min ITR for eight trials with 10 healthy subjects.

A systematic review of hybrid BCI was done by [57] in terms of taxonomy and usability. This review discussed two modes of operation: simultaneous and sequential modes. In simultaneous mode, any two BCI systems (e.g., P300 and SSVEP) work simultaneously controlling two functions at a time and this combined system might achieve higher accuracy and ITR. As explained previously in [52], the hybrid BCI used simultaneous mode which includes ERD (imagined movement) to control the cursor in vertical position and SSVEP to control the cursor in horizontal position. In sequential mode, output of one BCI system is used as the input for another to control various functions of the second BCI system or as a switch in asynchronous mode [57]. These two modes are depicted in **Figure 4a** and **b**.

Among all other EEG signals, SSVEP possess a better suitability to combine with P300 [58] for constructing efficient hybrid BCI due to the following reasons [55]:

- SSVEP and P300 both are elicited by visual stimuli, so subjects only need visual attention.
- Both are noninvasive so reduction in experimental setup time, complexity, effort, and cost.
- No mental count is required for SSVEP thus reducing the mind workload.

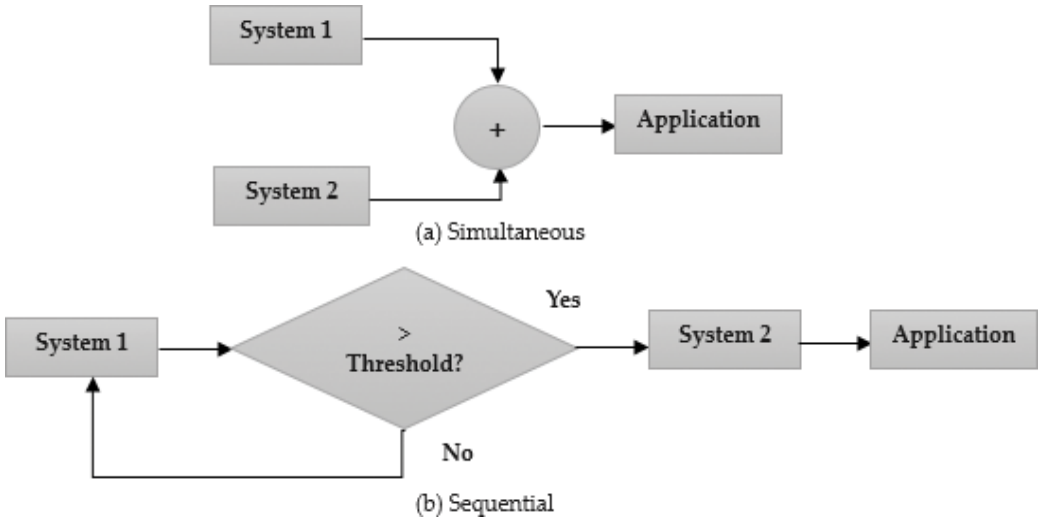

Figure 4. Hybrid BCI modes of operation [57].

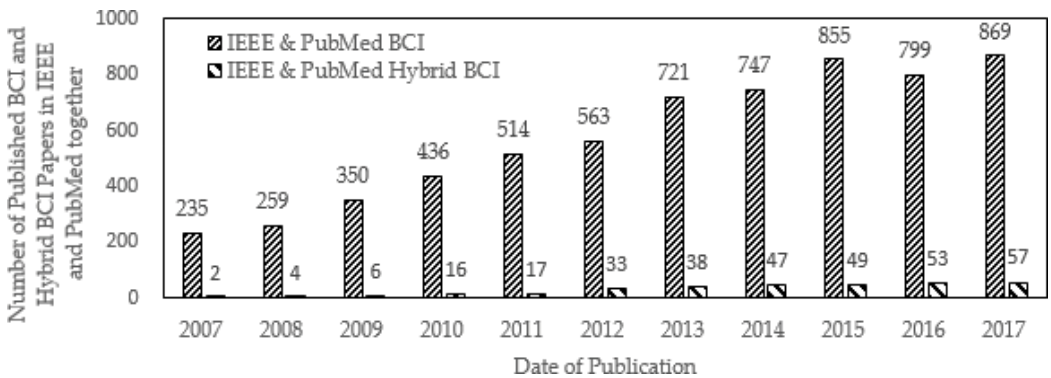

Figure 5. BCI and hybrid BCI papers in IEEE and PubMed.

- Both are measured in different domains (time domain for P300 and frequency domain for SSVEP).
- Both are detected from almost different cranial regions with independency enabling higher accuracy.

The research on hybrid BCI is growing and **Figures 5** and **6** illustrate number of publications in this field. The two figures are based on searches at IEEE Xplore [59] and PubMed [60] with keywords: "BCI," "Hybrid BCI," "SSVEP and MI," "P300 and SSVEP," and "P300 and MI "published in Conference, Journals, Magazines, Books, and e-books in the fields of "Engineering," "Psychology," "Neuroscience," "Medicine," and "Computer Science."

Figures 5 and **6** illustrate the number of published articles in IEEE Xplore and PubMed which are added together. They depict the growing numbers of research in hybrid BCI and among hybrid BCIs, number of P300 and SSVEP hybrid is comparatively higher as illustrated in **Figure 6**.

http://dx.doi.org/10.5772/intechopen.75132

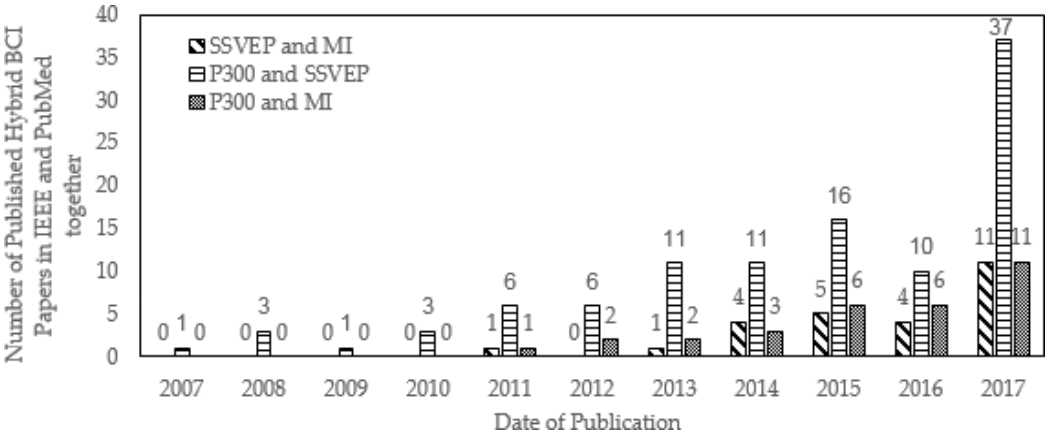

Figure 6. Hybrid BCI papers in IEEE and PubMed together.

3. Hybrid BCI classification

The most common signals for BCI are P300, SSVEP, and ERD, and there are various approaches used to combine two or more these signals to make a hybrid to enhance performance. The most common methods for hybrid BCI are discussed below and their classifications based on various parameters are illustrated in **Table 1**.

3.1. SSVEP-MI hybrid

SSVEP and ERD signals are used to form a BCI hybrid that combines visual attention and motor imagination. In [61], 14 healthy subjects (six women and eight men of ages 17–31 years) were chosen to perform three different tasks: MI only (ERD signals generated from left-hand or right-hand movement), SSVEP only (visual signals generated from two flickering LEDs at 8 Hz and 13 Hz), and simultaneous hybrid SSVEP-MI. Linear discriminant classifier was used and the classification accuracy was higher for SSVEP than MI and was highest for the hybrid.

An artificial upper limb was controlled by [62] combining SSVEP and MI in two degrees of freedom (DoF) in which MI controlled grasp function and SSVEP controlled elbow function (flexion and extension) of the limb. The experiment was conducted with 12 healthy subjects (7 male and 5 female) in offline and 7 healthy subjects (4 male and 3 female) in online. In offline experiment, 4 runs each with 40 trials were taken and the subjects were instructed to imagine feet dorsiflexion from two to four runs focusing the two flickering lights 7 and 13 Hz. The online experiment consisted a 2 DoF artificial upper limb and subjects controlled grasp and elbow functions as per instructions.

In [63], SSVEP-MI hybrid was proposed to control the speed (accelerate or deaccelerate the wheelchair based on flashing stimuli of 7, 8, 9, and 11 Hz) and direction (left- and right-hand imageries to control the direction) of a wheelchair in real time. Both virtual and real-time tests were conducted to observe the performance. Three options: straight driving, left and right turns were provided for direction, and accelerate, deaccelerate, or drive options for speed control using eight separate commands: turn left, turn right, drive forward, accelerate,

Hybrid type	Subj.	Modes of operation	Classifiers	Acc. (%)	ITR (bits/min)	Improvements	Reference
P300 + SSVEP	8	Simultaneous	SVM and DFT	90	22	"Go/stop" control signal with higher accuracy	[54]
P300 + SSVEP	12	Simultaneous	SWLDA and CCA	93	56	Classification accuracy and ITR	[55]
SSVEP + MI	14	Simultaneous	LDA	81	—	Reduction in BCI illiteracy	[61]
SSVEP + MI	12	Simultaneous	CCA	80	15	False activations reduction with binary decision	[62]
SSVEP + MI	3	Simultaneous	SVM & CCA	90	295	Time reduction with higher reliability	[63]
SSVEP + MI	6	Sequential	Filter and Threshold	78	—	Improved performance over conventional FET	[64]
SSVEP + MI	24	Sequential	CSP & CCA	87	—	Enhanced MI performance	[65]
SSVEP + MI	17	Simultaneous	LDA	85	—	Improved performances with single channel	[66]
P300 + SSVEP	10	Simultaneous	BLDA and CCA	90	22	Improved performance and easiness for users	[56]
P300 + SSVEP	10	Simultaneous	SWLDA and CCA	93	31	Reduced stimulation time for P300 and improved ITR	[67]
P300 + SSVEP	10	Sequential	FLDA and BLDA	88	19	Improved classification accuracy and ITR	[68]
P300 + SSVEP	12	Simultaneous	SWLDA	93	34	Transformed frequency locked SSVEP to time locked in a single speller	[69]
P300 + SSVEP	10	Simultaneous	BLDA and CCA	83	12	Improved SSVEP but not P300	[51]
P300 + MI	4	Sequential	SVM and FLDA	82	—	Finished more complex tasks in virtual environment	[70]
P300 + MI	4	Sequential	FLDA	82	—	Less exhaustive and reliable control of robotic devices	[71]

Hybrid type	Subj.	Modes of operation	Classifiers	Acc. (%)	ITR (bits/min)	Improvements	Reference
P300 + MI	11	Sequential	SVM	93	—	Enhanced accuracy and lowers trial duration	[72]
P300 + MI	11	Sequential	SWLDA and CSP	92	41	Control applications	[73]
P300 + MI	12	Simultaneous	LDA and CSP	92	—	Enhanced discriminating performances	[74]

Table 1. Different hybrid BCI systems' descriptions based on a number of subjects, modes of operation, classifiers used, accuracy, ITR, and improvements in the model.

deaccelerate, drive at uniform speed, and turn on or off the switch. Three healthy male subjects (21–30 years old) were participated in the experiment and the classification accuracy was more than 90% using Support Vector Machine (SVM) for MI and canonical correlation analysis (CCA) for SSVEP.

The sequential operation of SSVEP and ERD signals was used in [64] for advanced functional electrical therapy (FET) in which six right-handed healthy subjects (5 males and 1 female, mean age around 25 years) were selected. SSVEP signals from flickering LEDs of frequencies 15, 17, 19, and 21 Hz were used to select the types of grasp: palmar, lateral, and pinch followed by MI which was used as a brain switch that activated the intention of grasp.

In [65], hybrid BCI paradigm was proposed to enhance MI tasks using SSVEP. Twenty-four right-handed healthy subjects aged 23–30 years (19 males and 5 females) were used for the experiment to perform MI focusing on flickering SSVEP, where SSVEP was used initially to train the subjects for MI tasks providing accurate feedback, and afterward, the weight was shifted to MI gradually keeping SSVEP at less weights. Common spatial pattern (CSP) was used for MI and CCA for SSVEP classifications. This paradigm hypothesized that accurate feedback enhances MI.

The multiple channels hybrid was replaced in [66] combining SSVEP and MI in a single channel C3 or C4 improving performance. Seventeen healthy subjects (12 male and 5 female subjects with an average age around 23 years) were preinformed about the experiment to focus simultaneously on flickering visual stimuli of frequencies 15 and 20 Hz, and perform right- and left-hand MI, respectively. The average classification accuracy was around 85% for both channels.

3.2. P300-SSVEP hybrid

An asynchronous control of wheelchair was proposed by [54] combining SSVEP and P300 in which four groups of buttons were displayed, each group having one large central button surrounding eight small buttons with 45° spacing in a circumference of 60 mm radius. The four

groups flickered at frequencies 6, 6.67, 7.5, and 8.57 Hz to evoke SSVEP, while 100 ms interval was used to intensify and change the color of large central button to elicit P300. SVM and discrete Fourier transform (DFT) were used for classification of P300 and SSVEP, respectively, with an overall classification accuracy of about 90% from eight healthy subjects (20–31 years) performing "go/stop" control task using a real wheelchair.

A hybrid SSVEP-P300 BCI was proposed by [55] as mentioned earlier to improve spelling accuracy combining random flashing and periodic flickering to evoke P300 and SSVEP, respectively. All the cells of 6x6 matrix were flickered on black background with six frequencies 8.18, 8.97, 9.98, 11.23, 12.85, and 14.99 Hz, and selection of these frequencies were based on the higher SSVEP amplitude and easier target detection while orange crosses were flashed for 120 ms in random manner. Twelve healthy subjects (5 male and 7 female subjects, age 21–29 years) with good visions were used and the performance of the hybrid system was evaluated online using single trial. This experiment claimed to have the best performance.

In [56], a BCI with shape changing and flickering speller was designed, rather than traditional color changing as in [67], combining SSVEP and P300 in which the classification accuracy was improved in each of the individual systems. Shape changing of red boxes to arrows was used for P300 and flickering of those four boxes with frequencies 6, 8, 9, and 10 Hz for SSVEP. Ten healthy right-handed subjects with normal vision (9 male and 1 female subjects, age 22–27 years) were used for five offline experimental sessions having 20 runs of each sessions lasting for 4 s so the one session was 40 min including 10 min rest. The subjects found the new hybrid less annoying.

An asynchronous hybrid BCI combining P300 and SSVEP was proposed by [68] where the information transfer and control state (CS) detection was accomplished using P300 and SSVEP, respectively. This system operated in sequential manner in both offline and online experiments. Ten healthy subjects (7 males and 3 females aged 19–28 years) were participated in both experiments where P300 was elicited from flashing of a 6x6 matrix of 36 characters (A-Z and 0–9), and SSVEP was obtained from flickering of the characters black and white alternatively with frequency around 17.7 Hz. Two classifiers: Fisher's linear discriminant analysis (FLDA) for first three subjects and Bayesian linear discriminant analysis (BLDA) for remaining subjects were used for P300 classification. Inclusion of SSVEP into P300 improved the classification accuracy.

In [69], same target stimulus was used to elicit P300 and SSVEP blocking (SSVEP-B). A new speller of 3x3 matrix with characters 1–9 was proposed while all the characters flickered at a constant repetitive rate, and each character stopped flickering randomly within a short time. The repetitive flickering elicited SSVEP and the interrupted flickering of a character would elicit SSVEP-B and P300, a rare event at the same time which was detected simultaneously. Twelve right-handed healthy subjects (7 male and 5 female subjects, age 23–36 years) were participated in the experiment. The size and font of characters were changed with a variance of 0.49 ms for event-related potential, and brightness altered between light and dark with about 14.96 Hz for evoked potential. Stepwise linear discriminant analysis (SWLDA) was used for classification and the hybrid system produced better result than the individual systems.

In [51], SSVEP and P300 were combinedly evoked to improve accuracy using four red boxes with black background participating 10 healthy male subjects of age 21–25 years for three runs of 80 trials each in pseudorandom order. P300 was elicited by counting 32 flashings of the four red boxes for 8 times in each trial in the order: top, down, left, and right, and box changed from red to white for 100 ms during each flash while SSVEP was evoked by focusing on the target box which flickered at particular frequencies 9, 6, 10, and 8 Hz for 4 sec in the same order as of flashing, and the subjects needed to count the flashes and focus on flickering simultaneously for the hybrid paradigm. The P300 and SSVEP signals were analyzed separately and the average performances are mentioned in **Table 1**. This experiment highlighted the need for efficient hybrid as the hybrid performances improved relative to SSVEP but not to P300, and the subjects were comfortable with the hybrid.

A hybrid SSVEP-P300 BCI generating dual-frequency SSVEP was proposed by [67] using 9 panels speller, each panel with 4 characters flickering at different frequencies, and flickering panel and periodically updating characters evoked dual-frequency SSVEP. Ten graduate students (8 male, 2 female subjects, and average age 26 years) participated in both the offline and online experiments and there were improvements in stimulation time and ITR.

3.3. P300-MI hybrid

A hybrid P300-MI was used in [70] to control appliances in a virtual environment, in which P300 was used as a device control to operate control panel of virtual devices and MI as a navigation tool to turn left/right in the virtual environment, and the detection was sequential based on the activation of either MI or P300. Four healthy adults (1 male, 3 female subjects, age 23–25 years) participated and P300 was elicited using oddball paradigm, and MI using left-hand/right-hand movement imagination. The average online classification accuracy was achieved around 82% and authors claimed that more complex tasks in virtual environment could be performed compared to single pattern BCI.

The possibility of combining various brain signals for hybrid BCI was discussed by [71] merging P300 and ERD to control a robotic device such that additional features of one system could be used to improve classification accuracy of another. In this case, object selection from various options, called discrete decision, was done using P300 and movement control of the robot was done using ERD from motor imagination. EEG was filtered to a band 0–10 Hz for P300 classification. Optimum filter band varied with subject for ERD and the filter band was obtained from training data. Principal component analysis (PCA) and CSP was used in feature extraction for P300 and MI, respectively, and the discriminant classification was done by FLDA. Four healthy subjects were experimented with at least three MI trainings before the experiment by each subject with tasks: one out of five P300 symbols (1–5) and one out of two MI hand movements (left/right). Each subject performed one experimental session consisting of 60 trials, 30 trials for P300 in which targets were 1–5 numbers random flashings, and remaining 30 trials for MI where subjects needed to focus only one either on P300 or MI during each trial. Hybrid classification accuracy achieved was about 82% with average MI classification accuracy of 71%.

The selection of a target based on hybrid P300-MI BCI was developed by [72] on 1166×721 pixels monitor using two sequential tasks: cursor movement with the help of ERD from left-/right-hand movement imaginations and selection/rejection of the target from focused attention on flashing to evoke P300 keeping one system passive when other is active. Eleven healthy subjects (10 male, 1 female subjects, and age 22–32 years) were used in both online and offline analysis and each experiment was performed within 2 s with each trial duration for about 18 s. Two targets such as Green Square for selection and Blue Square for rejection were randomly appeared on the screen and the classification accuracy was about 93% in real time.

MI-based brain switch was merged with P300 sequentially by [73] in which right-/left-hand movement imaginations was used for control signal acting as a brain switch to turn ON/OFF P300 speller. Eleven healthy subjects (8 male, 3 female subjects, and age 23–30 years), with a few subjects having previous experience to P300 or MI, were experimented. Offline training was done for P300 and MI before real tests in a 22″ LED monitor containing 6×7 matrix of 26 English letters, 10 numbers, a few special characters, and commands. SWLDA was used for P300 classification and filtration in the alpha-beta rhythm range with two bands discrimination using CSP for MI and the classification accuracy achieved was about 92% for P300.

An efficient approach was proposed by [74] combining MI with P300 in a block diagonal matrix form to improve classification accuracy concatenating features of each paradigm where first-order information was used for P300 and second order for MI. Twelve volunteers (10 male, 2 female subjects, age 22–35 years) were experimented provided with eight flashing buttons and an arrow cue such that screen remained blank for initial 2.25 s and a cross appeared on the screen from 2.25 to 4 s to attract subject's visual attention. Arrow cue was displayed from 4 to 8 s such that up arrow was for P300 task to focus on the random flashing buttons without MI tasks and right arrow for MI task to make left-/right-hand imaginations. Test data was obtained from second experimental session and the classification accuracy was about 92%.

4. Signal processing approaches

The signal processing steps in BCI are signal acquisition, preprocessing, feature extraction, feature selection, feature classification, and postprocessing. The common classification approaches in hybrid BCI are briefly discussed here.

4.1. Fast Fourier transform (FFT)

FFT is an efficient algorithm for calculation of DFT reducing order of N^2 operations to $N \log_2 N$ that decomposes signal from time domain to its individual frequency components whose pairs are given as [75]:

$$X(k) = \sum_{n=0}^{N-1} x(n)\, W_N^{kn} \tag{1}$$

$$x(n) = \frac{1}{N}\sum_{k=0}^{N-1} X(k)\, W_N^{-kn} \tag{2}$$

where $W_N = e^{-j\left(\frac{2\pi}{N}\right)}$ and N = length [$x(n)$].

Amplitude vs. frequency is plotted and the dominant amplitude at a particular frequency is obtained for SSVEP signal analysis in BCI. FFT classifier has been replaced by other better classifiers in BCI research.

4.2. Linear discriminant analysis (LDA)

LDA, also known as Fisher's LDA (FLDA), is a useful classification technique that transforms features into a low-dimensional space with high degree of separation. Suppose, there are a certain set of samples belonging to classes "A" and "B" whose mean and scatterings within each classes are represented as μ_A, μ_B and S_A^2, S_B^2, respectively, and LDA is calculated as [76].

$$LDA = \frac{(\mu_A - \mu_B)^2}{S_A^2 + S_B^2} \tag{3}$$

This method is simple to use, has low computational cost with high accuracy, and is widely used in number of BCI applications for P300 and MI-related tasks [77]; but, it also suffers from small sample size and linearity problems [78]. BLDA, a Bayesian version of LDA, is useful for P300 in which parameters are estimated with Bayesian regression whose probabilistic output value lies between zero and one. It gives good results for small number of train sets or noise contaminated data and may give poor result for a complex nonlinear EEG data [78, 79]. SWLDA is a stepwise LDA that performs space reduction by selecting suitable features and stepwise analysis to remove least significant features which is an effective classification technique for online classification of P300 [80].

4.3. Support vector machine (SVM)

SVM is used for classification of linearly separable binary data sets that uses a discriminant hyperplane to identify classes and the best choice is the hyperplane that leaves maximum margin from both classes. The kernel generally used in P300 BCI is the Gaussian kernel and the corresponding SVM is Gaussian SVM which is given as:

$$\mathrm{K(x, y)} = \exp\left(\frac{-||x-y||^2}{2\sigma^2}\right) \tag{4}$$

where K(x, y) is kernel function and σ is kernel width.

SVM is simple and stable, and has a low variance which may be a key for low classification error for unstable and noisy P300 signals. SVM produces good results with high-dimension feature vectors and a small training set, thus outperforming LDA, but are generally slower than other classifiers [79]. BLDA is most robust for P300 application compared with LDA and SVM [81].

4.4. Canonical correlation analysis (CCA)

CCA is a multivariate statistical method to analyze frequency components of SSVEP in EEG [82]. It extracts narrowband frequency components of SSVEP in EEG using maximum correlation between reference stimulus signals and EEG signals. Suppose X be the EEG all channels data and Y_f be the reference signals at f Hz stimulus frequency with N number of harmonics, the reference signals Y_f are given as:

$$Y_f = \begin{pmatrix} \sin(2\pi ft) \\ \cos(2\pi ft) \\ \vdots \\ \sin(2\pi Nft) \\ \cos(2\pi Nft) \end{pmatrix} \tag{5}$$

The maximum correlation among X and Y_f is obtained as:

$$\rho_{max} = \max\left[correlation\ coefficient\ \left(X, Y_f\right)\right] \tag{6}$$

CCA is more common method for analysis of SSVEP signals in frequency domain that improves SNR, classification accuracy, and ITR [81, 83].

4.5. Common spatial patterns (CSPs)

CSP is used to analyze spatial patterns of MI calculating spatial filters to find optimum variances for two different classes of EEG data. It uses simultaneous diagonalization of two covariance matrices, and the spatially filtered signal Z of a single-trial EEG data is obtained as:

$$Z = WE \tag{7}$$

where E is $N \times T$ matrix of single-trial raw EEG data, N is the number of channels, T is the number of measurement samples per channel, and W is CSP projection matrix. The rows of W are stationary spatial filters and the columns of W^{-1} are common spatial patterns. Spatial patterns of motor action are dependent on the specific region of brain like left-hand movement on right cerebral hemisphere [84]. A higher classification accuracy for multitask learning with very few training samples among 19 healthy subjects was achieved by [85] in which spatial filter was replaced by Laplacian filter in CSP algorithm.

5. Applications

Hybrid BCI is in the state of development and various BCI signals are combined to form a hybrid enhancing performance for numerous experimental-related applications which are summarized in **Table 2**. Most of the applications are based on wheelchair control. Other

Application type	Specific control	Hybrid type	References
Wheelchair	Direction	P300 + MI	[50]
	"Go" and "Stop" movement	P300 + SSVEP	[54]
	Speed	SSVEP + MI	[65]
	Multi-degree	SSVEP + MI	[86]
	Speed and direction	SSVEP + MI	[63]
		P300 + MI	[87, 88]
	Autonomous navigation	P300 + MI	[89]
Computer cursor	2-D	SSVEP + MI	[52, 90]
		P300 + MI	[72]
Speller	Spelling accuracy	P300 + SSVEP	[55, 68]
		P300 + MI	[71, 73]
Artificial limb	Upper limb	SSVEP + MI	[62, 64]
	Multidimensional robotic arm		[91]
Functional electrical therapy	Advanced	SSVEP + MI	[66]
ALS patients	Communication	P300 + MI	[92]
	Awareness	P300 + SSVEP	[93]
Virtual environment	Smart home	P300 + SSVEP	[94, 95]
	Intelligent nursing bed		[96]

Table 2. Hybrid BCI applications.

applications include use of computer and communication, prosthetics using artificial limbs, advanced functional electrical therapy, monitoring ALS patients, entertainment and care in virtual smart home where MI is used mostly in prosthetics. Although BCI application is potentially safe, it needs regulatory approval before the experiment.

6. Limitations

Phenomenon of acquiring and processing information by human brain is still unknown. A very few hybrid BCI are experimented with target users and most of the subjects are healthy with small sample size. Rehabilitation using BCI is still not used in clinical practice [97]. Various methods have been incorporated to improve accuracy and ITR, and some hybrid with different classifiers combination have shown some improved results, but mostly subject's specific. Type and design of electrodes have impact on subject's head which influence EEG signals and demands for high compatible systems. These systems are not free from physical and mental fatigue that challenges their adaptability. Moreover, there are obstacles

in EEG acquisition due to electrodes placement, skull muscle movement, environment noises, limitations in hardware, and their calibrations. Two or more tasks need to be performed simultaneously in hybrid that might increase mental workload and cause discomfort to some users. Due to complexity, prior knowledge is required to use hybrid systems for target users. This demands for further research and hybrid BCI is still under development inside laboratory [57, 70].

7. Future scopes

Hybrid BCI has wider future scope and combining three or more signals may result better performances. Optimum combination of signals with high degree of compatibility may be obtained which is accessible to all [98]. Virtual environment-controlled applications [72] may turn to a real one which may provide easy access to target as well as healthy users. These applications may be broadened to people without disabilities too. Various researches are going on to calculate mental workload of armed soldiers, and brain automation control of wheelchair may be extended to control automobiles and airplanes [99]. Efficient algorithms need to be developed in future to make BCI practical with high accuracy and speed which act as a neurorehabilitation for stroke patients suffering from movement and language deficits. Human's intentions, emotions, and behaviors might be predicted in future using EEG which will ease for identifying fatigue in soldiers during war. It might be used in children to study various psychological measures such as behavior and learning tendency relative to age, and can be extended to animals besides human [97]. The laboratory experiment may be extended to the real world to ease our daily lives. Eventually, these might attract stakeholders to invest in BCI industry to produce commercialized BCI products in future.

8. Discussion and conclusion

Brain is a self-sustained oscillator where individual neurons oscillate at certain harmonics. Major rhythms of motor outputs generate through bifurcation. Several linear (spectral coherence and cross-correlation) and nonlinear (phase synchronization, mutual information and entropy) measures have been adopted to measure the oscillations [100]. Structural and functional connectivity of the brain works in coherence to perform a common action. Structural connectivity relates to the physical connection between different regions of the brain, while functional connectivity is the correlation between various regions over time that shows dynamic behavior [101].

During cognitive tasks requiring attention, certain brain regions become more active while the other regions activity decreases. A flashing or flickering visual stimulus eliciting event or evoked potential (P300 or SSVEP) increases activity in frontal and visual cortex. Due to more repetitive mental tasks, brain activity increases in the specific region, whereas activity in the other regions is reduced. The reason for reduction may be due to unrelated or difficult tasks [102]. This increase in brain activity corroborates growth in working memory of brain illustrating brain dynamic states. Brain changes its state according to the environment similar

to an artificially intelligent machine which adapts to learn from the input attributes without being explicitly programmed. So, a BCI illiterate at one point of time may adapt to learn with continuous trials due to dynamic brain states [103].

Human brain is a nonlinear dynamic system behaving as a chaotic and fractal system [104]. Therefore, EEG is a complex, nonlinear, and nonstationary signal. However, EEG signals have been analyzed based on linear/nonlinear and stationary/nonstationary techniques for feature extraction and classification. Fourier transforms, wavelet decomposition, power spectral density, autoregression, CCA, LDA, SVM, and CSP are some of the linear methods for EEG classification. However, only commonly used linear classifiers in hybrid BCI are discussed here. Due to the dynamical nature of the brain and the associated EEG signal, widely used linear approaches are not enough to obtain promising results. Therefore, the nonlinear dynamical behavior of EEG should be carefully considered during brain signal analysis. EEG signals need to be analyzed along with the dynamic states to reveal additional features that cannot be assessed with the linear methods.

EEG signals were analyzed dynamically in [105] to identify and code the attractors related to mental states using artificial neural network. It was shown that binary patterns of attractors resulting from neural firing of identical cognitive or sensory stimuli are similar, but they might appear as distinct features with different stimuli. The chaotic behavior of attractors highlights the fact that the neural signals are coherent. Indeed, brain dynamics has unveiled an emerging area of research to quantify information using attractors and fractals from EEG signals for useful operations applying hybrid BCI. It should be noted that attractors and fractals are the dynamic variables to measure complexity (correlation dimension and Hurst exponent) and stability (Lyapunov exponent and entropy) of EEG data [106–108]. The phenomenon of brain receiving the sensory inputs, storing the information, and processing output is still unknown. Hybrid BCI can be an efficient tool to transform the interesting brain dynamics into actions.

In this chapter, hybrid BCI is reviewed, and advancements from single BCI system to hybrid BCI systems, associated signal processing methods, usages, shortcomings and future scopes are discussed. The common hybrid systems based on signal combinations as well as operation methods, their performances, and improvements are mentioned. Statistical analysis of BCI and hybrid BCI related to P300 and SSVEP are illustrated based on publications. Transitioning from laboratory to the possible commercial applications is well discussed along with the limitations onward. This review illustrates P300, SSVEP, and MI which are mostly used EEG signals for BCI. Simultaneous operation is very common in P300-SSVEP hybrid and sequential operations are incorporated mostly in MI-related hybrid experiments. Average accuracy and ITR among reviewed hybrid BCI papers are 90% and 28 bits/min, respectively, which demand the need for a more efficient hybrid BCI system.

Author details

Bijay Guragain, Ali Haider and Reza Fazel-Rezai*

*Address all correspondence to: reza.fazelrezai@engr.und.edu

Biomedical Signal and Image Processing Laboratory, University of North Dakota, USA

References

[1] Millett D. Hans Berger: From psychic energy to the EEG. Perspectives in Biology and Medicine. 2001;**44**(4):522-542

[2] Başar E. Brain oscillations in neuropsychiatric disease. Dialogues in Clinical Neuroscience. Sep. 2013;**15**(3):291-300

[3] Sutton S, Braren M, Zubin J, John ER. Evoked-potential correlates of stimulus uncertainty. Science. Nov. 1965;**150**(3700):1187-1188

[4] Farwell LA, Donchin E. Talking off the top of your head: Toward a mental prosthesis utilizing event-related brain potentials. Electroencephalography and Clinical Neurophysiology. Dec. 1988;**70**(6):510-523

[5] Salvaris M, Sepulveda F. Visual modifications on the P300 speller BCI paradigm. Journal of Neural Engineering. Aug. 2009;**6**(4):46011

[6] Fazel-Rezai R, Abhari K. A region-based P300 speller for brain-computer interface. Canadian Journal of Electrical and Computer Engineering. 2009;**34**(3):81-85

[7] Fazel-Rezai R. Human error in P300 speller paradigm for brain-computer interface. In: 2007 29th Annual International Conference of the IEEE Engineering in Medicine and Biology Society. 2007. pp. 2516-2519

[8] Guan C, Thulasidas M, Wu J. High performance P300 speller for brain-computer interface. In: IEEE Int. Work. Biomed. Circuits Syst. Singapore Res. Collect. Sch. Inf. Syst. 2004. pp. 1-3

[9] Guger C et al. How many people are able to control a P300-based brain–computer interface (BCI)? Neuroscience Letters. Sep. 2009;**462**(1):94-98

[10] Fazel-Rezai R, Gavett S, Ahmad W, Rabbi A, Schneider E. A comparison among several P300 brain-computer Interface speller paradigms. Clinical EEG and Neuroscience. Oct. 2011;**42**(4):209-213

[11] Townsend G et al. A novel P300-based brain–computer interface stimulus presentation paradigm: Moving beyond rows and columns. Clinical Neurophysiology. Jul. 2010;**121**(7):1109-1120

[12] Haider A, Fazel-Rezai R. Application of P300 event-related potential in brain-computer interface. In: Event-related Potentials and Evoked Potentials. INTECH; 2017. pp. 19-38

[13] Vidal JJ. Real-time detection of brain events in EEG. Proceedings of the IEEE, 1977; **65**(5):633-641

[14] Wang Y, Gao X, Bo H, Jia C, Gao S. Brain-computer interfaces based on visual evoked potentials. IEEE Engineering in Medicine and Biology Magazine. Sep. 2008;**27**(5):64-71

[15] Haider MA, Cosatto B, Alam N, Tavakolian K, Fazel-Rezai R. A new region-based BCI speller design using steady state visual evoked potentials. In: International Brain-Computer Interface (BCI) Meeting; 2016. p. 1

[16] Lesenfants D et al. An independent SSVEP-based brain–computer interface in locked-in syndrome. Journal of Neural Engineering. Jun. 2014;**11**(3):35002

[17] Allison BZ, McFarland DJ, Schalk G, Zheng SD, Jackson MM, Wolpaw JR. Towards an independent brain–computer interface using steady state visual evoked potentials. Clinical Neurophysiology. Feb. 2008;**119**(2):399-408

[18] Zhu D, Bieger J, Garcia Molina G, Aarts RM. A survey of stimulation methods used in SSVEP-based BCIs. Computational Intelligence and Neuroscience. Mar. 2010;**2010**:702357

[19] Shu X, Yao L, Meng J, Sheng X, Zhu X. Visual Stimulus Background Effects on SSVEP-Based Brain-Computer Interface. Berlin, Heidelberg: Springer; 2013. pp. 453-462

[20] Hwang H-J, Lim J-H, Jung Y-J, Choi H, Lee SW, Im C-H. Development of an SSVEP-based BCI spelling system adopting a QWERTY-style LED keyboard. Journal of Neuroscience Methods. Jun. 2012;**208**(1):59-65

[21] Pastor MA, Artieda J, Arbizu J, Valencia M, Masdeu JC. Human cerebral activation during steady-state visual-evoked responses. The Journal of Neuroscience. Dec. 2003;**23**(37):11621-11627

[22] Müller-Putz GR, Scherer R, Brauneis C, Pfurtscheller G. Steady-state visual evoked potential (SSVEP)-based communication: Impact of harmonic frequency components. Journal of Neural Engineering. Dec. 2005;**2**(4):123-130

[23] Muller-Putz GR, Pfurtscheller G. Control of an electrical prosthesis with an SSVEP-based BCI. IEEE Transactions on Biomedical Engineering. Jan. 2008;**55**(1):361-364

[24] Gollee H, Volosyak I, McLachlan AJ, Hunt KJ, Gräser A. An SSVEP-based brain–computer Interface for the control of functional electrical stimulation. IEEE Transactions on Biomedical Engineering. Aug. 2010;**57**(8):1847-1855

[25] Lim J-H et al. An emergency call system for patients in locked-in state using an SSVEP-based brain switch. Psychophysiology. Nov. 2017;**54**(11):1632-1643

[26] Chen J, Zhang D, Engel AK, Gong Q, Maye A. Application of a single-flicker online SSVEP BCI for spatial navigation. PLoS One. May 2017;**12**(5):e0178385

[27] Yan W et al. Steady-state motion visual evoked potential (SSMVEP) based on equal luminance Colored enhancement. PLoS One. Jan. 2017;**12**(1):e0169642

[28] Allison B, Luth T, Valbuena D, Teymourian A, Volosyak I, Graser A. BCI demographics: How many (and what kinds of) people can use an SSVEP BCI? IEEE Transactions on Neural Systems and Rehabilitation Engineering. Apr. 2010;**18**(2):107-116

[29] Wolpaw JR, Wolpaw EW. Brain-Computer Interfaces: Principles and Practice. USA: Oxford University Press; 2012

[30] Liang S, Choi K-S, Qin J, Wang Q, Pang W-M, Heng P-A. Discrimination of motor imagery tasks via information flow pattern of brain connectivity. Technology and Health Care. Jun. 2016;**24**(s2):S795-S801

[31] Blankertz B et al. The Berlin brain-computer interface presents the novel mental typewriter hex-o-spell. In: 3rd Int. BCI Work. Train. Course, Graz 2006; 2006 January. Graz, Austria. 2006. pp. 2-3

[32] Cao L, Xia B, Maysam O, Li J, Xie H, Birbaumer N. A synchronous motor imagery based neural physiological paradigm for brain computer Interface speller. Frontiers in Human Neuroscience. May 2017;**11**:274

[33] Ang KK, Guan C. Brain-computer interface in stroke rehabilitation. Journal of Computing Science and Engineering. 2013;**7**(2):139-146

[34] Pfurtscheller G, Müller GR, Pfurtscheller J, Gerner HJ, Rupp R. 'Thought'—Control of functional electrical stimulation to restore hand grasp in a patient with tetraplegia. Neuroscience Letters. Nov. 2003;**351**(1):33-36

[35] Lotte F, Cuntai Guan C, Ang KK. Comparison of designs towards a subject-independent brain-computer interface based on motor imagery. In: 2009 Annual International Conference of the IEEE Engineering in Medicine and Biology Society, vol. 2009. 2009. pp. 4543-4546

[36] Kitahara K, Kondo T. Modulation of ERD/S by having a conscious target during lower-extremity motor imagery. In: 2015 37th Annual International Conference of the IEEE Engineering in Medicine and Biology Society (EMBC), vol. 2015. 2015. pp. 6630-6633

[37] Song M, Kim J. Motor imagery enhancement paradigm using moving rubber hand illusion system. In: 2017 39th Annual International Conference of the IEEE Engineering in Medicine and Biology Society (EMBC). 2017. pp. 1146-1149

[38] Prasad G, Herman P, Coyle D, McDonough S, Crosbie J. Applying a brain-computer interface to support motor imagery practice in people with stroke for upper limb recovery: A feasibility study. Journal of Neuroengineering and Rehabilitation. Dec. 2010;**7**(1):60

[39] Cincotti F et al. EEG-based brain-computer interface to support post-stroke motor rehabilitation of the upper limb. In: 2012 Annual International Conference of the IEEE Engineering in Medicine and Biology Society, vol. 2012. 2012. pp. 4112-4115

[40] Silvoni S et al. Brain-computer interface in stroke: A review of progress. Clinical EEG and Neuroscience. Oct. 2011;**42**(4):245-252

[41] Ang KK et al. A large clinical study on the ability of stroke patients to use an EEG-based motor imagery brain-computer Interface. Clinical EEG and Neuroscience. Oct. 2011;**42**(4):253-258

[42] Teo W-P, Chew E. Is motor-imagery brain-computer Interface feasible in stroke rehabilitation? PM&R. Aug. 2014;**6**(8):723-728

[43] Kai Keng Ang KK et al. A clinical study of motor imagery-based brain-computer interface for upper limb robotic rehabilitation. In: 2009 Annual International Conference of the IEEE Engineering in Medicine and Biology Society, vol. 2009. 2009. pp. 5981-5984

[44] Naeem M, Brunner C, Leeb R, Graimann B, Pfurtscheller G. Seperability of four-class motor imagery data using independent components analysis. Journal of Neural Engineering. Sep. 2006;**3**(3):208-216

[45] Bai O, Lin P, Vorbach S, Floeter MK, Hattori N, Hallett M. A high performance sensorimotor beta rhythm-based brain–computer interface associated with human natural motor behavior. Journal of Neural Engineering. Mar. 2008;**5**(1):24-35

[46] Qibin Z, Liqing Z, Andrzej C. EEG-based asynchronous BCI control of a car in 3D virtual reality environments. Chinese Science Bulletin. 2009;**54**(1):78-87

[47] Bonnet L, Lotte F, Lecuyer A. Two brains, one game: Design and evaluation of a multiuser BCI video game based on motor imagery. IEEE Transactions on Computational Intelligence in AI and Games. Jun. 2013;**5**(2):185-198

[48] Allison BZ, Brunner C, Kaiser V, Müller-Putz GR, Neuper C, Pfurtscheller G. Toward a hybrid brain–computer interface based on imagined movement and visual attention. Journal of Neural Engineering. Apr. 2010;**7**(2):26007

[49] Scherer R, Müller-Putz GR, Pfurtscheller G. Self-initiation of EEG-based brain–computer communication using the heart rate response. Journal of Neural Engineering. Dec. 2007;**4**(4):L23-L29

[50] Rebsamen B et al. Hybrid P300 and mu-beta brain computer interface to operate a brain controlled wheelchair. In: Proceedings of the 2nd International Convention on Rehabilitation Engineering & Assistive Technology. Singapore Therapeutic, Assistive & Rehabilitative Technologies (START) Centre. 2008. pp. 51-55

[51] Allison BZ, Jin J, Zhang Y, Wang X. A four-choice hybrid P300/SSVEP BCI for improved accuracy. Brain-Computer Interfaces. 2014;**1**(1):17-26

[52] Allison BZ, Brunner C, Altstätter C, Wagner IC, Grissmann S, Neuper C. A hybrid ERD/SSVEP BCI for continuous simultaneous two dimensional cursor control. Journal of Neuroscience Methods. Aug. 2012;**209**(2):299-307

[53] Amiri S, Fazel-Rezai R, Asadpour V. A review of hybrid brain-computer interface systems. Advanced Human-Computer Interaction. Feb. 2013;**2013**:1-8

[54] Li Y, Pan J, Wang F, Zhuliang Y. A hybrid BCI system combining P300 and SSVEP and its application to wheelchair control. IEEE Transactions on Biomedical Engineering. Nov. 2013;**60**(11):3156-3166

[55] Yin E, Zhou Z, Jiang J, Chen F, Liu Y, Hu D. A novel hybrid BCI speller based on the incorporation of SSVEP into the P300 paradigm. Journal of Neural Engineering. Apr. 2013;**10**(2):26012

[56] Wang M et al. A new hybrid BCI paradigm based on P300 and SSVEP. Journal of Neuroscience Methods. Apr. 2015;**244**:16-25

[57] Choi I, Rhiu I, Lee Y, Yun MH, Nam CS. A systematic review of hybrid brain-computer interfaces: Taxonomy and usability perspectives. PLoS One. Apr. 2017;**12**(4):e0176674

[58] Haider A, Fazel-Rezai R. Issues and challenges in designing P300 and SSVEP paradigms. In: Brain-Computer Interfaces Handbook: Technological and Theoretical Advances. Boca Raton, Florida, USA: CRC Press; 2017. p. TBA

[59] "IEEE Xplore Digital Library." [Online]. Available: http://ieeexplore.ieee.org/Xplore/home.jsp

[60] "PubMed - NCBI." [Online]. Available: https://www.ncbi.nlm.nih.gov/pubmed/

[61] Brunner C et al. Improved signal processing approaches in an offline simulation of a hybrid brain-computer interface. Journal of Neuroscience Methods. Apr. 2010;**188**(1):165-173

[62] Horki P, Solis-Escalante T, Neuper C, Müller-Putz G. Combined motor imagery and SSVEP based BCI control of a 2 DoF artificial upper limb. Medical & Biological Engineering & Computing. May 2011;**49**(5):567-577

[63] Cao L, Li J, Ji H, Jiang C. A hybrid brain computer interface system based on the neurophysiological protocol and brain-actuated switch for wheelchair control. Journal of Neuroscience Methods. May 2014;**229**:33-43

[64] Savić AM, Malešević NM, Popović MB. Feasibility of a hybrid brain-computer interface for advanced functional electrical therapy. Scientific World Journal. 2014:1-11

[65] Yu T et al. Enhanced motor imagery training using a hybrid BCI with feedback. IEEE Transactions on Biomedical Engineering. 2015;**62**(7):1706-1717

[66] Ko L-W, Ranga SSK, Komarov O, Chen C-C. Development of single-channel hybrid BCI system using motor imagery and SSVEP. Journal of Healthcare Engineering. Aug. 2017:1-7

[67] Chang MH, Lee JS, Heo J, Park KS. Eliciting dual-frequency SSVEP using a hybrid SSVEP-P300 BCI. Journal of Neuroscience Methods. Jan. 2016;**258**:104-113

[68] Panicker RC, Puthusserypady S, Sun Y. An asynchronous P300 BCI with SSVEP-based control state detection. IEEE Transactions on Biomedical Engineering. Jun. 2011;**58**(6):1781-1788

[69] Xu M, Qi H, Wan B, Yin T, Liu Z, Ming D. A hybrid BCI speller paradigm combining P300 potential and the SSVEP blocking feature. Journal of Neural Engineering. Apr. 2013;**10**(2):26001

[70] Su Y et al. A hybrid brain-computer interface control strategy in a virtual environment. Journal of Zhejiang University-Science A. May 2011;**12**(5):351-361

[71] Riechmann H, Hachmeister N, Ritter H, Finke A. Asynchronous, parallel on-line classification of P300 and ERD for an efficient hybrid BCI. In: 2011 5th International IEEE/EMBS Conference on Neural Engineering. 2011. pp. 412-415

[72] Long J, Li Y, Yu T, Gu Z. Target selection with hybrid feature for BCI-based 2-D cursor control. IEEE Transactions on Biomedical Engineering. 2012;**59**(1):132-140

[73] Yu Y et al. A self-paced brain-computer interface speller by combining motor imagery and P300 potential. In: 2016 8th International Conference on Intelligent Human-Machine Systems and Cybernetics (IHMSC). 2016. pp. 160-163

[74] Long J, Wang J, Yu T. An efficient framework for EEG analysis with application to hybrid brain computer interfaces based on motor imagery and P300. Computational Intelligence and Neuroscience. Feb. 2017;**2017**:1-6

[75] Akin M. Comparison of wavelet transform and FFT methods in the analysis of EEG signals. Journal of Medical Systems. 2002;**26**(3):241-247

[76] Tharwat A, Gaber T, Ibrahim A, Hassanien AE. Linear discriminant analysis: A detailed tutorial. AI Communications. May 2017;**30**(2):169-190

[77] Lotte F, Congedo M, Lécuyer A, Lamarche F, Arnaldi B. A review of classification algorithms for EEG-based brain–computer interfaces. Journal of Neural Engineering. Jun. 2007;**4**(2):R1-R13

[78] Lei XX, Ping Yang P, Dezhong Yao D. An empirical Bayesian framework for brain–computer interfaces. IEEE Transactions on Neural Systems and Rehabilitation Engineering. Dec. 2009;**17**(6):521-529

[79] Xu P, Yang P, Lei X, Yao D. An enhanced probabilistic LDA for multi-class brain computer Interface. PLoS One. Jan. 2011;**6**(1):e14634

[80] Krusienski DJ et al. A comparison of classification techniques for the P300 speller. Journal of Neural Engineering. Dec. 2006;**3**(4):299-305

[81] Lin Z, Zhang C, Wu W, Gao X. Frequency recognition based on canonical correlation analysis for SSVEP-based BCIs. IEEE Transactions on Biomedical Engineering. Jun. 2007;**54**(6):1172-1176

[82] Nakanishi M, Wang Y, Wang Y-T, Jung T-P. A comparison study of canonical correlation analysis based methods for detecting steady-state visual evoked potentials. PLoS One. 2015;**10**(10):e0140703

[83] Bin G, Gao X, Yan Z, Hong B, Gao S. An online multi-channel SSVEP-based brain–computer interface using a canonical correlation analysis method. Journal of Neural Engineering. Aug. 2009;**6**(4):46002

[84] Ang KK, Chin ZY, Zhang H, Guan C. Filter bank common spatial pattern (FBCSP) in brain-computer interface. In: 2008 IEEE International Joint Conference on Neural Networks (IEEE World Congress on Computational Intelligence). 2008. pp. 2390-2397

[85] Alamgir M, Grosse-Wentrup M, Altun Y. Multitask learning for brain-computer interfaces. In: Proc. Thirteen. Int. Conf. Artif. Intell. Stat., vol. 9. 2010. pp. 17-24

[86] Li J et al. Evaluation and application of a hybrid brain computer interface for real wheelchair parallel control with multi-degree of freedom. International Journal of Neural Systems. Jun. 2014;**24**(4):1450014

[87] Yu Y et al. Self-paced operation of a wheelchair based on a hybrid brain-computer Interface combining motor imagery and P300 potential. IEEE Transactions on Neural Systems and Rehabilitation Engineering. Dec. 2017;**25**(12):2516-2526

[88] Jinyi Long J, Yuanqing Li Y, Hongtao Wang H, Tianyou Yu T, Jiahui Pan J, Feng Li F. A hybrid brain computer interface to control the direction and speed of a simulated or real wheelchair. IEEE Transactions on Neural Systems and Rehabilitation Engineering. Sep. 2012;**20**(5):720-729

[89] Zhang R et al. Control of a wheelchair in an indoor environment based on a brain-computer interface and automated navigation. IEEE Transactions on Neural Systems and Rehabilitation Engineering. Jan. 2016;**24**(1):128-139

[90] Ma T et al. The hybrid BCI system for movement control by combining motor imagery and moving onset visual evoked potential. Journal of Neural Engineering. Apr. 2017;**14**(2):26015

[91] Gao Q, Dou L, Belkacem AN, Chen C. Noninvasive electroencephalogram based control of a robotic arm for writing task using hybrid BCI system. BioMed Research International. 2017;**2017**

[92] Guger C et al. Complete locked-in and locked-in patients: Command following assessment and communication with vibro-tactile P300 and motor imagery brain-computer interface tools. Frontiers in Neuroscience. May 2017;**11**:251

[93] Pan J et al. Detecting awareness in patients with disorders of consciousness using a hybrid brain–computer interface. Journal of Neural Engineering. Oct. 2014;**11**(5):56007

[94] Edlinger G, Holzner C, Guger C. A Hybrid Brain-Computer Interface for Smart Home Control. Berlin, Heidelberg: Springer; 2011. pp. 417-426

[95] Edlinger G, Guger C. A hybrid brain-computer interface for improving the usability of a smart home control. In: 2012 ICME International Conference on Complex Medical Engineering (CME). 2012. pp. 182-185

[96] Peng N et al. Control of a nursing bed based on a hybrid brain-computer interface. In: 2016 38th Annual International Conference of the IEEE Engineering in Medicine and Biology Society (EMBC), vol. 2016. 2016. pp. 1556-1559

[97] Huggins JE et al. Workshops of the sixth international brain–computer interface meeting: Brain–computer interfaces past, present, and future. Brain-Computer Interfaces. Apr. 2017;**4**(1-2):3-36

[98] Pfurtscheller G et al. The hybrid BCI. Frontiers in Neuroscience. 2010;**4**:30

[99] Kim BH, Kim M, Jo S. Quadcopter flight control using a low-cost hybrid interface with EEG-based classification and eye tracking. Computers in Biology and Medicine. Aug. 2014;**51**:82-92

[100] Guevara Erra R, Perez Velazquez JL, Rosenblum M. Neural synchronization from the perspective of non-linear dynamics. Frontiers in Computational Neuroscience. 2017;**11**:98

[101] Girgis F, Lee DJ, Goodarzi A, Ditterich J. Toward a neuroscience of adult cognitive developmental theory. Frontiers in Neuroscience. Jan. 2018;**12**:4

[102] Fox MD, Snyder AZ, Vincent JL, Corbetta M, Van Essen DC, Raichle ME. The human brain is intrinsically organized into dynamic, anticorrelated functional networks. Proceedings of the National Academy of Sciences of the United States of America. 2005

[103] Kenett YN et al. Driving the brain towards creativity and intelligence: A network control theory analysis. Neuropsychologia. Jan. 2018. In press

[104] Boeing G, Geoff. Visual analysis of nonlinear dynamical systems: Chaos, fractals, self-similarity and the limits of prediction. Systems. Nov. 2016;**4**(4):1-18

[105] Pizzi R, Pizzi R, Musumeci M. Coding mental states from EEG signals and evaluating their integrated information content: A computational intelligence approach. 2018;**11**:464-470

[106] Natarajan K, Acharya R, Alias UF, Tiboleng T, Puthusserypady SK. Nonlinear analysis of EEG signals at different mental states. Biomedical Engineering Online. Mar. 2004;**3**(1):7

[107] Stam CJ. Nonlinear dynamical analysis of EEG and MEG: Review of an emerging field. Clinical Neurophysiology. Oct. 2005;**116**(10):2266-2301

[108] Rodríguez-Bermúdez G, García-Laencina PJ, Sousa Ramos J. Analysis of EEG signals using nonlinear dynamics and chaos: A review. Applied Mathematics & Information Sciences. 2015;**9**(5):2309-2321

Chapter 8

Image-guided Placement of Magnetic Neuroparticles as a Potential High-Resolution Brain-Machine Interface

Irving N. Weinberg, Lamar O. Mair, Sahar Jafari,
Jose Algarin, Jose Maria Benlloch Baviera,
James Baker-McKee, Bradley English,
Sagar Chowdhury, Pulkit Malik,
Jamelle Watson-Daniels, Olivia Hale,
Pavel Y. Stepanov, Aleksandar Nacev, Ryan Hilaman,
Said Ijanaten, Christian Koudelka, Ricardo Araneda,
Jens Herberholz, Luz J. Martinez-Miranda,
Benjamin Shapiro, Pablo S. Villar, Ilya Krivorotov,
Sakhrat Khizroev and Stanley Fricke

Additional information is available at the end of the chapter

http://dx.doi.org/10.5772/intechopen.75522

Abstract

We are developing methods of noninvasively delivering magnetic neuroparticles™ via intranasal administration followed by image-guided magnetic propulsion to selected locations in the brain. Once placed, the particles can activate neurons via vibrational motion or magnetoelectric stimulation. Similar particles might be used to read out neuronal electrical pulses via spintronic or liquid-crystal magnetic interactions, for fast bidirectional brain-machine interface. We have shown that particles containing liquid crystals can be read out with magnetic resonance imaging (MRI) using embedded magnetic nanoparticles and that the signal is visible even for voltages comparable to physiological characteristics. Such particles can be moved within the brain (e.g., across midline) without causing changes to neurological firing.

Keywords: magnetic, particles, image-guided MRI, brain-machine interface

1. Introduction

Brain-machine interfaces (BMIs) have made great progress as prostheses (e.g., for vision-impaired individuals). Those patients were willing to undergo major surgery, expense, and to have centimeter-scale electrical devices implanted in their nervous systems. The scope of influence of BMI of the future is clearly large, potentially including cognitive enhancement and memory storage, and quite likely with ramifications beyond anybody's present imagination [1, 2]. To fully exploit the power of BMI, some big steps need to be taken. For wide and long-term public use, the invasiveness of the implant procedure and toxicity of the implant materials need to be eliminated. The number of neuronal channels an implanted device must address needs to be increased by many orders of magnitude, and the entire nervous system must be accessible. The spatial resolution should be smaller or equal to the diameter of small groups of neurons (i.e., micron-sized), and the temporal resolution should be faster than or comparable to neurons in the native brain (i.e., sub-millisecond response time).

Most medical researchers attempt to translate therapeutic approaches from animal models to human use. Unfortunately, there are significant barriers to taking this approach to BMI. Optical dyes that are the mainstay of animal research do not work for animals larger than a few centimeters because of light scattering and the photon-stopping power of tissue. The multi-decade-long history of failure to bring optical mammography into clinical practice suggests that light scatter is not a problem that is easily solved [3]. Implanted tethered electrodes and high-intensity-focused ultrasound can only address one section of the nervous system at a time. Genetic manipulation of brain circuitry (e.g., with optogenetic or sonogenetic techniques) has significantly increased our understanding of preclinical neurosciences, but would still require invasive focal delivery of gene vectors, optical fibers, or ultrasonic transducers that would limit wide use in humans [4, 5].

Oscillating magnetic fields do not interact much with tissue, especially below several gigahertz in frequency, and therefore penetrate the human head readily. Magnetic resonance imaging methods that examine blood oxygen-level dependency (BOLD) rely on vascular changes that have a poor spatial and temporal resolution. Magnetic resonance imaging (MRI) pulse sequences that read out electrical current (e.g., from Lorentz forces causing neuronal displacement) can detect micro-amp levels (far from the nanoampere currents generated from individual or small neuronal bundles) although technical improvements such as fast magnetic gradients may improve performance in the future [6]. Imaging of electrical currents (magnetoencephalography) is limited to millimeter spatial resolution due to the variable impedance of the brain and the detector resolution [7].

In this chapter, we summarize contrast-enhancement approaches to BMI that could yield readout and writing of the entire brain with high spatial and temporal resolution. Contrast enhancement from radioactive and other materials has been used in radiology practices for the past century to explore and diagnose diseases of the nervous system. The contrast materials that appear the most promising are based on magnetic nanoparticles, which we attempt to describe more fully in this chapter.

http://dx.doi.org/10.5772/intechopen.75522

2. Brain access

To date, developers of the smart-dust [8] concept have constructed millimeter-sized particles using wafer-based lithographic methods typically employed for electronic circuitry (e.g., CMOS). Traditional electronic particles below a millimeter in size are difficult to power without a tether to the outside world, because of poor electromagnetic coupling to small antennas. In order to implant or remove electronic particles of these sizes, practitioners need millimeter-sized holes, requiring either surgery or interventional procedures to go through the vessels or subarachnoid spaces. Because of the potential for damage to eloquent nervous structures, such procedures carry risks and expensive and are therefore inappropriate for wide (e.g., consumer) applications.

As will be discussed below, we and others have formulated contrast solutions containing high concentrations of nano-sized particles with magnetic properties (e.g., spintronic, magnetoelectric) that do not need to rely on traditional approaches to enter or interact with the brain. As in drug delivery, we have shown that nanoscale particles can be delivered intranasally, which is considered a noninvasive administration mode in the clinical literature [9, 10]. The cribriform plate separates the nasal from the cranial cavities, with foramina that decline slightly in size with age, with an overall area of 6 mm^2 at age 25 and 4 mm^2 at age 66 [11]. Our group and others have demonstrated that magnetic particles with diameters of up to 250 nm readily enter the cranium with the assistance of a 20-mT magnetic gradient, with no appreciable intracranial entry in the absence of an imposed magnetic field (**Figure 1**). Minimally invasive routes other than intranasal are possible, for example, via lumbar puncture or via intravenous administration. However, both of these routes require overcoming countervailing current flows (of cerebrospinal fluid and blood, respectively) that make them less attractive.

Once in the intracranial cavity, magnetic particles can be manipulated using magnetic gradients for delivery to specific brain foci. The tracks that such particles make are micron-sized, unlike the millimeter scale holes made during conventional deep-brain stimulation surgery. Magnetic particle manipulation is difficult with a conventional MRI, since it is very hard to create magnetic gradients that can overcome the static MRI field strength. However, our group and others have constructed MRI systems where the static field can be temporarily

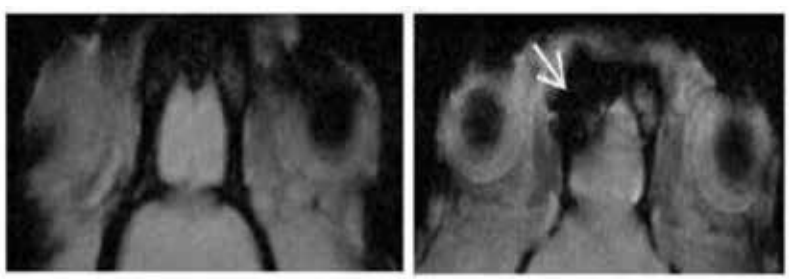

Figure 1. Transport into brain. Rat olfactory bulb before (left) and after (right) intra-nasal administration of particles under magnetic gradient.

eliminated in order to apply magnetic gradients without interference [12]. The MRI's static magnetic field can then be reapplied to assist in real-time image-guided manipulation.

In the past, it was believed that it was impossible to propel magnetic particles deep within tissues because of the particles' tendency to realign and become attracted to the propelling magnets and because particles tend to dissipate instead of aggregate when being pushed through tissue. With appropriate magnetic pulse sequences, it is possible to transiently polarize the particles in the direction opposite to the propelling magnets ("dynamic inversion"), so that the particles can be delivered deep into tissue [13]. With appropriate particle design choices, it is also possible to twist the particles during propulsion, which assists in penetrating tissues without increasing the particle track diameter [14]. Particles transported interstitially through the brain do not rely on vascular transport and therefore effectively bypass the blood-brain barrier.

Once the particles have been delivered to the intended location in the brain, the average distance between particles and neurons is inversely related to the local particle concentration. The distance between particles and neurons is critical to reading out or writing to the brain, since the electrical field decreases rapidly from kilovolts/meter (across the neuronal membrane) to tens of volts per meter (10 μm from the neuron). It may be possible to decrease the effective particle-neuron distance by coating the particle with materials in configurations that promote penetration of the neural membrane, as has been done with experimental brain electrodes [15].

3. Particle toxicity

For magnetic particles to become widely used, the particles must have a negligible potential for toxicity [16]. This very high bar is reflected in the Food and Drug Administration's (FDA) classification of devices for the brain as class III, requiring a premarket approval (PMA) application. In comparison, devices for the peripheral nervous system are often treated as class II devices. Note that particles are often treated by the FDA as drugs, although in Europe, they may be treated as devices. Studies of ex vivo vital rodent brain slices have shown that the presence of magnetic particles does not cause a measurable disruption of function [17]. In fact, it is not unusual for humans living in industrial cities to have magnetic particles in their brains, with no known related diseases [18]. It is also very common for humans over 50 years of age to have radio-dense "calcifications" in the basal ganglia, again with no definite disease association [19]. Small animal studies have examined the toxicity of magnetoelectric particles with no adverse effects [20].

4. Particle fabrication

Traditionally, implantable medical devices for neurostimulation have been built with CMOS processes (like other electronic devices). This approach is not scalable to nano-sized products that are needed for noninvasive access. Most of the magnetic particle literature was contributed in the field of bioassays, where particle uniformity is not critical. However, for medical applications (e.g., magnetic particle imaging), lack of particle uniformity is often a limiting factor [21].

http://dx.doi.org/10.5772/intechopen.75522

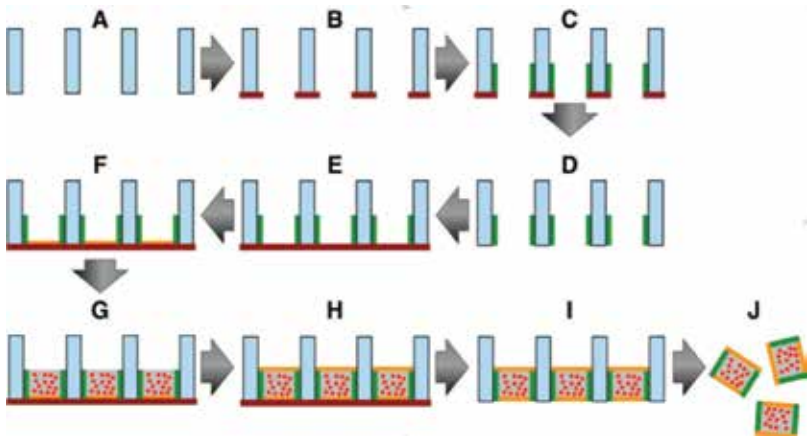

Figure 2. Example of template-guided shape-engineered synthesis of magnetic particles. Particles are made via sequential processing of polycarbonate track etched (PCTE) membrane films. PCTE films have pores extending through the thickness of the film. Templates (A) are first partially sealed on one surface with a conductive layer (B), followed by deposition of a polymer (e.g. poly-lactic-co-glycolic acid) shell inside the pores of the PCTE (C). Selectively etching the partially sealing conductive layer (D) and replacing it with a completely sealing conductive layer (E) allows for deposition of a conformal gold layer (F), after which a payload (e.g. liquid-crystal-magnetic composite) can be deposited by vacuum impregnation into the sealed pores of the PCTE film (G). Deposition of a final sealing layer (H), followed by selective etching of the conductive sealing layer (I) and removal of PCTE film (J) results in free-floating particles.

We have used template-guided methods to build shape-engineered highly uniform magnetizable particles with features important for transport and effectiveness [22] (**Figure 2**). For example, different sections of the particles can be built with aspect ratios that favor a particular magnetization direction. With appropriate use of precessing magnetic fields, the particles can be drilled through tissue [14]. The template-guided methods are also economical: it is possible to fabricate micromolar quantities of particles for less than $20 in raw materials. We have evaluated nanoscale spintronic devices for voltage sensing and stimulation, which have very tight tolerances. Transitioning these devices in their current morphologies to template-guided manufacturing (with tolerances of a few nm) may be challenging and may require device redesign.

5. Neuronal readout

Although neurons affect each other over nanoscale distances through chemical means (e.g., neurotransmitters), longer neuronal transmissions are electrical in nature. Noninvasive neuronal sensing in humans has generally employed either electrical methods to detect electrical fields or magnetic methods to detect electrical currents. Noninvasive external measurements of electrical fields from deep in the brain (e.g., with electroencephalography) yield centimeter-scale resolution because of the complicated impedance of the brain and surrounding tissues. Direct measurements of magnetic fields can be obtained with magnetoencephalography, but the resolution is limited to millimeter scales because of detector-size limitations.

Our working hypothesis is that the magnetic readout of contrast materials with magnetic resonance imaging (or the related field of magnetic particle imaging) is the way to go. With fast high magnetic gradients, magnetic resonance imaging (MRI) can achieve 30 μm spatial resolution (**Figure 3**) and kHz temporal resolution. In the past, it was believed that such rapid changes of magnetic fields would induce unwanted neurological stimulation, but we have shown in a prospective human study that if the frequency is high enough, such effects do not occur [23]. Magnetic particle imaging should theoretically be able to detect a single particle; however, experimentally, this has been difficult to achieve because of prior limits on gradient strength and particle uniformity [21, 24]. We have found that with very fast MRI pulse sequences that directly measure the reduction in local proton signal decay time, it is possible to detect as few as 1000 particles.

5.1. Readout with magnetic particle/liquid-crystal composites

There are several ways that magnetic particles can report on local electrical fields. The most promising in terms of field sensitivity takes advantage of liquid crystals, whose orientation can be used to detect low local electrical fields, for example, at a few volts per meter [25]. For purposes of comparison, voltage-sensitive dyes report on changes on the orders of kilovolts per meters (e.g., tens of millivolts across a 5-nm membrane) [26]. The high spatial and electrical field resolution of liquid crystals enables mapping of electronic layers with a sub-micron resolution [27]. Magnetic nanoparticles have been used to make the liquid crystals more sensitive to electric fields (dielectric permittivity) [28]. The liquid crystals' change in orientation (due to changes in local electric fields) can be transferred to magnetic particles, as validated with X-ray scattering methods (**Figure 4**) [29]. This orientation changes the local magnetic susceptibility, which can be detected with proton MRI (**Figure 5**) [30]. With MRI, we have detected electric fields as low as 20 V/m with this method.

5.2. Readout with piezoelectric magnetic particles

Particles have been built with magnetic cores and piezoelectric shells, where the magnetic moment of the core changes in response to an applied electric field. These magnetic moment

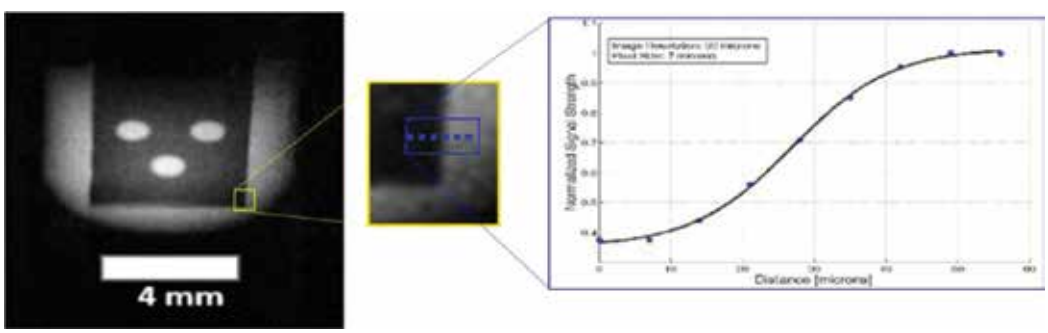

Figure 3. Spatial resolution of low-field MRI with high magnetic gradient strength. Left: spin echo sequence of a water phantom with 7-μm pixels in 2D projection. Right: calculation of spatial resolution of 30 μm.

http://dx.doi.org/10.5772/intechopen.75522

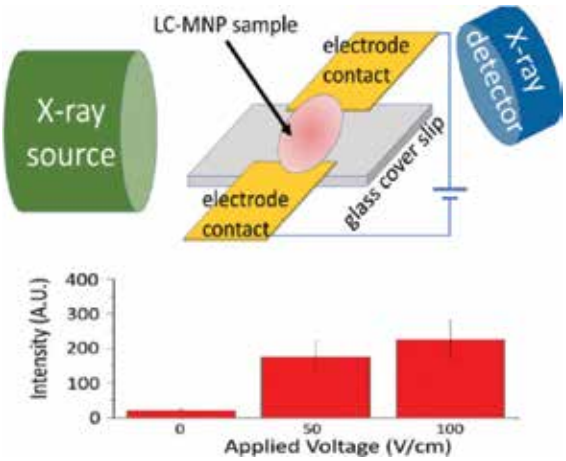

Figure 4. X-ray diffraction experiments with liquid crystal/magnetic particle composites (LC-MNP). Top: LC-MNP films placed in X-ray beam. Bottom: X-ray scattering measurements reveal changes in liquid crystal layer-to-layer spacings based on applied voltage.

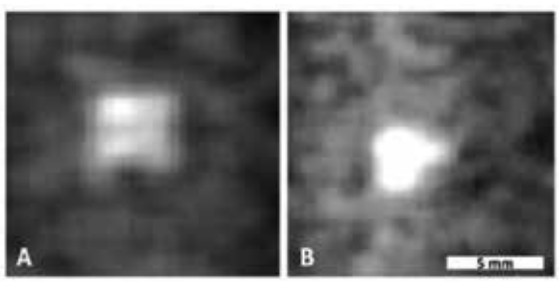

Figure 5. MRI of novel contrast agent. MRI results with no voltage applied (A) and with voltage applied (B). A 5% change in MRI signal is observed with electric fields of 20 V/m (comparable to the field within 10 μm of neurons).

changes can be read out with proton MRI (**Figure 6**). The same particles can be used to generate electric fields in response to an applied magnetic field (discussed subsequently in Section 6) [20, 31, 32].

5.3. Readout with spintronic particles

Spintronic devices act as nano-valves that convert electrical currents into radiofrequency (RF) waves. The devices are also sensitive to applied magnetic fields, which is important since the particles can thereby be localized by applying magnetic gradients (as in MRI). We have shown that a single nano-sized on-chip spintronic device can convert electrical currents in the micro-amp range into radio waves that can be detected centimeters away [33]. Spintronic devices can be ganged synchronously to amplify signals [34]. The micro-amp range is probably too low to detect the state of single neurons, but might be appropriate for tracts. Work needs to be done (e.g., with template-guided synthesis) on freeing the spintronic devices from substrates

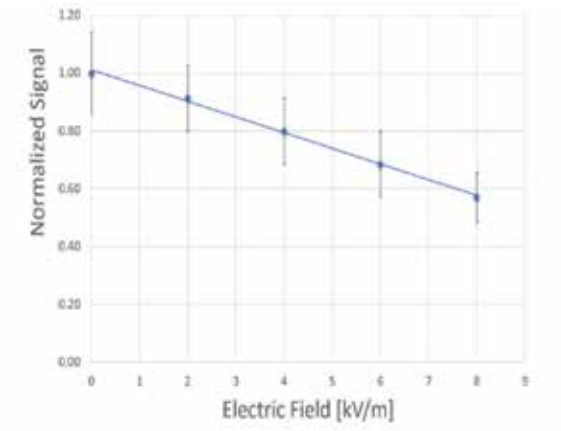

Figure 6. Voltage-sensitive MRI signal from piezo-magnetic particle.

for deployment as a contrast agent. The spintronic particles can be used in a reverse mode for stimulation (with radio-frequency energy converted to low-frequency currents) again with the possibility of localization with applied magnetic gradients [35].

6. Writing to the brain

The brain can be stimulated electrically, chemically and even mechanically. Most brain-machine interface work has been performed with electrical stimulation from invasive focal electrodes, which have advantages of high speed and spatial precision, but can only access a small portion of the brain. Noninvasive electrical stimulation has been performed with transcranial magnetic stimulation, where externally applied changing magnetic fields are used to induce electrical fields and currents in the brain. This technique yields relatively poor spatial resolution (e.g., centimeter scale) at the brain surface, with spatial resolution worsening appreciably in deeper parts of the brain. Externally applied electrical currents have even worse spatial localization capability, since the impedance of various tissues in the head is highly nonuniform. Theoretically, radio-frequency energy could be focused in small regions with high-field MRI, but this technique has not been intentionally used for stimulation [36]. Externally Administered chemical brain modulation is an ancient technique, practiced in pubs daily by millions of people. In a few rare cases, the focal concentration of receptors in certain sections of the brain allows chemical stimulants to target specific regions (e.g., substantia nigra by 1-methyl-4-phenyl-1,2,3,6-tetrahydropyridin) [37]. Microinfusions of chemicals via brain-implanted catheters have been applied in animal studies for research. Catheters have been implanted in the neuronal sections of human brains to deliver cancer treatment (i.e., convection-enhanced delivery). Externally applied high-intensity-focused ultrasound (HIFU) has been used experimentally to stimulate the brain, although the exact mechanism is not well understood [38]. We hypothesize that magnetic particles may be useful in focal brain stimulation, with focality realized either through noninvasive selective placement of particles (e.g., after magnetically-assisted intranasal

administration) in desired locations or with diffusely delivered particles that can be addressed selectively. In the next sections, we list various candidate magnetic particles for brain stimulation, some of which overlap the prior section for brain readout.

6.1. Mechanical stimulation with magnetic particles

Anecdotal surgical data from the placement of deep-brain stimulation leads have shown that mechanical vibration can stimulate neurons [39, 40]. Cultured neuron studies have demonstrated mechanoreceptors that react by opening calcium channels [41]. Invertebrate experiments suggest that externally applied magnetic gradients can wiggle magnetic particles enough to cause nerve stimulation (**Figure 7**) [42].

6.2. Composite piezoelectric/magnetic particles

With appropriately designed piezomagnetic particles, externally applied magnetic fields can be applied to the particles in order to generate powerful electric fields focally (e.g., strong enough to electroporate cells) [32]. Indirect evidence of global brain stimulation has been collected through electroencephalography of animals [20].

6.3. Electret-based magnetic particles

Recent innovations in harvesting harvesting from mechanical motion have been driven because of the proliferation of wearable devices. Some of the principles of energy harvesting can be reversed in order to generate electrical currents and voltages. Electrets, which rely on changes in capacitance to generate power, are very efficient vibrational energy harvesters. Liquid crystals have been used as electrets for energy harvesting [43]. Typically, liquid crystals require very high magnetic fields to change their capacitance, but the addition of magnetic

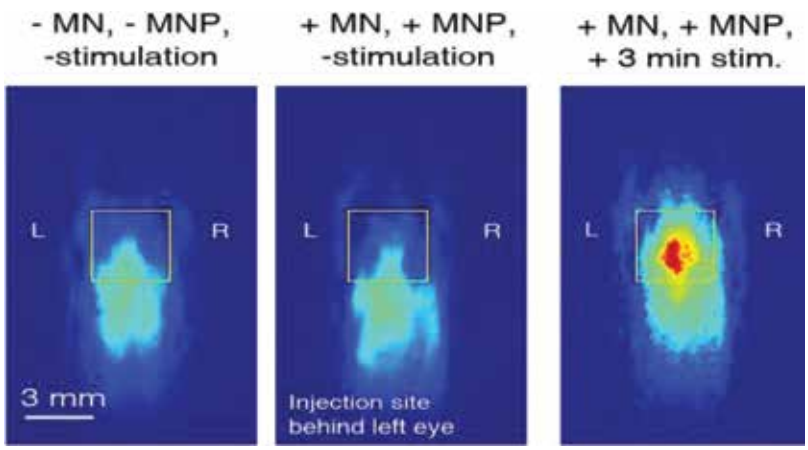

Figure 7. Magnetic particle neurostim-ulation visualized with manganese-enhanced MRI (MEMRI). Particles were injected behind the left eye of crawfish and stimulated for 3 min using magnetic wiggling of particles. Increased MEMRI signal is seen in the left brain.

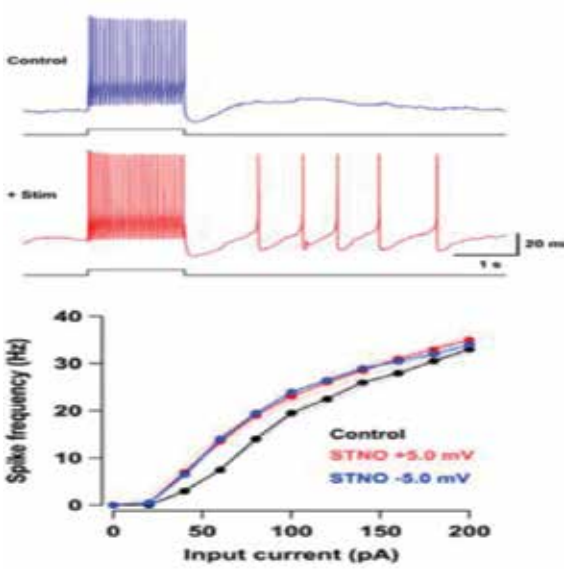

Figure 8. Spintronic particle writing to single neuron. Top: neuro-modulation in vital mouse brain slice (red) when spintronic nano-oscillator (STNO) particle is triggered by RF signal. Bottom: neuronal frequency changes in as a function of applied RF pulse.

dopants dramatically reduces the magnetic field strength required to alter capacitance [28]. Therefore, a composite of magnetic particles and liquid crystals (as discussed above) might be able to convert a changing externally applied magnetic field into local electrical stimulation.

6.4. Spintronic particles

As discussed above, spintronic particles have been used to convert low-frequency electrical currents into high-frequency radio-frequency emissions. Our group successfully reversed this process, to convert applied radio-frequency (RF) radiation into low-frequency electrical currents that were able to affect the firing frequency of a single neuron (**Figure 8**) [35]. An attractive potential application of this technology is that the efficiency of conversion of the RF radiation exhibits frequency dependence that is also a function of the ambient magnetic field. This mechanism would permit spintronic devices to be addressed with micron-level spatial resolution.

7. Conclusion

Magnetic neuroparticle solutions to brain-machine interface were predicted a long time ago and are under development today. As shown above, animal data show that nontoxic magnetic particles could be noninvasively directed to specific locations in the brain under real-time imaging guidance. Particles could be placed with high spatial resolution in focal regions for specific clinical indications (addiction, Parkinson's disease). Alternatively, the particles could be globally spread in the brain and selectively addressed for local stimulation and/

or readout with appropriate RF or magnetic tuning. Many of the particles listed above (e.g., magnetoelectric, electret-based particles) can both read and write electrically and therefore potentially fit the bill for high-speed bidirectionality. Building on the work of deep-brain stimulation, one might expect that the focal stimulation of specific brain nuclei would be the first clinical target for noninvasive or minimally invasive bidirectional BMI. The high temporal and spatial resolution of voltage-sensitive contrast media would likely shed additional light on large-scale brain processes (e.g., attractors [44]) that would be useful in building more eloquent BMIs. System architectures for reading from and writing to the brain would be similar to conventional MRI systems, preferably with the ability to rapidly turn off the static magnetic field in order to manipulate the magnetic particles with high flexibility [12]. Once the particles were placed in the appropriate location, stimulation could be implemented with a wearable coil. Readout with voltage-sensitive contrast media could be performed with conventional MRI systems.

Author details

Irving N. Weinberg[1]*, Lamar O. Mair[1], Sahar Jafari[1], Jose Algarin[2], Jose Maria Benlloch Baviera[2], James Baker-McKee[3], Bradley English[3], Sagar Chowdhury[3], Pulkit Malik[3], Danica Sun[3], Jamelle Watson-Daniels[3], Olivia Hale[3], Pavel Y. Stepanov[3], Aleksandar Nacev[4], Ryan Hilaman[4], Said Ijanaten[4], Christian Koudelka[4], Ricardo Araneda[5], Jens Herberholz[5], Luz J. Martinez-Miranda[5], Benjamin Shapiro[5], Pablo S. Villar[5], Ilya Krivorotov[6], Sakhrat Khizroev[7] and Stanley Fricke[8]

*Address all correspondence to: inweinberg@gmail.com

1 Neuroparticle Corporation, Rockville, Maryland, USA

2 Polytechnic University of Valencia, Valencia, Spain

3 Weinberg Medical Physics, North Bethesda, Maryland, USA

4 Promaxo Corporation, North Bethesda, Maryland, USA

5 University of Maryland, College Park, Maryland, USA

6 University of California, Irvine, California, USA

7 Florida International University, Miami, Florida, USA

8 Children's National Medical Center, Washington, DC, USA

References

[1] Kurzweil R. How to Create a Mind. New York City: Viking & Penguin; 2012

[2] Kennedy P. Brain-machine interfaces as a challenge to the "moment of singularity". Frontiers in Systems Neuroscience. 2014;**8**:213

[3] Xia W, Steenbergen W, Manohar S. Photoacoustic mammography: Prospects and promises. Breast Cancer Management. 2014;**3**(5):387-390

[4] Pashaie R, Anikeeva P, Lee JH, Prakash R, Yizhar O, Prigge M, Chander D, Richner TJ, Williams J. Optogenetic brain interfaces. IEEE Reviews in Biomedical Engineering. 2014;**7**:3-30

[5] Ibsen S, Tong A, Schutt C, Esener S, Chalasani SH. Sonogenetics is a non-invasive approach to activating neurons in Caenorhabditis elegans. Nature Communications. 2015;**6**(1):8264

[6] Truong T-K, Song AW. Finding neuroelectric activity under magnetic-field oscillations (NAMO) with magnetic resonance imaging in vivo. In: Proceedings of the National Academy of Sciences of the USA. 2006 Aug 15;**103**(33):12598-12601. Epub 2006 Aug 7

[7] Gosseries O, Demertzi A, Noirhomme Q, Tshibanda J, Boly M, Op de Beeck M, Hustinx R, Maquet P, Salmon E, Moonen G, Luxen A, Laureys S, De Tiège X. Functional neuroimaging (fMRI, PET and MEG): What do we measure? Revue Médicale de Licge. 2008;**63**(5-6):231-237

[8] Seo D, Carmena JM, Rabaey JM, Alon E, Maharbiz MM. Neural Dust: An Ultrasonic, Low Power Solution for Chronic Brain-Machine Interfaces Neurons and Cognition (q-bio.NC); Instrumentation and Detectors (physics.ins-det). arXiv:1307.2196 [q-bio.NC]

[9] Nacev A, Sarwar A, Weinberg IN, Rodriguez O, Albanese C, Shapiro B, Stepanov PY, Beylin D, Urdaneta M, Probst R, Fricke S. Non-invasive brain access with gradient propulsion of magnetic nanoparticles. IEEE Medical Imaging. 2012

[10] Kumar H, Mishra G, Sharma AK, Gothwal A, Kesharwani P, Gupta U. Intranasal drug delivery: A non-invasive approach for the better delivery of neurotherapeutics. Pharmaceutical Nanotechnology. 2018;**5**(3):203-214

[11] Kalmey JK, Thewissen JGM, Dluzen DE. Age-related size reduction of foramina in the cribriform plate. The Anatomical Record. 1998;**251**(3):326-329

[12] Nacev A, Hilaman R, Jafari S, Patel D, Chowdhury S, Mair L, Stepanov P, Weinberg I. Tunable electropermanent system for magnetic resonance imaging and magnetic particle propulsion. In: Gordon Research Conference, In-vivo Magnetic Resonance Imaging. 2016

[13] Nacev A, Stepanov PY, Weinberg IN. Dynamic magnetic inversion concentrates ferromagnetic rods to central targets. Nano Letters. 2015; **15**(1):359-364

[14] Mair LO, Nacev A, Hilaman R, Stepanov PY, Chowdhury S, Shapiro B, Weinberg IN. Doing the twist: Nanorods with orthogonally magnetized segments twist their way through viscoelastic media. In: Scientific and Clinical Applications of Magnetic Carriers Meeting. 2016

[15] Verma P, Melosh NA. Gigaohm resistance membrane seals with stealth probe electrodes. Applied Physics Letters. 2010;**97**:033704. https://doi.org/10.1063/1.3464954

[16] Silva AC, Lee JH, Aoki I, Koretsky AP. Manganese-enhanced magnetic resonance imaging (MEMRI): Methodological and practical considerations. NMR in Biomedicine. 2004; **17**(8):532-543

[17] Ramaswamy B, Kulkarni SD, Villar PS, Smith RS, Eberly C, Araneda RC, Depireux DA, Shapiro B. Movement of magnetic nanoparticles in brain tissue: Mechanisms and impact on normal neuronal function. Nanomedicine. 2015;**11**(7):1821-1829

[18] Maher BA, Ahmed IAM, Karloukovski V, MacLaren DA, Foulds PG, Allsop D, Mann DMA, Torres-Jardón R, Calderon-Garciduenas L. Magnetite pollution nanoparticles in the human brain. Proceedings of the National Academy of Sciences of the United States of America. 2016;**113**(39):10797-10801

[19] Brannan TS, Burger AA, Chaudhary MY. Bilateral basal ganglia calcifications visualised on CT scan. Journal of Neurology, Neurosurgery, and Psychiatry. 1980;**43**(5):403-406

[20] Guduru R, Liang P, Hong J, Rodzinski A, Hadjikhani A, Horstmyer J, Levister E, Khizroev S. Magnetoelectric 'spin' on stimulating the brain. Nanomedicine (London, England). 2015;**10**(13):2051-2061

[21] Ferguson RM, Minard KR, Krishnan KM. Optimization of nanoparticle core size for magnetic particle imaging. Journal of Magnetism and Magnetic Materials. 2009; **321**(10):1548-1551

[22] Mair LO. Fabrication and Manipulation of Micro- and Nanoscale Magnetic Particles: Application to Magnetofection, Nanopositioning, and Drug Delivery. Chapel Hill: University of North Carolina; 2012

[23] Weinberg IN, Stepanov PY, Fricke ST, Probst R, Urdaneta M, Warnow D, Sanders H, Glidden SC, McMillan A, Starewicz PM, Reilly JP. Increasing the oscillation frequency of strong magnetic fields above 101 kHz significantly raises peripheral nerve excitation thresholds. Medical Physics. 2012;**39**(5):2578-2583

[24] Gleich B, Weizenecker J. Tomographic imaging using the nonlinear response of magnetic particles. Nature. 2005;**435**(7046):1214-1217

[25] Mathews S, Farrell G, Semenova Y. Directional electric field sensitivity of a liquid crystal infiltrated photonic crystal fiber. IEEE Photonics Technology Letters. 2011;**23**(7):408-410

[26] Tyner KM, Kopelman R, Philbert MA. "Nanosized voltmeter" enables cellular-wide electric field mapping. Biophysical Journal. 2007 Aug 15;**93**(4):1163-1174. DOI: 10.1529/biophysj.106.092452

[27] Möreke J, Hodges C, Mears LLE, Uren MJ, Richardson RM, Kuball M. Liquid crystal electrography: Electric field mapping and detection of peak electric field strength in AlGaN/GaN high electron mobility transistors. Microelectronics and Reliability. 2014;**54**(5):921-925

[28] Maleki A, Ara MHM, Saboohi F. Dielectric properties of nematic liquid crystal doped with Fe_3O_4 nanoparticles. Phase Transitions. 2017;**90**(4):371-379

[29] Martinez-Miranda L, McCarthy K, Kurihara LK, Noel A. Effect of magnetic nanoparticles and their functionalization on liquid crystal order. Molecular Crystals and Liquid Crystals. 2005;**435**(1):87-93

[30] Mair LO, Martinez-Miranda L, Nacev A, Hilaman R, Jafari S, Chowdhury S, Weinberg IN. Electric field responsive contrast agent based on liquid crystals and magnetic nanoparticles. In: Proceedings of the Magnetism and Magnetic Materials Conference. 2017

[31] Nair M, Guduru R, Liang P, Hong J, Sagar V, Khizroev S. Externally controlled on-demand release of anti-HIV drug using magneto-electric nanoparticles as carriers. Nature Communications. 2013;**4**:1707

[32] Guduru R, Khizroev S. Magnetic field-controlled release of paclitaxel drug from functionalized magnetoelectric nanoparticles. Particle and Particle Systems Characterization. 2014;**31**(5):605-611

[33] Ramaswamy B, Algarin JM, Weinberg IN, Chen Y-J, Krivorotov IN, Katine JA, Shapiro B, Waks E. Wireless current sensing by near field induction from a spin transfer torque nano-oscillator. Applied Physics Letters. 2016;**108**:242403. https://doi.org/10.1063/1.4953621

[34] Prokopenko O, Bankowski E, Meitzler T, Tiberkevich V, Slavin A. Spin-torque nano-oscillator as a microwave signal source. IEEE Magnetics Letters. 2011;**2**:3000104

[35] Algarin JM, Ramaswamy B, Weinberg IN, Waks E, Shapiro B, Herberholz J, Araneda RC. Modulation and detection of single neuron activity using spin transfer nano-oscillators. Spintronics X. 2017

[36] Patel G, Haas M, Darji N, Speck O. Evaluation of 2D spatially selective MR spectroscopy using parallel excitation at 7 T. Quantitative Imaging in Medicine and Surgery. 2015;**5**(3):344-355

[37] Langston JW. The MPTP story. Journal of Parkinson's Disease. 2017;**7**(s1):S11-S22

[38] Lee W, Lee SD, Park MY, Foley L, Purcell-Estabrook E, Kim H, Fischer K, Maeng L-S, Yoo S-S. Image-guided focused ultrasound-mediated regional brain stimulation in sheep. Ultrasound in Medicine & Biology. 2016;**42**(2):459-470

[39] Kondziolka D, Lee JYK. Long-lasting microthalamotomy effect after temporary placement of a thalamic stimulating electrode. Stereotactic and Functional Neurosurgery. 2004;**82**:127-130

[40] Chang S-Y, Shon YM, Agnesi F, Lee KH. Microthalamotomy effect during deep brain stimulation: Potential involvement of adenosine and glutamate efflux. In: Conf. Proc. … Annu. Int. Conf. IEEE Eng. Med. Biol. Soc. IEEE Eng. Med. Biol. Soc. Annu. Conf., vol. 2009. 2009. pp. 3294-7

[41] Tay A, Di Carlo D. Magnetic nanoparticle-based mechanical stimulation for restoration of mechano-sensitive ion channel equilibrium in neural networks. Nano Letters. 2017;**17**(2):886-892

[42] Nacev A, Weinberg IN, Mair LO, Hilaman R, Algarin J, Jafari S, Ijanaten S, Da Silva C, Baker-McKee J, Chowdhury S, Stepanov PY, DaSilva C, Baker-McKee J, Chowdhury S. Neurostimulation using mechanical motion of magnetic particles wiggled by external oscillating magnetic gradients. In: Nacev A, Weinberg IN, Mair LO, Hilaman R, Algarin J, editors. Proc. Eighth Int. IEEE EMBS Neural Eng. Conf. Shanghai; 2017. 2017

[43] Kittipaisalsilpa K, Kato T, Suzuki Y. Liquid-crystal-enhanced electrostatic vibration generator. In: 2016 IEEE 29th International Conference on Micro Electro Mechanical Systems (MEMS); January. 2016. pp. 37-40

[44] Miller P. Dynamical systems, attractors, and neural circuits. F1000 Res. 2016;**5**:F1000 Faculty Rev-992. DOI: 10.12688/f1000research.7698.1

Edited by Denis Larrivee

As a strategic response to cognitive and CNS impairments, BCI is a theoretical outgrowth of several generations of endogenous devices for peripheral nerves, which have as a prime goal the direct replacement of lost neural function. In these earlier applications therapeutic intervention has been premised only on the restoration of signal generating capacity where nerve transmission is largely unidirectional and temporally sequenced. It is increasingly apparent, however, that the brain not only employs a very different type of syntax from that of peripheral nerves but also structures the semantic content of motor activity, fundamentally altering the conception of BCI as a therapeutic medium. The book presented here documents this change, proposing a multi-faceted strategy in which BCI therapy can restore the loss of multi-tiered, brain based motor function.

Published in London, UK

IntechOpen

ISBN 978-1-83881-588-2